CZECH TECHNICAL UNIVERSITY IN PRAGUE
FACULTY OF MECHANICAL ENGINEERING
DEPARTMENT OF ENVIRONMENTAL ENGINEERING

DOCTORAL THESIS

OPTIMUM REPRESENTATION OF HEAT SOURCES IN SIMULATIONS OF AIR FLOW IN INDOOR ENVIRONMENT

Ing. Petr Zelenský

Doctoral Study Programme:
Mechanical Engineering

Study Field:
Environmental Engineering

Supervisor:
prof. dr. ir. Jan L. M. Hensen

Supervisor Specialist:
Ing. Martin Barták, Ph.D.

Prague, September 2018

SHRNUTÍ

Výzkum byl motivován problematikou správné distribuce vzduchu ve velkých prostorech s velkým počtem zdrojů tepla a/nebo variabilním obsazeností návštěvníky, jako jsou např. přednáškové síně, divadla, kina, atria apod. Projektanti systémů techniky prostředí pro tyto prostory často čelí nejistotě, zda navržená řešení splní požadavky na kvalitu vnitřního prostředí.

Dosažení vysoké kvality vnitřního prostředí velkých prostor při současném zohlednění energetických nároků může být náročné. Jedním z nástrojů, které mohou pomoci analyzovat a pochopit složité interakce ve vnitřním prostředí, je modelování a simulace pomocí počítačové mechaniky tekutin (CFD). Nicméně v současné době existují omezení CFD, vyplývající zejména z omezené kapacity dostupné výpočetní techniky. Numerické modely simulovaných prostor je tak vždy nutné do určité míry zjednodušovat.

Byla vyvinuta nová metoda modelování zdrojů tepla pro studium proudění vzduchu ve vnitřním prostředí s cílem snížit výpočetní nároky CFD simulací se zdroji tepla a zajistit spolehlivost získaných výsledků. Výzkum byl založen na numerickém modelování a simulacích v CFD softwaru ANSYS Fluent. Bylo provedeno několik numerických a experimentálních studií zaměřených na problematiku přirozené konvekce ve vnitřním prostředí a její simulaci:

- byly stanoveny optimální parametry výpočetní sítě v blízkosti ohřívané stěny modelovaného zdroje tepla;
- byl stanoven optimální model turbulence pro CFD simulace s převažujícím účinkem přirozené konvekce na proudění vzduchu;
- byla zkoumána citlivost konvekčních proudů nad zdroji tepla na okolní teplotu;
- byla vyhodnocena vzájemná interakce konvekčních proudů nad více zdroji tepla, které jsou umístěny blízko u sebe.

Byla zpracována řada simulací trojrozměrného konvekčního proudění ve vnitřním prostředí. K validaci navržené metody modelování zdrojů tepla byly použity výsledky vlastního měření v experimentální místnosti společně s porovnáním modelů s různým stupněm zjednodušení. Navržená metoda byla adaptována tak, aby odrážela různé tepelné podmínky okolního prostředí a byla vytvořena uživatelsky definovaná funkce (UDF) pro software ANSYS Fluent. Metoda byla následně aplikována ve vybrané případové studii a byla demonstrována její použitelnosti v praktických aplikacích.

SUMMARY

The research was motivated by the issue of proper air distribution in large indoor spaces with a high number of heat sources and/or variable occupancy patterns, such as e.g. lecture halls, theatres, cinemas, atriums etc. Designers of heating, ventilation and air conditioning (HVAC) systems for these spaces frequently cope with the uncertainty whether the proposed design will meet the requirements for adequate indoor environment quality.

Achievement of high indoor environment quality with simultaneous consideration of energy demands in large indoor environments can be challenging. Modelling and simulation tools, such as computational fluid dynamics (CFD) can help to analyse and understand the complex interactions in the indoor environment. However, there are currently some limits of CFD arising especially from the limited capacity of available computers and resulting in the necessity to simplify numerical models of the simulated cases.

A new modelling method to represent models of heat sources for indoor air flow studies was developed in order to reduce the computational burden of CFD simulations with heat sources and ensure high reliability of the obtained results. The research was based on numerical modelling and simulation in the CFD software ANSYS Fluent. Several numerical and experimental studies were conducted, targeting issues related to natural convection indoors and its simulations:

- optimal characteristics of the near-wall region mesh around the modelled heat source was determined;
- an optimal model of turbulence for CFD simulations with prevailing effect of natural convection on the air flow was proposed;
- the sensitivity of the thermal plumes above heat sources on the ambient air temperature conditions was studied;
- the mutual effect of thermal plumes rising above multiple heat sources positioned close to each other was assessed.

Various cases of three-dimensional convective flow in the indoor environment were simulated. The results of the experiment performed in the experimental room were used for validation of the proposed modelling method to represent heat sources, together with comparative testing of models at different levels of simplification. The proposed method was adapted to reflect different thermal conditions of the ambient environment and a user defined function (UDF) for ANSYS Fluent was developed. The method was applied in a selected case study in order to demonstrate its usability in practice.

DECLARATION OF AUTHORSHIP

I declare that this doctoral thesis entitled “Optimum Representation of Heat Sources in Simulations of Air Flow in Indoor Environment” is my own work performed under the supervision of prof. dr. ir. Jan L.M. Hensen and Ing. Martin Barták, Ph.D., with the use of available literature.

Further, I certify that this work is free of plagiarism and all materials appearing in this thesis have been properly quoted and attributed.

Prague, 17.9.2018

Petr Zelenský

ACKNOWLEDGMENT

I would like to express my deep gratitude to Dr. Martin Barták for his support and guidance over the past years. Without his enthusiasm and advices, I would never have been able to conclude my research. My special thanks go to Prof. Jan Hensen for his valuable suggestions and help to get my research out of the box and to see it in different perspectives.

I would like to thank all of my friends and colleagues that I have met both during my stay at the Czech Technical University in Prague and at the Eindhoven University of Technology. Without them, my study years would never have been so enjoyable.

Finally, my family has been a constant source of support, encouragement, and inspiration not only during my academic career, but also during my entire life. Namely, I would like to thank my wife Rebeca, who endured all the evenings and weekends, when the Ph.D. work was a priority. Finally yet importantly, my biggest gratitude goes of course to my parents, to whom I would like to dedicate this thesis.

TABLE OF CONTENTS

LIST OF FIGURES

LIST OF TABLES

NOMENCLATURE

c	[J/kg·K]	specific heat capacity
d	[m]	diameter
k	[m^2/s^2]	turbulence kinetic energy
l	[m]	characteristic dimension
p	[Pa]	pressure
t	[°C]	temperature
u	[m/s]	velocity
u_x, u_y, u_z	[m/s]	velocity components
u_τ	[m/s]	friction velocity
u^+	[-]	dimensionless velocity
w	[m]	width
y^+	[-]	dimensionless wall distance
A	[m^2]	area
D	[m]	thickness
H	[m]	height
$\dot{I}$	[kg·m/s^2]	momentum transfer rate
P_c	[W]	heat output
R	[-]	residual
T	[K]	temperature
$\dot{V}$	[m^3/s]	volume flow rate
ε	[m^2/s^3]	turbulent dissipation rate
λ	[W/m·K]	thermal conductivity coefficient
μ	[Pa·s]	dynamic viscosity
ν	[m^2/s]	kinematic viscosity
ρ	[kg/m^3]	density
τ_w	[Pa]	wall shear stress
ω	[1/s]	specific dissipation rate
x	[m]	position coordinate (Cartesian axis)
y	[m]	position coordinate (Cartesian axis)
z	[m]	position coordinate (Cartesian axis)

List of indexes

x, y, z	Cartesian axis
max	maximum
min	minimum
amb	ambient

List of abbreviations

AC	Active chilled beams
BES	Building enregy simulation
CFD	Computational fluid dynamics
DC	Data centre
HVAC	Heating ventilation and air conditioning
HRN	High Reynolds number
IT	Information technology
LRN	Low Reynolds number
LDA	Laser Doppler anemometry
PI	Performance indicator
PIV	Particle image velocimetry
SBC	Subsidiary zone with simple boundary condition (see Chapter 6.1)
UDF	User defined function

1 INTRODUCTION

The innovation and optimization of heating, ventilation and air conditioning (HVAC) systems for any occupied space is the number one task of HVAC engineering. Every improvement of the indoor environment quality increases comfort of occupants and can enhance work productivity, reduce sickness rate, raise overall physical and psychological wellbeing of the occupants etc. A very important reason for optimization of HVAC systems is also reduction of energy consumption.

The main aim of the current research is to target issues of improper air distribution risk and discomfort risk in large indoor spaces with large number of heat sources and/or variable occupancy patterns, such as atriums, lecture halls, theatres, cinemas and other entertainment facilities, etc. Designers of HVAC systems for these spaces frequently cope with the uncertainty of the proposed design meeting requirements for adequate thermal comfort and proper air distribution under different conditions of occupancy. The improvement of indoor environmental quality and simultaneous reduction of energy demand in large indoor environments with various conditions of use can be challenging. There are very complex interactions in the indoor air flow, which may not be obvious at first sight.

One of the techniques that can help to analyse and understand these interactions is computational fluid dynamics (CFD) modelling and simulation. It is increasingly applied in building design practice, as it allows the user to study the indoor environment at several levels of resolution at the same time, providing both overall insight and detailed information. Thus, it uncovers the complex interactions and helps to test whether the specified requirements can be met before the design realization. Although the availability of CFD simulation is rising, there are still some limits, especially in the capacity of available computers. It is very often necessary to simplify the reality to a certain level. However, as the quality of the results is determined by the accuracy of the input, the simplification must be done in a proper way, considering the aim of the simulation.

Heat sources are very common elements of the indoor environment. They act as a source of sensible heat and sometimes also latent heat and contaminants (as for example occupants). They can have a strong influence on the air flow in rooms, temperature gradient, contaminant distribution and stratification etc. They influence thermal comfort in the indoor space and also performance of HVAC systems. With rising demand for better indoor environment quality and lower energy consumption of buildings, it is necessary to consider the indoor heat sources as precisely as possible. It is of a great importance to be able to model heat sources in an appropriate way, so the necessary simplification of the models does not alter the effect of the heat sources on the air flow conditions in the simulated environment, considering the evaluated performance indicators.

The main impact of indoor heat sources on the surrounding air flow is caused by convective flow rising around them. The warm air is driven upwards by buoyancy forces, forming a rising thermal plume above the heat source. The characteristics of the plume are influenced by many various factors such as the shape of a heat source and its heat output, properties of the surrounding environment, arrangement of other heat sources and sources of forced flows, etc. Thus, it is very problematic to simulate convective flow adequately with a simplified model of heat sources. This research addresses specifically the appropriate representation of heat sources for simulation of indoor air flow. It was based on numerical modelling and simulations in CFD software ANSYS Fluent.

A new modelling method to represent heat sources in CFD simulations of the air flow in the indoor environment has been proposed. The method is aimed to reduce computational demands of CFD simulations with indoor heat sources and ensure high reliability of the obtained results. Several numerical and experimental studies related to the simulation of thermal plumes around heat sources have been carried out during the development of the method and its adaptation for practical use. The method was tested and applied in a selected case study in order to show its usability for practical applications.

1.1 Thesis layout

The thesis is divided into several sections. Chapter 2 summarizes the research background and current state of the art of the researched issue. It is based on the information found in the available literature and it places the current research into a wider context. It introduces different methods of air flow modelling in HVAC engineering, with emphasis on the CFD approach. Basic types of indoor heat sources are presented, including the ways of their modelling in air flow simulations. The approaches to experimental studies with heat sources are described as well, while the measurement of characteristics of thermal plumes rising above heat sources is discussed in detail.

Chapter 3 is summarizing the goals of the current research arising from the literature review. Methods and tools used for numerical and experimental studies in the presented research are described in Chapter 4. Current ways of turbulence modelling in CFD simulations are discussed in detail. Appropriate meshing of near-wall regions in the numerical models is discussed as well. The following chapters are describing development, validation and application of the new modelling method to represent heat sources in indoor air flow simulations.

The research achievements and contributions are discussed in Chapter 8 with differentiation of contributions for theory and for practice. Chapter 9 summarizes the conclusion of the current research and also proposes directions for possible future extension of the presented work.

2 RESEARCH BACKGROUND

This part of the thesis summarizes the theoretical background for the current research found in literature, professional journals and electronic sources of information (Science direct, EBSCOhost…). Chapter 2.1 introduces the use of indoor air flow modelling in the HVAC engineering, including different approaches towards its solution. Chapter 2.2 summarizes basic types of indoor heat sources and their effect on the indoor environment. Characteristics of thermal plumes and factors affecting their forming are described. The current position of CFD simulations as a design tool and the necessity of simplified modelling is discussed in detail in Chapter 2.3. Turbulence modelling in CFD simulations is addressed as well. Chapter 2.4 deals with simplified modelling of indoor heat sources for CFD simulations in HVAC engineering. It targets especially models of occupants, considering the main focus of the research. It also analyses how previous authors discretised their numerical models. The approaches to modelling of air-supply diffusers in CFD simulations are mentioned in the Chapter 2.5, as an inspiration for the development of a new modelling method to represent heat sources. Chapter 2.6 addresses possible approaches to validation of newly proposed methods. Chapter 2.7 summarizes methods of experimental investigation of thermal plumes generated by heat sources. The issue of the indoor environment quality assessment in real world scenarios with the use of performance indicators is discussed in Chapter 2.8.

2.1 Indoor air flow modelling

The lifestyle in developed countries has changed rapidly over the last several decades. We often spend most of our working and leisure time indoors – in schools, offices, entertainment facilities or at home. Thus, the innovation and optimization of buildings and their systems is the number one task of HVAC engineering, as every improvement of the indoor environment quality directly affects the quality of our lives. A great variety of both active and passive systems for indoor environment treatment has been proposed. In addition, the recent development in building construction brought new innovative design solutions, which frequently differ from traditional building forms and require advanced design tools.

The optimization of indoor environment quality can be a challenging task. There are often several sources of forced flow in the room to be considered, such as the influence of infiltration and heat sources, the effect of the room geometry, conditions of the external environment, etc. The technique that can help to understand these complex interactions is air flow modelling and simulation.

As computer simulation became a very popular design tool, several different approaches for building air flow prediction in terms of complexity and resolution level of the obtained results have evolved. The ones most often applied in the current practice are semi-empirical methods, multizone models, zonal models and CFD simulations (Hensen 2004; Zuo 2010). It is especially important to understand the general purpose, advantages, disadvantages and range of applicability of each type of method. Only then, it is possible to apply the correct method for a solved issue. It may be considered that a more complex, higher resolution approach does not always provide better answers to all design questions and also, that some questions can be answered more effectively (easier and faster) by a less complex, lower resolution method.

2.1.1 Semi-empirical methods

The semi-empirical modelling methods originate from traditional engineering practice. They are generally easy to set up and they have very little demands on computational power. The air flow is modelled conceptually, based on rules of thumb, engineering values and semi-empirical

relationships. However, these methods do not give any deep insight into air flow inside the modelled space. They provide rather general information about air flow – mostly they are used to predict air change rates, for example air change rate by infiltration based on estimation of building airtightness etc. (Hensen 2004).

2.1.2 Multizone models

Multizone approach is based on the assumption that the air in a room is well mixed and homogenous (considering pressure, temperature, contaminant distribution etc.) and it can be described by a single node representing the whole room. The building system is treated as a nodal network representing rooms and system components with inter-nodal connections representing air flow paths (windows, doors, ducts, cracks, fans, etc.). Multizone models can be used for fast prediction of air-change rates for the whole building, while keeping very low computational demands. However, its use can be problematic for simulations of spaces with poorly mixed air and contaminants (Wang & Chen 2007). Also, as it completely neglects momentum effects in a zone, it is not appropriate for any high resolution studies of indoor air flow, such as the ones targeted in this research.

2.1.3 Zonal models

The above mentioned multizone approach can be adapted for better resolution, i.e. to zonal modelling approach. The rooms are further divided into several virtual volumetric zones. It is assumed that each of the zones has uniform air conditions and it can be represented by an individual node within the nodal network. Thus, the basic information on temperature and contaminant distribution in the room, draft, asymmetric thermal radiation etc. can be obtained, while keeping low computational demands.

The zonal model approach is much faster than CFD simulation and provides better resolution results than the multizone model. However, its accuracy is still not good enough for various applications. Especially, it is necessary to know (or estimate) the air flow patterns and contaminant concentrations before the simulation, in order to reasonably divide the modelled room (Griffith & Chen 2003). Therefore, the zonal model approach is not effective for air flow modelling in spaces with unknown and/or complex air flow patterns and it is not a good choice for the current study.

2.1.4 CFD Simulations

CFD simulations are usually based on the finite volume method, i.e. division of the investigated domain into a large number of small control volumes and subsequent solution of conservation equations for mass, momentum, and energy for each of them. They can provide very detailed flow information, which can not be obtained by the previously discussed methods. Although the CFD simulations generally have very high demands on computational power (much higher than the three previously discussed approaches), there are various application, which benefit from the high complexity of the obtained results.

The detailed CFD air flow modelling can be important in the cases of design of rooms with high requirements on indoor environment quality, proper air distributions and thermal comfort of occupants. Ventilation of operating theatres can be mentioned as an example. Low infection rate must be assured at surgical sites in general and any optimization of air flow field has a direct effect on the health of patients. The air quality should remain as high as possible especially near the wound and the positions where implants and surgical instruments are situated. However, it is difficult to predict the air flow in the operating theatres due to the interaction of the supply air flow from air conditioning units and convective flow rising above the surgical equipment and

personnel (who act also as the prominent source of contaminants in the room). This requires detailed indoor air flow modelling using CFD simulation. (Loomans et al. 2008).

Another example of an internal environment with high requirements of proper air distribution are hospital rooms. This case combines the need to efficiently remove contaminants and at the same time ensure thermal comfort of the accommodated patients. Méndez et al. (2008) studied air flow patterns in a two-bedded hospital room and uncovered the deficiencies in the initial room design. The authors conducted a variant study of several configurations of the room equipment and proposed an optimized design leading to increased ventilation efficiency and better thermal comfort of the patients.

The design and optimization of active chilled beams (ACB) is also an area where air flow modelling plays an important role. The efficiency of ACB systems is influenced by various factors, such as primary and induced air flows, thermal uniformity in the space, geometry of the room, ACB placement etc. It is also necessary to consider condensation and draft risks. The design optimisation of ACB systems is thus challenging to achieve and air flow modelling is often used (Karimi 2018).

Air flow modelling may also be beneficial for the design of industrial premises without the occurrence of occupants. For example, proper air distribution is very important in the case of data centers (DCs). Although the best-practice of DC design is well established and documented, it is not unusual to approach it with the use of air flow modelling, as simply following the best-practice rules may not be sufficient for achieving optimum air distribution (Zelenský et al. 2014). Incorrect understanding of the air flow in DC and its poor management can lead to the occurrence of hot spots (undesirable local temperature rise caused by improper cooling of DC equipment), which consequently leads to a greater need of cold air causing energy inefficiency or, in extreme cases, to information technologies (IT) equipment failures. CFD simulation of air flow was used, for example, by Cho et al. (2009) who compared heat removal efficiency of various air distribution systems in a DC and Zhang et al. (2008), who studied the effect of various levels of rack-model simplification on the result of the CFD simulation of a DC.

The large spaces with large numbers of indoor heat sources are another example where air flow modelling can be a useful design tool. It can help to uncover complex interactions of thermal plumes rising above multiple heat sources. Barták et al. (2001) used air flow modelling for a study of indoor environment in a cultural centre housed in the former church of St. Anna in Prague. The authors revealed the air flow patterns in the building and discussed their possible effect on the delicate building structures of the landmark. However, they faced limitations of CFD simulation to correctly model large number of heat sources in one computational case (up to 350 visitors in the building).

Aside of the above mentioned cases, it has been encountered in the Department of Environmental Engineering at the Faculty of Mechanical Engineering, CTU in Prague, that consultancy for the air flow modelling in large indoor spaces is often requested by HVAC engineers and building developers. In recent years, various studies have been discussed, such as high resolution air flow simulations in large shopping galleries, open-space offices, railroad station, industrial storage of nuclear waste from a nuclear power plant, etc. Proper representation of heat sources in the numerical models, while keeping reasonable computational demands of CFD simulations, was often a limiting factor in these studies.

2.2 Heat sources in indoor environment

The indoor heat sources can be classified into three basic groups: occupants, equipment and strong heat sources. The equipment covers for example lights, IT devices, kitchen and other household appliances, etc. Strong heat sources can be found especially in industry. Heat sources providing thermal comfort in the indoor environment, such as combustion devices (boilers, stoves etc.) or heating devices (radiators, convectors, floor or wall heating surfaces etc.) can be identified as a separate category. The following text is focused only on heat sources without mechanically induced air flow.

Natural air flow formed above a heat source is called convective stream or thermal plume. It directly influences the air flow pattern in the surrounding environment. Its impact depends on its momentum, parameters of the environment and type of used air distribution system. In rooms without significant air mixing, even the weak convective plumes have very strong influence on the overall flow pattern, temperature gradient, contaminant distribution and thermal stratification. The momentum of convective flow formed around strong or multiple heat sources can be comparable, or even higher, than the momentum of the air flow supplied to the room by air-conditioning units. In such cases, the air flow from air distribution elements can be influenced, possibly in a negative way (Zukowska 2011; Awbi 2003; Zbořil et al. 2007; Loomans et al. 2008) which can affect comfort of occupants. On the other hand, in the rooms with displacement ventilation, thermal plumes have special importance, as they provide driving force for natural ventilation. They are important for appropriate air exchange and they also positively influence the quality of inhaled air (Xing et al. 2001; Skistad et al. 2002).

2.2.1 Convective flows

Upward rising convective flows are formed above the heat sources and near the walls with temperature higher than the ambient air temperature. They are driven by buoyant force arising from the air temperature difference (from the consequent air density difference). They are influenced by the shape and intensity of a heat source, its position and conditions of surrounding environment: room size (particularly the ceiling height), temperature, temperature stratification, arrangement of other heat sources and also sources of forced flows, etc. (Skistad et al. 2002; Awbi 2003).

The aspects influencing the heat plume must be understood for its effective measurement and simulation. Three regions can be recognized in the thermal plume above a freestanding heat source, see Fig. 2.1 (Zukowska 2011):

I. Initial region – the region closest to the heat source. It begins at convective boundary layer around the surface of the heat source as a laminar flow, which becomes turbulent in a higher distance. The temperature and velocity profiles are not developed in this region.
II. Region of self-similarity of the mean motion – region of turbulent flow with velocity and temperature profiles of Gaussian type. The flow in this region is considered as axisymmetric.
III. Region of complete flow similarity – the flow in this region is considered fully developed and axisymmetric. It spreads linearly in environments without thermal stratification. In thermally stratified environments, this region is called the region of maximum plume rise as the maximal elevation of the plume is reached, since the temperature gradient affects the height to which the plume rises. This is described below in more detail.

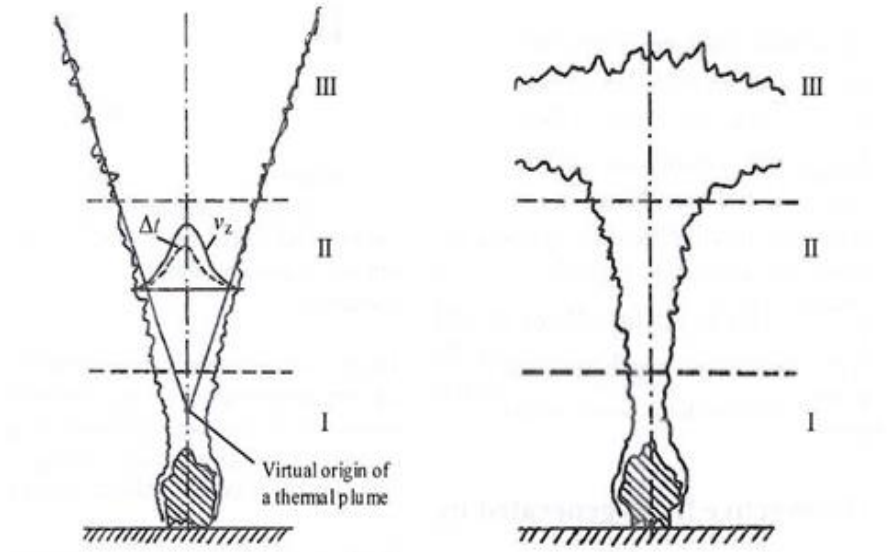

Fig. 2.1 – Thermal plume regions (Zukowska 2011)
Environment without thermal stratification (left), with thermal stratification (right)

An essential condition for forming of convective flow is the temperature difference between the air in the plume and the ambient air. In the environment with vertical temperature stratification and sufficient height of the ceiling (see Fig. 2.2), the rising convective plume reaches the height z_t, where the air temperature in the plume centre is the same as the temperature of the ambient air. After reaching this height the plume starts to spread horizontally. The maximum height of the plume reached by its inertia is indicated as z_{max} (Skistad et al. 2002).

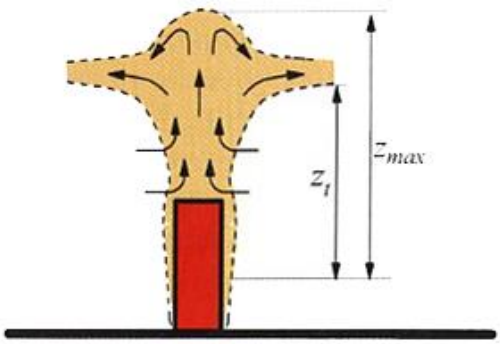

Fig. 2.2 – Maximal height of thermal plume (Skistad et al. 2002)

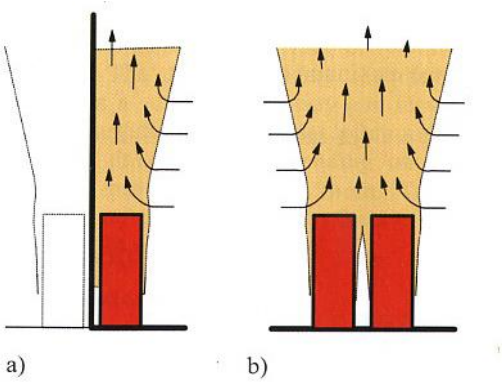

Fig. 2.3 – Interaction of thermal plumes (Skistad et al. 2002)

The shape of a thermal plume, its velocity and temperature distribution (velocity and temperature profiles) and also turbulence characteristics depend strongly on the geometry and parameters of the heat source (Mierzwinsky 1980). However, the form of convective flow can be influenced also by the proximity of other heat sources (i.e. other convective flows). Flows rising in parallel direction from several adjacent heat sources may interact, gradually coalesce and continue as a single plume with higher momentum, see Fig. 2.3 b). The vertical distance from the heat sources at which the plumes fully merge, depends mainly on the distance between individual heat sources and the character of the merging thermal plumes. As the process

is gradual, four regions can be seen: region of independent plumes, encroaching plumes, merging plumes and fully merged plumes, see Fig. 2.4 (Macdonald et al. 2002).

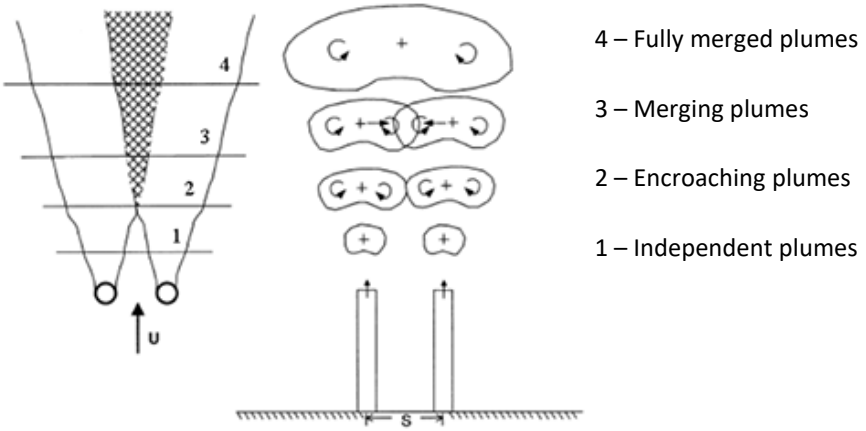

Fig. 2.4 – Merging of thermal plumes (Macdonald et al. 2002)

If the heat source is positioned close to a wall, then the formed convective flow may attach to the wall due to the Coanda effect. The proximity of the surface restricts the air entrainment on the side facing the wall. This creates a pressure difference and consequent inflection of the plume. The plume moves upward along the surface as a wall jet, see Fig. 2.3 a). Both of the mentioned phenomena (plumes merging and attachment to a surface) affect, for example, the rate of entrainment of the ambient air, maximum height z_{max} reached by the plume etc. (Skistad et al. 2002).

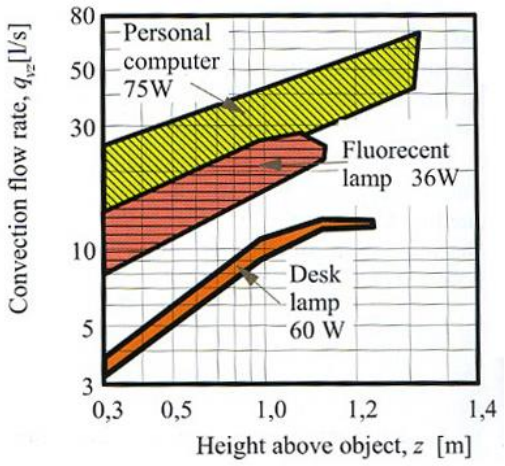

Fig. 2.5 – Thermal plumes above common heat sources (Skistad et al. 2002)

The mass flow in a thermal plume increases along the height as a result of entrainment of ambient air on the boundary of the convective flow. Ranges of volume flows of plumes above some common types of heat sources for usual indoor environment temperatures are shown in Fig. 2.5.

An important issue is the stability of thermal plumes. It has been previously noticed that the convective flows do not reach steady state even when the conditions in the plume surroundings seem to be constant (Zukowska et al. 2010a; Deevy et al. 2008; Hyldgaard 1998). This phenomenon is called plume axis wandering and it is characterized as a periodical deviation of the plume axis from its mean vertical position. The instability may be caused by small changes in the surroundings, as it is impossible to create ideally stable conditions (Popiolek 1987). Zukowska et al. (2010b) showed that the convective flow can be influenced even by small non-uniformity of the surrounding environment, such as deviation of 0.005 m/s in speed and around 0.01 °C in temperature. The instability can be also caused by unsteady flow in convective boundary layer around the heat source (Zukowska 2011). Both can be observed during experimental measurement, as well as in transient CFD simulations of heat sources.

2.2.2 Analytical solution of convective flows

Analytical solving of convective flows is possible only for a very limited number of rather simplified configurations, such as for example convective flow above a point source, line source, along a vertical surface and above a horizontal surface, see Fig. 2.6. The mathematical relations for calculating the quantities of thermal plumes above these sources (i.e. volume flow, momentum, velocity and temperature in the axis of the plume…) are available in the literature (Awbi 2003; Zukowska et al. 2010a). It is important to distinguish between a heat source in a neutral environment and in an environment with thermal stratification, which directly affects the plume development and its maximal elevation. In the case of rooms with temperature stratification, the velocity in a plume is lower because the vertical increase of the room air temperature reduces the buoyancy force.

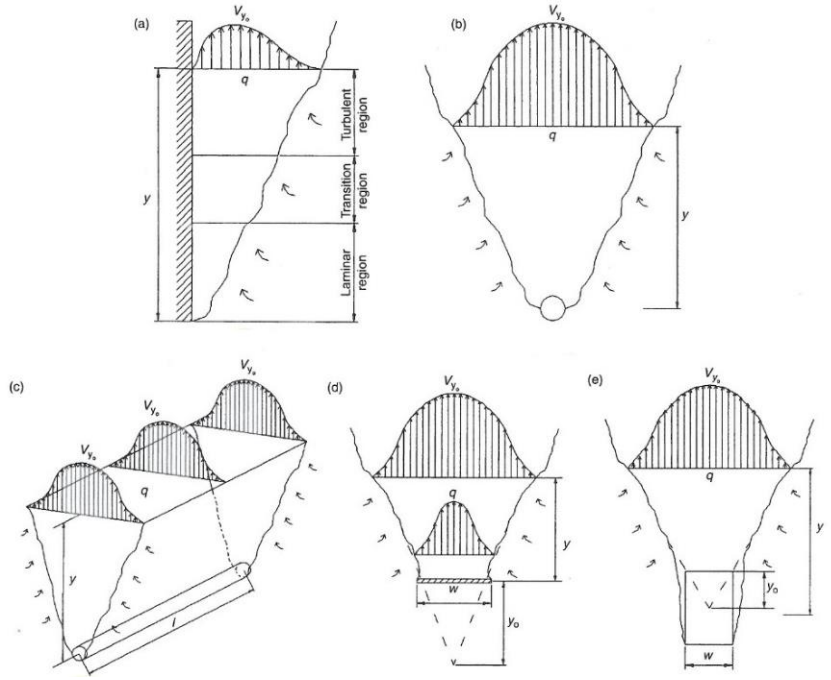

Fig. 2.6 – Basic configurations of heat sources for analytical solution (Awbi, 2003)
a) vertical surface, b) point source, c) line source, d) horizontal surface, e) vertical source

The influence of thermal conditions in the room on the plume development is predictable using basic analytical relations. The case of three basic analytical configurations (horizontal surface, point source and line source) in the environment without temperature stratification is further discussed as an example. The relations to calculate volume flow rate $\dot{V}_y$ at a chosen height y for heat source of heat output P_c are listed below (Awbi 2003).

- Horizontal Surface: $$\dot{V}_{surface,y} = 0.5\times10^{-3} l^{2/3} P_c^{1/3} (y+w)^{5/3} \quad (2.1)$$
- Point Source: $$\dot{V}_{point,y} = 5.5\times10^{-3} P_c^{1/3} (y+y_0)^{5/3} \quad (2.2)$$
- Line Source: $$\dot{V}_{line,y} = 14.0\times10^{-3} l^{2/3} P_c^{1/3} (y+y_0)^{5/3} \quad (2.3)$$

Additionally, Popiolek et al. (1987) present analytical relation to calculate volume flow rate at a chosen height y above objects of more complex shapes (sphere, cylinder of h/d ratio from 2.7 to 8.0, radiator) with heat output P_c:

- Complex objects: $$\dot{V}_{line,y} = 14.0\times10^{-3} l^{2/3} P_c^{1/3} (y+y_0)^{5/3} \quad (2.4)$$

The formulae (2.1), (2.2), (2.3) and (2.4) assume that the basic volume flow rate of convective flow above the horizontal surface heat source, point heat source, line heat source but also heat sources of more complex shapes is influenced only by the heat output of the heat source and it does not reflect temperature conditions in the surroundings. The same applies also for the maximum velocity in the plume v_{y0} (axis velocity) and temperature difference ΔT_{y0} at the plume centre, as demonstrated on the example of analytical solutions of point heat source (see formulae (2.5) and (2.6), respectively). Therefore, the change of temperature conditions in the room (indoor air temperature) should not affect the form of thermal plume above these heat sources, providing that their heat output remains constant.

$$u_{y_0,\text{point}} = 0.0128 P_c^{1/3} y^{-1/3} \tag{2.5}$$

$$\Delta T_{y_0,point} = 0.329\, P_c^{2/3} y^{-5/3} \tag{2.6}$$

However, analytical relation for the volume flow rate above a vertical surface does reflect temperature conditions (or more precisely, temperature difference between the surface temperature of the heat source and ambient air temperature) (Awbi 2003):

$$\dot{V}_{surface,y} = 2.75\times10^{-3} l \left(T_w - T_{amb}\right)^{2/5} y^{6/5} \tag{2.7}$$

where T_w is temperature of the surface, T_{amb} temperature of the ambient air and l is characteristic dimension.

The influence of the temperature difference is not always explicit in the available analytical solutions; it is often implied by the heat output term. Thus, it is not clear whether the temperature conditions influence the convective flow.

The basic cases of heat sources stated above are more or less idealized. It is usually problematic to outline the characteristics of convective flows just by analytical solution for more complex geometries that occur in real situations as they often do not meet the basic geometrical requirements of the analytical solutions. Moreover, in some cases it is not possible to simplify the sources in order to match one of the configurations suitable for the analytical solution.

In addition, if we deal for example with a number of heat sources in one space, with obstacles surrounding these heat sources (occupant sitting by the table…), or with interaction of natural buoyant flows with forced flows, then the analytical methods are insufficient. Very suitable tool for solving these cases can be experiments or CFD simulations, where simulations are nowadays generally cheaper and can be more efficient.

2.3 CFD simulations and simplified modelling

The design methods and tools in HVAC engineering are changing with growing demand and increasing capacity of IT. Standard (manual) methods are gradually complemented by computer-based alternatives. Building simulations generally have become one of the most important engineering tools in design of buildings and HVAC systems. This is caused by the increasing number of non-standard solutions in modern building construction, which can be hardly dealt with standard design methods. There is a strong demand for improving the indoor environment quality and simultaneously for reducing the energy consumption of HVAC systems and entire buildings. However, these two targets are often contradicting each other. With enhanced design tools, it is possible to address them both at the same time. Computer simulations enable better imitation of reality and provide new insights into solved problems. They help to understand the relations between various boundary conditions, design options, control strategies, etc., and performance of the whole system. Thanks to simulations, it is possible to design the systems in

different variants and mutually compare their predicted performance. The robustness of the systems and their performance under different conditions can be tested as well. Thus, it is possible to foresee and potentially avoid the drawbacks of the design before its realization and optimize the systems. The appropriate method for detailed modelling of the indoor environment aiming to uncover for example air flow patterns in rooms, temperature conditions, indoor air quality and contaminant distribution is CFD (Djunaedy et al. 2003; Schälin 2007).

Effective use of CFD simulations depends mainly on the ability of the person who sets up and performs the simulation, as well as on the capabilities of IT, which has undergone a very rapid development in the recent decades, resulting in a significant rise of accessible computer power. However, there are still considerable limitations. The more complex the problem is that we are solving, the longer its computational time takes and the more difficult it is to prepare the computational models. As it is vital to communicate the outcomes of the simulation with other participants who are involved in the design process, it is necessary to get relevant results in the horizon of days or weeks at maximum. One of the ways to reach the target of reasonable computational time is simplification of numerical models used for the simulation, which, aside of the computational time, also reduces the time necessary for computational model preparation and meshing.

2.3.1 Turbulence modelling in indoor air flow simulations

Selection of the method to approximate turbulent processes in fluid flow is a very important part of CFD simulations, as turbulence is often dominant over all other flow phenomena (Sodja 2007). It significantly influences the mixing in any flow and its correct modelling increases the quality of the simulation. There are several approaches to deal with turbulence; they differ in complexity and accuracy (Zhai et al. 2007).

The most computationally demanding method is the direct numerical simulation (DNS), in which the Navier-Stokes equations are numerically solved for instantaneous quantities. The large eddy simulation (LES) method directly solves the large-scale turbulent motions and approximates the turbulent transport, which occurs in small-scale eddies. Both methods are generally very accurate, but it is cumbersome to use them in solving more complex cases, due to their high demand for computational power and memory.

Reynolds decomposition and averaging of Navier-Stokes equations (RANS method) is a very usual approach to deal with turbulence in engineering applications. Only mean flow quantities are solved directly and the effect of turbulent fluctuations is approximated on the basis of turbulence models. The accuracy of this method is lower than that of DNS or LES approaches, but the demand for computational resources is considerably reduced. The RANS method is usually sufficient in the CFD simulations for HVAC engineering applications, as we are interested mainly in the prediction of mean flow and there is most of the time no interest in very detailed and accurate solution of turbulent processes (Zhai et al. 2007).

A number of turbulence models have been developed for the RANS method. Commonly used models are summarized for instance by Zhai et al. (2007). In HVAC engineering, the most frequently used turbulence models are the two-equation models such as k-ε and k-ω. They are based on two transport equations, one for turbulence kinetic energy k and another one either for turbulence dissipation rate ε or for specific dissipation rate ω.

The standard k-ε model (in ANSYS Fluent referred to as *k-ε Standard*) was proposed by Launder and Spalding (1974) and it is suitable for flows at higher values of turbulent Reynolds numbers (Zhai et al. 2007). Turbulence model according to Yakhot and Orszag (1986) gives slightly better

results when simulating air flow in enclosed spaces (Zhai et al. 2007). In ANSYS Fluent this model is denoted as *k-ε RNG*. Turbulence model by Shih et al. (1995) is suitable for the environment with swirling flows, buoyancy flows and flows involving separation (Zhai et al. 2007). In ANSYS Fluent it is referred to as *k-ε Realizable*.

The model developed by Wilcox (1988) shows higher accuracy for turbulent flow near the wall with adverse pressure gradient. However, it is less robust in the areas of wakes and in the case of flow without effect of shear stress on the wall (Zhai et al. 2007). In ANSYS Fluent it is referred to as *k-ω Standard* turbulence model.

Although there is currently a wide variety of different turbulence models to choose from, there is not yet a single, practical turbulence model that can reliably predict all turbulent flows with sufficient accuracy (Zhai et al. 2007). It is always necessary to consider problem on hand and physical phenomena in the solved simulation. The turbulence model must be carefully chosen according to it.

2.3.2 Near wall region in CFD simulations

Flow prediction in the near wall region (so called boundary layer) is crucial to the accuracy of CFD simulations of wall bounded turbulent flows which are often present in engineering applications. The presence of the solid wall significantly affects the transport of momentum, mass and heat (Karimpour & Venayagamoorthy 2013). Incorrect modelling of near wall region of flow with the effect of heat transfer can result in incorrect wall temperatures and/or incorrect heat transfer rates.

The boundary layer consists of a viscous sublayer nearest to the wall, followed by a buffer layer, logarithmic region and extends to the fully turbulent region. See Fig. 2.7. Even though it usually occupies only a small part of the simulated space, it can account for the majority of the computing time. The reason for this high computational cost is that boundary layer flow properties change at a rate typically two or more orders of magnitude faster than elsewhere in the flow (Bäckar & Davidson 2017).

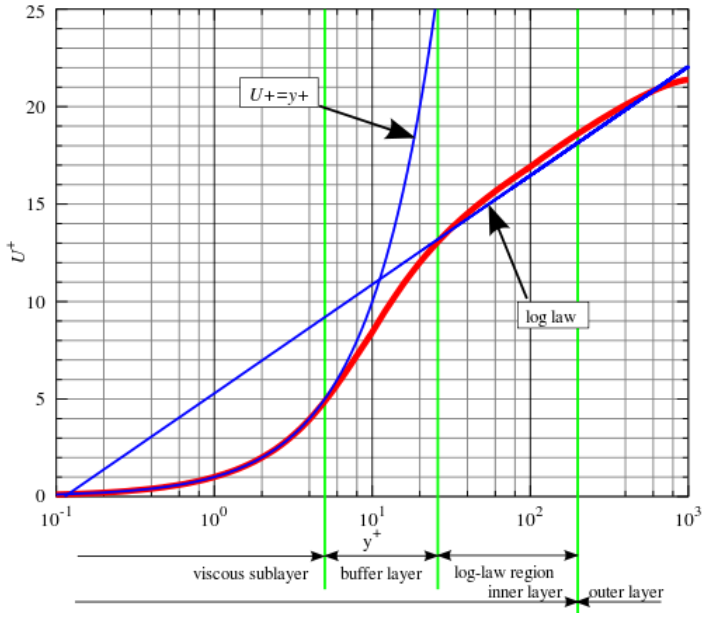

Fig. 2.7 – Boundary layer on a flat plate (Wikimedia, 2011)

There are two general approaches to solve high gradients in the boundary layer – integration of governing equations through the whole boundary layer and simulation without integration in the viscous sublayer and buffer layer, with the use of wall functions (Bäckar & Davidson 2017).

Integration of governing equations in the viscous sublayer

The first group of turbulence models that uses this strategy are the low-Reynolds-number (LRN) models. These models use the same set of equations for all parts of the flow and may be accurate for most types of flows (for example k-ω turbulence model). However, the resulting equation system can converge slowly, especially at high Reynolds number (HRN).

To mitigate the slow convergence of the LRN models, the boundary layer and the fully turbulent region can be decoupled, thus acknowledging the different computational requirements for the two regions. The second group of turbulence models uses a hybrid HRN and LRN modelling, where the boundary layer is resolved but with a slightly simplified set of partial differential equations compared to what is used in the rest of the domain (i.e. for example k-ε turbulence models).

The high gradients near the wall require a very fine computational mesh in order to be resolved accurately in both above mentioned cases. It is important to achieve value of dimensionless wall distance y^+ in the order of 10^{-1} to 10^0 for the first cell. Moreover, it is advised to have at least ten cells (but preferably twenty cells) within the viscosity-affected near-wall region (ANSYS 2013), i.e. covering the viscous sublayer and buffer layer. This can lead to enormous number of computational cells.

According to Wilcox (2006) the simulation results are more accurate in the case of even finer mesh covering the near wall region. He advises to achieve dimensionless wall distance $y^+ < 1$ for the first cell by the surface, while there are at least 7 to 10 cells with $y^+ \leq 2.5$.

Dimensionless wall distance y^+ is defined as:

$$y^+ = \frac{u_\tau \cdot y}{\nu} \tag{2.8}$$

where $u_\tau = \sqrt{\frac{\tau_w}{\rho}}$ is friction velocity (2.9)

$\nu = \frac{\mu}{\rho}$ is kinematic viscosity (2.10)

After rearrangement, we get the distance of the cell centre from the wall:

$$y = \frac{y^+ \cdot \mu}{\sqrt{\rho \cdot \tau_w}} \tag{2.11}$$

Near-wall region treatment using wall functions

Sufficient near-wall resolution is often prohibitive for HRN flows with complex geometries, due to high memory and processing requirements. A common approach in these cases is to use wall functions to bridge the region from the first grid node to the wall. In this case, the boundary layer and the fully turbulent region is decoupled and the HRN model is used together with a wall function. A coarse mesh is used where the first cell layer covers the inner boundary layer (i.e. viscous sublayer and buffer layer), including the inner part of the logarithmic region. Instead of solving partial differential equations on a fine mesh, an analytical expression is used to model the flow in this part of the boundary layer.

When applying wall functions, the dimensionless distance of the first cell centre should be in the order of 10^1 to 10^2, so it reaches to the inner part of the logarithmic region of the boundary layer. This results in much lower number of computational cells compared to the near-wall region

treatment by integration of governing equations in the viscous sublayer. However, the method of wall functions can negatively affect the accuracy of convective flows around the heat source, especially when the flow conditions are too different from the ideal conditions underlying the wall functions (Bradshaw & Huang 1995; ANSYS 2013).

2.4 Models of indoor heat sources for CFD simulations

There are various methods for modelling and simulation of indoor heat sources. The most straightforward is a detailed modelling, which captures all geometrical and physical details of the real objects. For example, Sørensen and Voigt (2003) used laser scanning technique to create identical geometry of a seated thermal manikin.

However, detailed modelling is usually difficult when it comes to design process of the model, but also to computation itself. Most of the heat sources are relatively small compared to the room size, with fine geometrical details requiring small cells of the surrounding numerical mesh to capture them. Moreover, there are big differences in properties of flow around the heat source and in the surrounding environment (differences in turbulent quantities, velocity magnitudes, velocity gradients, etc.). It can result in high number of control volumes in the domain and consequently slow calculation of the simulation. This may be addressed by simplified modelling.

When approaching the model simplification, we always have to take into consideration the question on hand and anticipate the possible influence of the simplification on the result of simulation (Nielsen et al. 2007). The method of simplification must be therefore carefully chosen. The common ways of simplification are:

- simplification of the shape and geometrical details;
- simplification of boundary conditions;
- simplification of operational characteristics.

2.4.1 Simplification of the shape and geometrical details

Geometrical shape of a heat source can be very complex, although in some cases (such as for example occupants) it may not have a significant influence on the results of simulation (Zukowska et al. 2007). Proper simplification can make the design of the model easier and can lower the computational burden of CFD simulations. However, substantial geometrical simplification is not always appropriate and the solved problem has to be considered specifically.

Geometrical simplification of thermal manikins (models of occupants) was extensively investigated by Zukowska et al. (2007). The authors carried out several experiments and CFD simulations to evaluate the influence of geometrical simplification on the character of the formed thermal plume. They compared four different models of occupant, see Fig. 2.8.

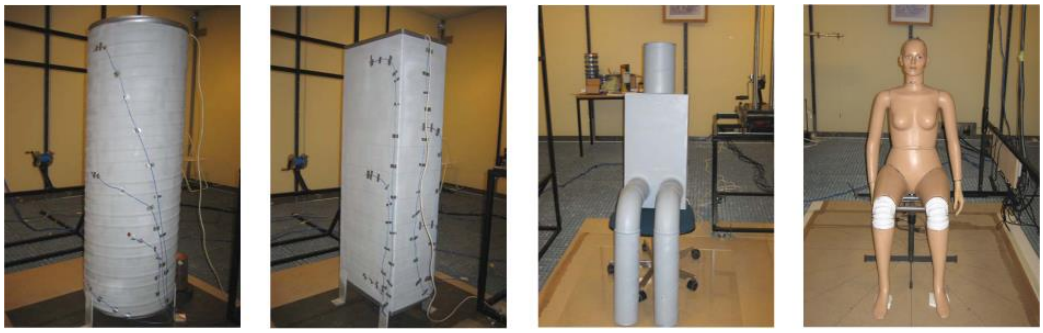

Fig. 2.8 – Different models of occupants (Zukowska et al. 2007)

They found that thermal plumes above models with significantly simplified geometry (cylinder, cuboid) did not correspond to the plumes above models with geometry close to the real human body shape (simplified thermal manikin and dummy). They were narrower and weaker (volume flow was by up to 40 % lower) and they did not provide necessary mixing with surrounding air. On the other hand, thermal plumes above thermal manikin and dummy corresponded sufficiently to each other. They were wider, asymmetric, with more significant mixing. An asymmetry was caused by thermal plumes rising above the legs of the manikins. The reason of intensive mixing was turbulence caused by more complex geometrical shape of the models. As the parameters of thermal plumes above both manikins (detailed and simplified) were very similar, certain simplification of the shape is possible, which was concluded also by Borges et al. (2007)

The authors also investigated the influence of thermal plumes above simplified models of occupants on the overall flow pattern in a room ventilated by displacement ventilation (Zukowska et al. 2008). They pointed out that weaker and narrower thermal plume above significantly simplified model (cylinder) leads to a distorted flow pattern and also inaccurate contaminant stratification in the room. The contaminants are more concentrated below the ceiling of the room and the quality of inhaled air is better than in reality. More complex geometry of both thermal manikins leads to more significant mixing of indoor air and to a different contaminant distribution in the room.

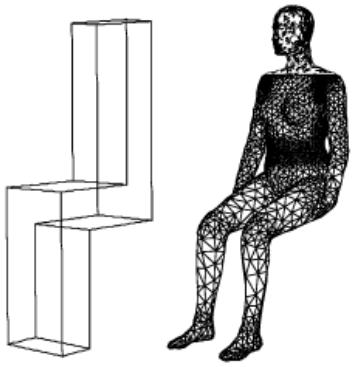

Fig. 2.9 – Different models of occupants (Topp 2002)

The influence of heat sources on the contaminant distribution was investigated by Topp (2002). The author compared two computational models with different levels of simplification, see Fig. 2.9. The models were placed in an enclosure according to the scheme in Fig. 2.10. For this arrangement, the simplification influenced especially the contaminant concentration in the close vicinity of the model surface. The concentration around the model with real geometry was higher, as the convective flow around the legs drew the contaminated air above the floor.

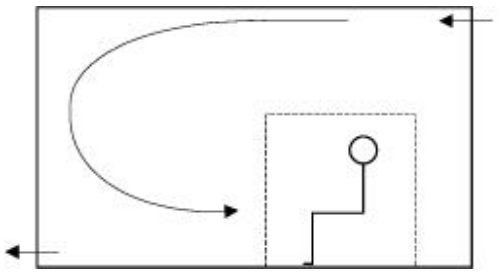

Fig. 2.10 – Scheme of the model (Topp 2002)

When simplifying models of occupants, one has to consider very carefully the influence of their geometry on the surrounding air flow. This has been investigated in several studies (Zukowska et al. 2008; Zukowska et al. 2007; Topp 2002; Murakami et al. 2000; Yan et al. 2009). Most of the authors conclude that significant simplification of the geometry does influence the overall air flow and contaminant distribution in the room (Zukowska et al. 2008; Topp 2002; Murakami et al. 2000). One can simplify the computational model just to a certain level, as shown by Zukowska. However, as much details as possible should be kept when solving air flow around a human body (Topp 2002). This applies especially if one deals with air flow and contaminants distribution in the facial area, where details such as nose or ears have significant influence (Sørensen & Voigt 2003).

Models of occupants in CFD simulations usually do not reflect surface properties, clothing or its porosity, hair, cover of the head etc. This simplification may lead to convective flows with higher velocities than in reality, because flow in the simulated boundary layer changes from laminar to turbulent at higher locations (Zukowska et al. 2010b).

Regarding the models of equipment as heat sources, the situation is more straightforward. The geometry is usually not as complex as in the case of occupants and the properties of surface are less complicated. Critical for modelling of this type of heat sources is usually correct determination of boundary conditions.

2.4.2 Simplification of boundary conditions

When designing the computational model, it is very often not possible to exactly prescribe the boundary conditions of real heat sources. In reality, the properties of the boundary surfaces may not be homogenous, the surface temperature may not be constant etc. It is necessary to idealize these characteristics. The temperature conditions at the surface of the model are then represented by boundary condition of the first or second type. However, simulation of boundary flow in the vicinity of a heat source can be very computationally demanding.

Specification of boundary conditions is very often more important than geometrical details of the model. Especially correct prescription of body temperature, heat output and convection-to-radiation ratio of heat transfer (Yan et al. 2009) is critical for the case of models of occupants. The correct setting of heat output and distribution of the temperature on the surface is very important, especially for models of strong heat sources.

2.4.3 Simplification of operational characteristics

Operational characteristics of heat sources can be for example mechanical functions, variation of geometry, variation of heat source placement etc. These characteristics are simplified very often.

CFD simulations usually neglect the movements of occupants. It was previously demonstrated that small localized movements (movements of hands and fingers on keyboard or on table, movements of head, etc.) influence neither the formed thermal plumes nor the overall flow pattern in the premise (Rim & Novoselac 2009). However, the neglect of occupants' movement around the room can have significant influence on the results of the simulation.

It was demonstrated by Hyldgaard (1998) that respiration processes do not influence the rising thermal plume. It was also shown that they neither influence the overall flow pattern in the surrounding environment (Gao & Niu 2006). In the most cases of CFD simulations these processes are neglected, but they must be considered when simulating the air flow and contaminants distribution in the human breathing zone or, for example, if the quality of inhaled air is studied (Gao & Niu 2006).

The above listed basic methods of simplification are not effective in all situations. It can be problematic to simulate, for example, the environment with high number of heat sources. In this case, even when the models of heat sources are geometrically simplified, with idealized boundary conditions on their surface, the method of fine boundary layer mesh for heat transfer calculation can lead to enormous number of computational cells. On the other hand, the method of wall functions can negatively affect the accuracy of convective currents around the heat sources, especially when the flow conditions are too different from the conditions underlying the wall functions (ANSYS 2013). Therefore, it may not be appropriate for complex model geometries and for complex indoor environments.

2.4.4 Meshing of CFD models with heat sources

In general, the three most important issues for correct meshing of models for CFD simulations with heat sources are:

- appropriate dimension of numerical cells in the domain;
- reasonable transition from small cells surrounding fine geometric details to large cells filling the rest of the meshed volume;
- correct meshing of boundary layer regions near the heated surfaces (i.e. height of the first mesh cells, growth rate, number of layers and related total height of the fine boundary layer mesh).

These issues are discussed in detail on examples of CFD simulations with models of occupants.

Voigt (2001) created a detailed model of thermal manikin, using a laser imaging method. Its surface was meshed by 500,000 triangular cells. The dimension of the individual cells was from 3 to 10 mm. Voigt together with Sørensen (2003) subsequently created set of models of the same thermal manikin, in three levels of surface mesh density:

- coarse: 125,000 surface cells;
- medium: 250,000 surface cells;
- fine: 500,000 surface cells.

However, even the most coarse resolution (i.e. 125,000 cells) was found to be too detailed for practical use of the model in CFD simulations. The surface mesh of the manikin was therefore considerably simplified, which resulted in 23,000 numerical cells on the surface of the model. Finer mesh was kept in more geometrically complex areas, such as face, nose or fingers. The height of the first cell of the fine boundary layer mesh near the manikin was 0.2 mm and the authors created in total 20 layers of prismatic cells, with growth factor 1.13. The fine boundary layer mesh near the face of the numerical model is displayed in Fig. 2.11.

Fig. 2.11 – Numerical mesh near the face (Sørensen & Voigt 2003)

Zukowska et al. (2010b) created a simplified model of person composed from blocks. Surrounding volume was meshed by hexagonal mesh with global cell size 80 x 80 x 80 mm. The area around the model of occupant was meshed by smaller cells with the edge dimension of 20 mm, which was followed by area of cells with edges 40 mm. The total number of cells in the domain was 303,870.

Fig. 2.12 and Fig. 2.13 show numerical mesh with a model of occupant according to Deevy et al. (2008). The edge length of the triangular cells can be estimated on the basis of a simple manual measurement as 20 mm at the geometrically very complex areas of the manikin, and 40 mm at the rest of the body. In the remaining space, the dimension of cells is approximately 80 mm.

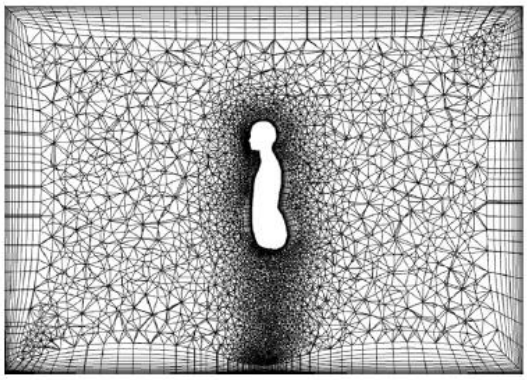

Fig. 2.12 –Volume mesh of experimental chamber (Deevy et al. 2008)

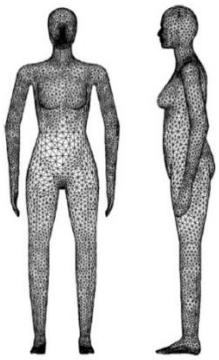

Fig. 2.13 – Surface mesh of thermal manikin (Deevy et al. 2008)

Gao and Niu (2006) created a numerical model of two occupants placed in an experimental chamber with the dimensions 2.6 x 2.2 m and the height of 2.7 m. They divided the chamber into approximately 2,525,000 control volumes. According to the authors, the fine boundary layer mesh surrounding the models of occupants should have at least 10 layers with the height of the first cell 0.2 mm.

Srebric et al. (2008) simulated an experimental chamber with the dimensions 5.16 x 3.65 x 2.16 m. They discretised the model into 180,000 computational cells. Consequently, they have refined the mesh (resulting in total number of cells 655,000) and performed grid-independence study. They have proved that the 180,000 cells were sufficient to achieve grid independent results.

2.5 Modelling of air supply diffusers as an inspiration for the new modelling method to represent heat sources

Appropriate description of the forced flow from air supply diffusers in CFD simulations is important for reaching reliable and trustful results (Srebric & Chen 2002; Nielsen et al. 2007). Similarly to heat sources, most of the diffusers are small compared to the size of the common rooms and they have complex geometry with a lot of details influencing the flow. There are also

considerable differences of velocities inside the diffuser and in the room, which makes their joined simulation challenging.

The requirements for precise simulation of the flow in the diffuser are significantly different and often incompatible with the requirements for simulation of overall flow in the room. This has been previously addressed by several methods of simplification describing how to more or less sufficiently deal with issues such as big differences in velocities or length scales in the CFD simulations (Srebric & Chen 2002). These methods also lower computational burden of simulation when compared to detailed modelling of air supply diffusers.

Available methods of air supply diffusers modelling can be generally classified into six categories (Zhang et al. 2009):

- **Direct description**
  Direct description of air supply diffusers without using any approximation is problematic, as mentioned above. Huge difference of length and velocity scales may even impose difficulties in convergence of computations (Fontaine et al. 2005).
- **Simplified geometry**
  It is the basic method of air supply diffusers simplification. It is based on approximating of real diffuser to simplified alternative with the same effective area. Great number of air flow simulations has been based on this method of simplification (Srebric & Chen 2002). This method offers great simplicity, but the result accuracy is not assured, which has been identified by many researchers as a significant limiting factor.
- **Momentum method**
  The diffuser is modelled as an opening with the same gross area, mass flow and momentum flux as the real diffuser (Srebric & Chen 2002).
- **Prescribed velocity method**
  The diffuser is modelled as an opening with the same gross area and mass flow as the real diffuser. The inlet velocity is prescribed higher than in the real case, which compensates the momentum loss.
- **Box method**
  It determines flow and thermal conditions in certain distance from the diffuser. The quantities of the flow are determined in advance by a measurement and defined in a simulation as a boundary condition at an imaginary box surrounding the diffuser, see Fig. 2.14.

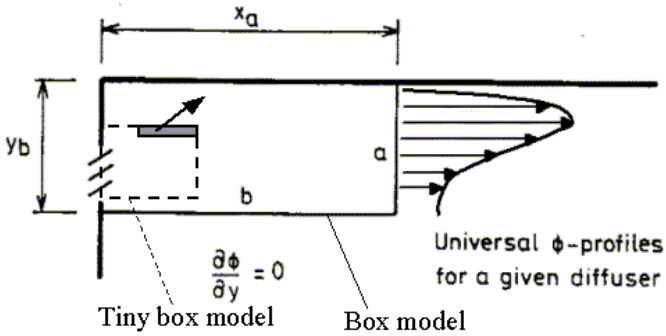

Fig. 2.14 – Box method of air supply diffusers modelling (Srebric & Chen 2002)

The flow field inside the box is ignored and thus the diffuser itself does not have to be modelled. However, the determination of the box dimensions is not a trivial task. The boundary condition inducing the flow should be set in the fully developed region of the jet, but on the other hand, the box should be as small as possible to minimize its impact on the surrounding environment, such as impact on the room air recirculation, thermal plumes etc. (Nielsen 1997).

- **Method of random blocking of CFD cells**
  The method proposed by Zhang et al. (2009) assigns real velocities to random cells on the surface of the diffuser, while the remaining cells are blocked for the flow, see Fig. 2.15. The total area of the diffuser is same as in the real case and blocking of the random cells may assure that the effective area ratio of the diffuser is correct.

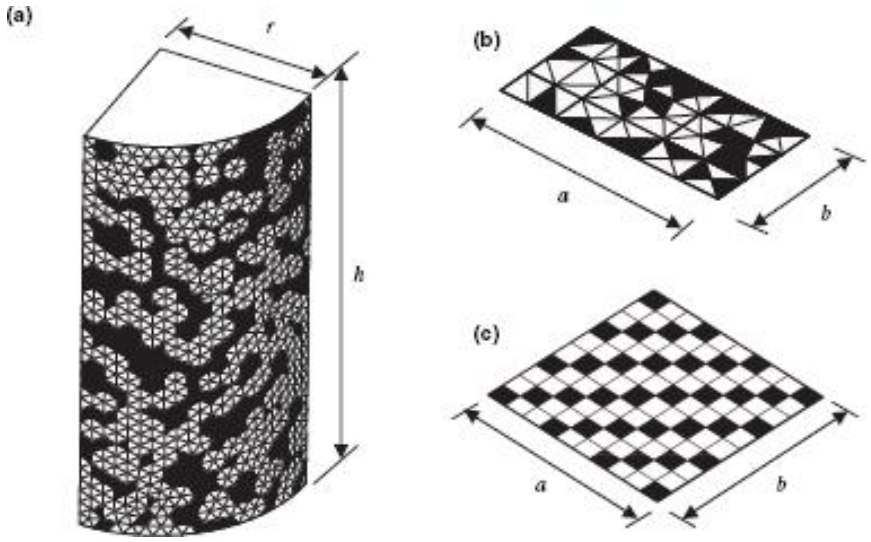

Fig. 2.15 – Method of random blocking of CFD cells (Zhang et al. 2009)

2.6 Validation in CFD simulations

Every new method of modelling should be thoroughly tested and validated to uncover any possible drawbacks of the method. There are three basic ways to do it: using analytical methods, comparison with experiments or comparative testing (i.e. comparison of several simulations) (Hensen, 2012). The best way is to combine more of them, as each has its strengths, but also limitations.

Validation using analytical methods is very limited as it is based on comparison with cases for which analytical solutions can be obtained. These cases are usually very simple and in the case of heat sources, they often isolate only one heat transfer mechanism.

Comparison with experiments (empirical validation) is a very rigorous test of performance. However, it can be expensive and time consuming to measure data set for validation in a good quality. Moreover, some of the complex physical processes cannot be tested by this method as there are limitations of measurement techniques.

Comparative testing (inter-model comparison) is very effective way of validation. The results of several simulations (possibly done in several computational programs) are mutually compared and evaluated. However, it does not provide absolute measure of the method accuracy.

2.7 Experimental studies of thermal plumes

There are various different approaches to investigation of thermal plumes generated by heat sources. It is possible to measure velocity and temperature solely along the vertical axis of the plume and their decay with increasing height above the heat source, assess profiles of velocity and temperature at various horizontal axes or planes intersecting the plume, or to monitor the whole temperature and velocity fields around the heat source. Consequently, several experimental techniques can be used.

In general, the most basic way is to measure the temperature and velocity of the air flow at a given point in space at a given time. Although it sounds simple, it is not always easy to perform the measurement. Particularly for slow air flow (e.g. thermal plumes), the airstream can be affected by the measuring device. This effect is magnified when multiple points are measured close to each other. This leads to the second difficulty, which is measuring enough points to define the air flow patterns around a heat source or velocity and temperature profiles of a thermal plume. Various frames and traversing mechanisms with attached measuring devices can be used for this. Nevertheless, traditional techniques are nowadays complemented by various non-intrusive techniques that can measure flow quantities without affecting it, as described below in more detail.

2.7.1 Temperature measurement

Air temperature is relatively easy to measure, however the investigator must be aware that it is subject to considerable variation through space and time. A device that senses temperature traditionally consists of some confined substance, whose volume (or other measurable physical property) changes with a change in temperature. Modern thermometers may be based on the change in electrical properties of the transducing device. A variety of sensors are available for measuring air temperature, including mercury-in-glass thermometers, bimetallic thermometers, pressure thermometers, thermocouples, resistance temperature detectors, infrared thermometers, thermistors and monolithic (ICTT) temperature sensors. Detailed information can be found in literature, for example in the publication of Matuška (2005).

Mainly copper-constantan thermocouples have been previously used for the measurement of temperature around heat sources, as mentioned for example by Mierzwinski (1980), Zukowska (2011) and Borges et al. (2007).

Another method was used by Jančík and Bašta (2011), who measured convective flow above an electric convector. They used thermal imaging to visualize the rising thermal plume on a sheet of carton paper, which was stretched above the convector. The temperature field above the convector was recorded by a thermovision camera.

2.7.2 Velocity measurement – mechanical and thermal anemometry

The most straightforward methods to measure velocity of air are based on mechanical principles. There are two types of probes for mechanical anemometry: cup anemometers, which are used for high air flow velocities (such as outdoor wind measurements), and various types of vane anemometers, for low and high velocity measurements. The mechanical anemometers generally tend to be less accurate for measuring very low velocities and they are not widely used for measurement of air flow around heat sources. Among the reviewed literature, it was mentioned only in the work of Mierzwinski (1980). Therefore, this method is not discussed in detail . More information can be found in the literature (Matuška 2005).

An alternative to the mechanical anemometry is thermal anemometry. In this case, the probes measure air flow velocity by sensing changes in heat transfer from a small, electrically-heated element exposed to the fluid. A key feature of the thermal anemometer is its ability to measure very rapid changes in velocity. This is accomplished by coupling a very fine sensing element with a fast feedback circuit which compensates for the drop in the natural sensor response. Time response to flow fluctuations as short as a few microseconds can be achieved.

There are three possible ways of the thermal anemometry: constant temperature anemometers, constant current anemometers and constant voltage anemometers. In all the arrangements, the cooling effect caused by the fluid passing the element is balanced by the circuit, so the probe is

held with a constant specific variable (temperature, current or voltage), when the change in the other variable is monitored. For the constant temperature and constant current anemometers it is voltage output, for the constant voltage anemometers it is change in the electric current through the circuit.

Thermal anemometry has been widely used to measure velocities of air flow around heat sources. For example by Zukowska (2011), who investigated thermal plumes above several objects simulating occupants, by Borges et al. (2007), who measured velocity profiles at several heights in the vertical plane crossing the shoulders of a sitting occupant, heated thermal manikin and above a heated cylinder or by Hyldgaard (1998), who measured air velocity above a thermal manikin.

2.7.3 Non-intrusive techniques

Temperature and velocity of air flow around heat sources can be measured by several non-intrusive techniques, which do not affect the air stream. One of them is a Laser Doppler Anemometry (LDA), using the Doppler shift in a laser beam to measure the velocity in transparent or semi-transparent fluid flows. It accurately measures low velocity and direction, but it is expensive and difficult to set up on a full size room. This technique was used for example by Hyldgaard (1998).

An alternative to the Laser Doppler Anemometry is Particle Image Velocimetry (PIV), an optical method of flow visualization. The fluid is seeded with tracer particles and illuminated, so that the particles become visible and it is possible to monitor them. It is necessary to use sufficiently small particles, so they follow the flow dynamics, yet large enough to scatter light sufficiently so it can be captured by a photo detector. In air flow velocity measurements the particles are typically oil drops with size in the range of 1 μm to 5 μm (Mao 2005). The PIV can capture the velocity and direction information in many points over a plane of fluid almost instantaneously, which can be useful for validation of CFD simulations.

Another a non-intrusive technique is an acoustic anemometry (Mao 2005). The air flow velocity is in this case derived on the basis of difference of the measured sound speed from the sound speed in still air of the same properties (namely temperature, pressure, humidity and CO_2 concentration).

2.7.4 Published experimental data

Several experiments evaluating convective thermal plumes above heat sources were found in the literature. Most of them were focused on thermal plumes above occupants or their simulators (thermal manikins, simplified objects).

Mierzwinsky (1980) measured parameters of thermal plumes above a sitting and standing person. The results of his work are very detailed regarding the experimental data of thermal plume quantities. However, it would be very complicated to use them for any validation as the conditions in the experimental premise were very unstable (air temperatures varied within the range of 18 to 25 °C). Moreover, the measurement was performed above a real person, so the change of heat output and activity level of the object could have influenced the measurements.

Hyldgaard (1998) performed several experiments with a sitting and standing breathing thermal manikin with different heat outputs (90, 115 and 130 W). He measured air velocity profiles in several heights above the manikin head. However, he did not report exact temperatures in the experimental chamber. He only stated that the surroundings were almost isothermal and the chamber was not ventilated.

Borges et al. (2007) performed measurement above a seated person, thermal manikin and a cylindrical dummy. He measured velocity and temperature profiles at 7 heights in the vertical plane intersecting the shoulders of the occupant (and occupant simulators). He specified that temperature in the experimental chamber was 18 to 19 °C. It was concluded that the temperature was probably closer to 18 °C. The results of the experiment could be used to compare results of CFD simulations with real heat sources. The results of the experiment with a cylindrical dummy could be also used for validation of CFD models.

Very extensive research aimed at thermal plumes above occupants was elaborated by Zukowska et al. (2007; 2008; 2010a; 2010b; 2011; 2012a; 2012b). The authors investigated impact of thermal manikin geometry and influence of various factors, such as clothing, breathing or furniture arrangements on the parameters of thermal plumes. They also dealt with plume axis wandering. They published contour maps of velocity and temperature in different heights above the heat source from several experiments with different geometries of occupant simulators, different arrangements of the experimental chamber and different conditions. The authors give very good guidelines on the factors influencing convective flow above occupants.

2.8 Indoor environment quality assessment in real world scenarios

The indoor environment is a system with complex interactions of various factors, such as thermal, visual and acoustic conditions, indoor air movement, air quality, etc. Consequently, the overall indoor environment quality is a complex integration of a large number of physical attributes. When evaluating and comparing different experimental or numerical data in real word scenarios, it is important to do it in an understandable and systematic way, in order to target the issues in question and to be able to efficiently communicate the outcomes. This can be achieved by the use of appropriate performance indicators (PIs).

PIs can be also very useful for the usability testing of the new modelling methods. When evaluating results of complex simulations, we are usually not interested in every detail of the indoor environment. Performance indicators help to evaluate the results considering the problem on hand and neglecting insignificant negative effects of the simplification. Thus, it can be decided if the simplification is suitable for a particular problem or not.

Multiple performance indicators have been developed and used in the past as a useful instrument for simplification and quantification of the indoor environment performance and for the communication between researchers and designers. Framework with a set of key PIs for the indoor environment has been proposed by Loomans et al. (2011) within the European Coordination Action PERFECTION (Performance Indicators for Health, Comfort and Safety of the Indoor Environment). The standard indicators were listed in more detail by Steskens and Loomans (2010; 2010). The most widely used PIs related to thermal comfort and sensation are:

- PMV – predicted mean vote;
- PPD – predicted percentage of dissatisfied;
- PD – percentage of dissatisfied;
- ET – effective temperature;
- SET – standard effective temperature;
- operative temperature;
- draught rate;
- vertical air temperature difference;
- radiant asymmetry.

Next to the standard performance indicators, it is also possible to find in the literature various PIs related to particular, more specialized problems or design questions. Some of them are related to simulations with simplified heat sources. For example Djunaedy et al. (2003) or Xing et al. (2001) mentioned:

- whole body thermal comfort;
- local discomfort;
- turbulence intensity;
- mean age of air;
- air exchange rate;
- ventilation efficiency;
- contaminant distribution.

Méndez et al. (2008) analysed ventilation air flow patterns in a two-bedded hospital room with several alternative configurations of the furniture and different positioning of curtains and internal partitioning walls. They used air change per hour (ACH) as the basic performance indicator and the air exchange efficiency (ratio between the minimum and the mean replacement time of the air) as an integral performance indicator. However, they also concluded that it is not sufficient for a more detailed evaluation (to find for example hyperventilated or under-ventilated zones) for which the detailed air flow patterns should be used. One of the PIs to assess the air flow patterns is for example the mean age of air.

Loomans et al. (2008) dealt with operation theatre ventilation both with the use of CFD simulations and experiments. The authors evaluated contaminant concentration at chosen places as a performance indicator (as it directly affects possibility of surgical site infection rate). They briefly mentioned several other PIs that can be used for assessment of indoor environment quality in the operation theatres (such as thermal comfort, hypothermia, etc.). Similar indicators were used also by Zoon et al. (2011).

One of the most important issues when using performance indicators is to decide which of them are relevant for a particular case. It is possible to use standard performance indicators or to propose new ones appropriate for the application in question. Considering the indoor heat sources modelling simplification, it is possible to measure directly the velocity of air flow around and above the heat source. However, more overall indicators, such as temperature gradient, draught or turbulence intensity should be used as well. When testing the method on case studies, indicators such as air exchange rate, ventilation efficiency, contaminant removal efficiency or comfort parameters could be used.

3 RESEARCH GOAL – NEW MODELLING METHOD TO REPRESENT HEAT SOURCES

The main goal of the presented research was to develop a new modelling method to represent heat sources in numerical models of indoor environment in order to enhance the use of CFD simulation in practice. It is targeting especially assessment of proper air distribution in large indoor spaces with a large number of heat sources and/or variable occupancy patterns (such as atriums, large meeting rooms, lecture halls, theatres, cinemas and other entertainment facilities, etc.). The method reflects the issues which are not addressed by the basic ways of simplification currently used for numerical modelling of indoor heat sources, as discussed in the previous chapter.

Nowadays, it is difficult to simulate large spaces with large number of heat sources in a reasonable time, not mentioning limited possibility of more complex case studies. The developed method is targeting simulations of air flow in the space, evaluation of temperature conditions and ventilation efficiency in an indoor environment. It should reduce computational demands of CFD simulations with heat sources and ensure high reliability of the obtained results.

As the issue of heat sources modelling is similar to modelling of air supply diffusers, the development of the new method was inspired by the currently used methods to model air supply diffusers for CFD simulations, particularly box method proposed by Nielsen (1997), see Chapter 2.5. The flow and thermal conditions in a jet are defined in a certain distance from the diffuser. They are determined in advance by measurement at an imaginary boundary box surrounding the diffuser. The diffuser itself does not have to be modelled, as the flow field inside the imaginary box is ignored. This method was found to be the most relevant for the current development of simplified modelling of heat sources.

Similarly to the jet streams from the air supply diffusers, the flow and thermal conditions of the thermal plume rising above a heat source can be defined by previously determined boundary condition set at a certain distance above the heat source. Thus, the geometry of the heat source can be simplified and there is no need to create a fine mesh in the region around the heat source, which is otherwise necessary for correct heat transfer calculation, as discussed in Chapter 2.3.2. This results in an easier preparation of numerical models and significantly easier meshing. Additionally, the absence of the fine mesh near the surface of the heat source allows the whole computational domain to be meshed by a coarser mesh, which would otherwise be affected by small cells (as it is necessary to keep certain homogeneity of cell dimensions in a computational mesh in the domain). Fewer computational cells in the modelled domain results in a faster CFD simulation

Following the literature review, the RANS approach was chosen as the most suitable one for modelling turbulence in all the performed simulations. However, it was not clear from the literature which of the currently available RANS-based turbulence models is the most appropriate for the related types of applications (cases with prevailing effect of natural convection on the air flow). This issue had to be studied additionally. Also, the issue of the correct meshing of the near wall region had to be addressed, as it was important for some of the simulations.

Several physical phenomena mentioned in the previous chapter have an important effect on the air flow around heat sources and spreading of thermal plumes above them. These are especially the entrainment of the surrounding air into the thermal plume and effect of the ambient air temperature on the plume development, but also the interaction of multiple thermal plumes rising close to each other and the interaction of individual thermal plumes with the surrounding

environment (walls, ceiling etc.). All of the listed issues had to be considered during development of the proposed method and addressed by several additional test studies.

The main challenges of the research, following the proposition of the new modelling method to represent heat sources in the CFD simulations of air flow indoors, were summarized into the following tasks:

- to assess sensitivity of computations on the selection of turbulence model and propose an optimal model of turbulence for cases with prevailing effect of natural convection on the air flow;
- to assess physical correctness of the simulated results when using simplified model of heat source;
- to assess the optimal distance of the defined flow and thermal boundary condition from the heat source;
- to assess sensitivity of the method on the temperature of the ambient air;
- to assess usability of the method for CFD simulation with multiple heat sources (i.e. especially influence of the simplification on the merging of multiple thermal plumes);
- to summarize assets and drawbacks of the proposed method;
- to sum up limitations of the proposed method, considering its possible applications for real world scenarios;
- to provide guideline for the future use of the developed method.

4 RESEARCH MATERIALS, TOOLS AND METHODS

The main part of the research was based on CFD simulations solved in a commercial software ANSYS Fluent. The geometries of numerical models were created either in the pre-processors Gambit or ANSYS Design Modeller. Hexagonal or tetrahedral numerical meshes were generated in the pre-processors T-Grid or ANSYS Meshing, respectively. For more details see Chapter 4.1.

Development steps towards the proposition of the new modelling method to represent heat sources are described in Chapter 4.2. The validation of the results was accomplished by a combination of their comparative numerical testing, comparison with the experimental results found in the literature and comparison with the results of measurements in an experimental chamber. The executed experiment was based on thermo-graphic measurements of the thermal plume temperature field by a thermal imaging camera. The applicability of the developed method to represent heat sources in CFD simulations was tested in a case study.

4.1 CFD Simulations

4.1.1 Software

The geometry of the numerical models was created in the pre-processors Gambit or ANSYS Design Modeller, using the most recent tool. The hexagonal numerical meshes were created in the pre-processor T-Grid, using the most recent version (13.0 for the first models, 16.0 for the models testing the thermal plumes merging). The tetrahedral meshes were created in the pre-processor ANSYS Meshing 15.0. CFD simulations were solved in the software ANSYS Fluent, using the most recent version (6.3, 16.0 or 17.0).

The numerical solution of governing equations in the ANSYS Fluent software is based on the finite volume method (Patankar 1980). All simulations were solved as non-isothermal flow of incompressible air with the influence of thermal expansion. Heat radiation was simulated using the surface-to-surface (*S2S*) model (ANSYS 2013). The *Body Force Weighted* scheme was chosen for the discretisation of the pressure equation as it is recommended for solving buoyancy driven flows (ANSYS 2013). The convective terms in transport equations were solved using a second order upwind discretisation scheme. A segregated solver was used to solve the governing equations and the *SIMPLE* algorithm was applied to couple the pressure and velocity fields (unless specified otherwise in the text). The flow was considered as unsteady (unless mentioned otherwise in the text). All calculations were done in double precision, as it has been previously found that simulations of indoor air flow converge better in the double precision mode (Barták 2007).

4.1.2 Convergence of the simulations

The convergence was monitored by observing the residual values for each equation being solved and their development during the simulation. Ideally, the residuals will go to zero as the solution converges. But in an actual computation, the residuals decay to some small value and then stop changing. ANSYS Fluent uses globally scaled residuals to monitor the convergence of all the equations. It is a sum of the absolute values of the residuals in all control volumes divided by a parameter characterized by the total flow of the related variable through the computational domain at the iteration on hand. Only the residuals of the continuity equation are scaled by the largest sum of absolute value of the residuals of continuity equation obtained during the first five iterations. For detailed description of the residual calculation, see ANSYS Fluent User's Guide (ANSYS 2013). It is important that the globally scaled residuals can reflect small local instabilities anywhere in the computational domain caused by, for example, inappropriate

computational mesh or boundary condition. Thus, it can detect the faults of the computational case. However, it is always beneficial to use also other additional indicators of convergence, such us balance of flows across domain boundaries.

A residual with the highest value R_{max} was used as the main convergence criteria. In all the cases it was either the value of the continuity equation residual or one of the momentum equation residuals of the velocity components. In few stationary cases, the simulation was considered converged when $R_{max} < 10^{-3}$; in the non-stationary cases when $R_{max} < 10^{-4}$ at the end of each time-step. Moreover, development of all the residuals during the simulation was monitored as well. In the stationary cases, the residuals were required to decrease from the beginning of the calculation until levelling out or eventually slightly oscillating around the mean level, which was constant. Development of the residual value during one time step was monitored in the non-stationary cases. It was required that the residual decreased under the above-mentioned value during maximum 10 iterations.

In addition to monitoring the residuals, two more indicators of convergence were used, which were the balance of mass flow and the balance of heat flow through the whole computational domain.

4.1.3 Turbulence modelling

Two-equation turbulence models were used to close the RANS and thermal energy equations. These models are the most frequently used for CFD simulations in the field of HVAC engineering, as they offer a good compromise between numerical demands and computational accuracy.

There is no universal two-equation model of turbulence suitable for all indoor air flow simulations (Zhai et al. 2007). Therefore, a combined numerical-experimental study was done to assess the performance of four most common two-equation k-ε and k-ω turbulence models for simulations of thermal plumes, in order to determine the most appropriate model of turbulence. Simulations performed with different turbulence models were compared mutually and with a measurement, because solely inter-model comparison cannot indicate which turbulence model gives results that are correct. Based on the study, the appropriate turbulence model was selected for further simulations.

4.1.4 Meshing of near-wall regions

The near-wall modelling significantly influences the fidelity of numerical solutions of turbulent flows with heat transfer by natural convection. There are large velocity and temperature gradients in the vicinity of heated walls which act as the main sources of vorticity and turbulence. Therefore, special attention should be paid to near-wall regions meshing, see Chapter 2.3.2. It is important to achieve a correct value of dimensionless wall distance y^+ for the first cell near the wall, which should be in the order of 10^1 to 10^2 when using wall functions and in the order of 10^{-1} to 10^0 in the case when the boundary layer is integrated to the wall. Moreover, when using the latter approach, it is necessary to ensure that there is sufficient number of computational cells in the viscous sublayer which extends to $y^+ = 5$.

Unfortunately, as the y^+ value depends on the local friction velocity, it is not possible to know y^+ prior to running the simulation. Therefore, the value of y^+ has to be estimated in order to calculate the height of the cells near the wall when creating the numerical mesh.

Integration of governing equations in the entire boundary layer was used in most of the performed CFD simulations. The emphasis was placed on the numerical mesh near the heated surface. In these regions, $y^+ \leq 2.5$ was required for at least first seven cells near the wall (Wilcox 2006), while

the $y^+ \leq 1$ was required for the first cell by the heated surface. The estimation of the y^+ value was based on the initial test simulation of a heat source with the same surface area and heat output as the detailed heat source, but with a simplified geometry, see Fig. 4.1.

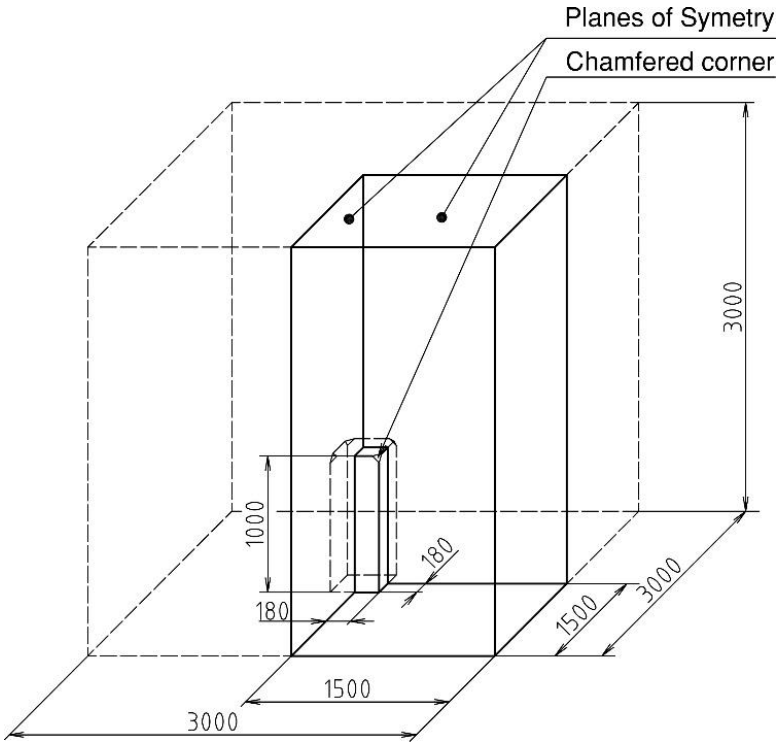

Fig. 4.1 – Geometry of the test model

Air flow was simulated in only one quadrant of the space in order to speed up the calculation. The remaining space was specified as symmetrical. The full lines depict the modelled geometry, the dashed lines full geometry behind the planes of symmetry. The corner of the object emitting heat was chamfered. The parameters of the simulation were set identical to the consequent simulations, as described in Chapter 4.1.1.

The density ρ of the warm air near the heated surfaces used for estimation of the y^+ value was determined from this initial test simulation – it was found as the lowest value of density in the simulated room (i.e. density of the warmest air rising near the heat source). The mean value of the shear stress τ_w on the heated surfaces was estimated on the basis of the initial simulation as well.

The required distance of the cell centre is defined by the formula (2.11), and it was calculated using the estimated values τ_w and ρ.

4.1.5 Evaluation of unsteady simulations

All unsteady simulations were evaluated in the same manner, reflecting the instability of the raising thermal plume and its eventual periodical oscillation, as discussed in Chapter 2.2.1. The simulations were initialized and run until the air-flow was developed. Additional ‘start-up’ period of at least 480 s was simulated and only after that the flow was considered as fully formed. Then the results were recorded for further 120 s of the simulated time, with a time step of 1 s. The values of temperature, velocity and turbulent quantities were recorded at measuring points at several heights above the heat source. For the distribution of the measuring points see Annex I. 120 data files were the outcome of each simulation. The final profiles of temperature, velocity and turbulent quantities were time-averaged over the period of 120 s.

4.2 Development steps towards proposition of the new modelling method

The proposition of the new modelling method to represent heat sources in CFD simulations of indoor air flow was done in two steps. First, a numerical simulation with detailed model of a sample heat source was conducted. The computational case was meshed by a fine mesh in order to ensure high quality of the simulation. The obtained results were empirically validated by comparison with experiment described in the following chapter. Some issues, as for example choice of an appropriate turbulence model for the simulations and the effect of the ambient air temperature on the thermal plume above the heat source were studied by comparison with the results from experimental measurement.

Following the initial studies, the new method to represent heat sources was proposed. It was taken into account that every new method of modelling should be thoroughly tested and validated to uncover any possible errors and examine the ways of its application. The validation of the developed modelling method to represent heat sources was based on comparative testing of numerical models with different levels of simplification. The reference case for the inter-model comparison was the simulation with the detailed model of the sample heat source, which was previously empirically validated by comparison with the experimental results.

Thermal manikin resembling a sitting occupant was selected as the sample heat source to test and validate the method, see Fig. 4.2. The geometry of the manikin was based on the previous prototype of the Centre for Indoor Environment and Energy at DTU in Lyngby, Denmark. Annex I provides a detailed technical drawing. The geometry of the manikin differed from the shape of a human body. Nevertheless, such simplified models of occupants are frequently used in indoor environmental studies. Previous experiments of Zukowska et al. (2010b) indicated that the simplification of thermal manikin geometry such as used by DTU in Lyngby (regarding the shape of human body) should not significantly affect the character of a thermal plume formed above the manikin and it can be considered as a suitable substitute to a detailed model of human body. An identical geometry of the heat source was used both for the numerical simulation and experimental measurement. Metal thermal manikin previously assembled by Koiš (2009) and tested by Zbořil (2008) was used for the experiments.

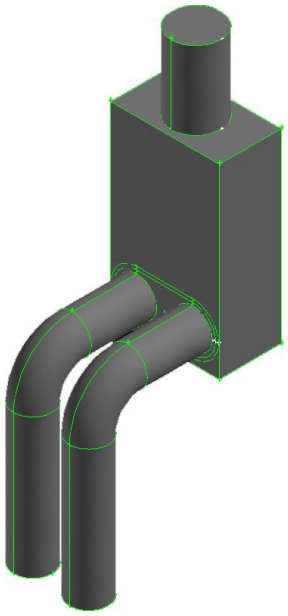

Fig. 4.2 – Thermal manikin

Following the empirical validation and comparative testing, the method was also applied in a case study using selected performance indicators in order to demonstrate its usability for practical applications.

4.2.1 Empirical validation

To ensure physical correctness, the simulation results for the thermal plume above detailed model of heat source (thermal manikin) were initially compared to experimental data found in literature (Hyldgaard 1998; Borges et al. 2007; Zukowska 2011). However, due to complex geometries of the experimental settings and also due to several important data missing in the studies, this approach turned out to be insufficient. Therefore, additional experiments in thermally stabile

chamber with heat sources identical to heat sources in reference CFD simulations were carried out in order to use more relevant experimental data.

When measuring convective flows we have to consider very low temperature differences and velocities of the convective flow, i.e. around 1 to 2 K and 20 cm/s, respectively (Mierzwinsky 1980). It is important to use probes with appropriate measuring range and good sensitivity. The measurements should be performed in an experimental chamber with boundary conditions as stable as possible, since the convective flows are influenced by the slightest changes in the surrounding environment, see Chapter 2.2.1. The adaptation of the experimental chamber for more accurate measurements was proposed by Barták and Zelenský (2011), who developed a method of thermal stabilization of the experimental chamber walls with use of heating and cooling capillary tube mats.

It is also important to take into account the fluctuation of the thermal plume, see Chapter 2.2.1. Zukowska (2011) carried out time-averaging measurements in order to capture the representative mean values of the measured quantities. The averaging time was 5 minutes for each measurement, the time for conditions to became stable after change of position of the probes was also 5 minutes. Hyldgaard (1998) measured for a period of 10 minutes in order to get the mean value.

In the performed experiment, the air temperature distribution in the thermal plume was measured by a thermal imaging camera. The two measured arrangements of the experiment are shown in Fig. 4.3. The metal thermal manikin was positioned in an experimental room with the ceiling height of 3 m. The floor dimensions of the experimental room were 4 m × 8 m. The air temperature in the experimental room was 20.5 °C. Thermal manikin was heated up from inside by four light bulbs positioned in its head, body and each leg. The heat was evenly distributed by forced flow from a fan placed inside the manikin. Total heat output of the manikin was 90 W, same as in the simulations.

The experiment was performed according to the recommendations found in literature (Jančík & Bašta 2011). A sheet of plain paper was stretched vertically above the centre of manikin's head. The temperature field was continuously transferred from the thermal plume to the paper by convection. Thermal images of the paper surface were recorded using the infrared camera Flir T620 at 1 Hz sampling rate for the total period of 120 s. The time-averaged horizontal temperature profiles were then evaluated at seven different heights above the manikin's head in two perpendicular planes (front view, side view).

Fig. 4.3 – Experimental chamber with thermal manikin, 2 measured arrangements

4.2.2 Validation by inter-model comparison

In order to test the proposed method, simulations with heat sources (sitting thermal manikins) represented by simplified numerical models were compared to the simulations with detailed models of the manikin, which were considered as reference cases (as they were previously validated by comparison with the experimental results).

The comparative testing was based on the assessment of velocity magnitude isolines in two vertical planes intersecting the centre of the thermal manikins' head (front view and side view) and profiles of velocity and temperature, which were determined for every computational case in several heights above the models of the manikins.

Two types of numerical studies were performed during the inter-model comparison. The first type was a set of simple studies with one manikin placed in the middle of an enclosed room with floor dimensions 4.5 m x 4.5 m, ceiling height of 3 m and no obstacles. See Annex I, drawing D3 / DT-PZ-2018 for the exact positioning of the thermal manikin model in the room. The grid of measuring points was defined above the thermal manikin in order to compare the rising thermal plumes in individual simulations, see drawings D4 and D5 / DT-PZ-2018 in Annex I. The distribution of the measuring points was based on the previous experiment of Borges et al. (2007), while more measuring points closer to each other were used.

The second type was a study with four sitting thermal manikins placed close to each other in the middle of a room. The room had floor dimensions 5 m x 5 m and ceiling height of 5.6 m, see Annex I, drawing D6 / DT-PZ-2018. Similarly to the previous case, a grid of measuring points was defined above the thermal manikins. See drawings D7 and D8 / DT-PZ-2018 in Annex I.

In both cases, the boundary conditions at the surface of the thermal manikins were considered as constant. The uniform sensible heat flux from the surface was set to 57.3 W/m^2, which gave the total heat output of 90 W. The boundary conditions on the walls of the room were identical for all the simulations in order to enable mutual comparison of the results. The surface temperature of the room walls was set to 19 °C (unless mentioned otherwise in the text), their emissivity was 0.94 and the emissivity of the thermal manikin surface was 0.98. No-slip boundary condition was prescribed to the walls of the room and surfaces of the heat source.

The inter-model comparison, aside of validation purposes, was expected to show especially the effect of the variant positioning of the subsidiary boundary condition and drawbacks of the developed modelling method to represent heat sources.

4.2.3 Usability demonstration

Following the validation and initial testing of the developed modelling method, a case study was performed in order to investigate the usability of the method for real-life situations. The main target was to show applicability of the method in practice and uncover possible drawbacks of the theoretical propositions.

The previously developed modelling approach to represent heat sources in air flow modelling simulations was applied in a real scenario of a recently refurbished former church built in the 14th century, now used as a concert and conference hall with up to 350 visitors staying for different periods during each day. Two cases of two different occupancy scenarios were simulated. Models of visitors in both CFD simulations were represented according to the developed method. Only natural ventilation through window openings at the street level and roof windows was considered.

5 DEVELOPMENT OF THE MODELLING METHOD

This chapter describes the preparatory steps necessary for proposing the new modelling method to represent heat sources in CFD simulations of indoor air flow. The numerical mesh appropriate for the selected sample heat source is described in Chapter 5.1. The results of the CFD simulation with detailed model of heat source (thermal manikin) were compared to measurement to prove the correctness of the simulated results, see Chapter 5.4.

Forming of thermal plume in CFD simulations of common indoor heat sources is significantly influenced by the choice of the turbulence model. It can affect the profiles of velocity, temperature and turbulent quantities of the thermal plume. Therefore, the appropriate turbulence model was determined, as described in Chapter 5.2 and Chapter 5.4.

The difference between the heated surface and the ambient air temperatures may influence thermal plume generation and heat transfer intensity. This had to be taken into account, see Chapter 5.3.

5.1 Numerical mesh for simulations of heat transfer by natural convection

Development and validation of the proposed method was based on CFD simulations of thermal manikin, placed in the middle of an experimental chamber. Discretisation of the whole domain was influenced mainly by appropriate meshing of near-walls regions around the heat sources, which are crucial for correct simulation of heat transfer by natural convection (Wilcox 2006). Therefore, it was first necessary to establish properties of the fine mesh in the boundary layer region in the closes vicinity of the heat source (so called boundary layer mesh).

Maximal growth rate 1.2 is advised for the generation of a fine boundary layer mesh, representing the geometric progression of the contiguous cell heights (ANSYS 2013). In addition, it is appropriate to achieve the height of the last cell of the boundary layer mesh comparable to the following cell of the domain volume mesh.

The emphasis was put on the correct value of the dimensionless wall distance y^+ of the cell layers above the surface of the thermal manikin, which was required to be $y^+ \leq 2.5$ for at least the first seven cell layers (Wilcox 2006). Moreover, it was checked that at least first ten cells near the heated surface were situated in the region of the viscous sublayer, i.e. with $y^+ \leq 5$.

The maximum distance from the wall $y_{max(v.s.)}$ where $y^+ \leq 2.5$ was determined on the basis of the formula (2.11), using the mean value of τ_w on the surface of the heat source and the air density ρ estimated from the initial CFD simulation described in Chapter 4.1.4. The air density near the heated surface was found as the lowest air density in the initial CFD simulation:

$\mu = 1.789 \cdot 10^{-5}$ Pa·s

$\rho = \rho_{min} = 1.156$ kg/m^3

$\tau_w = 1.2 \cdot 10^{-4}$ Pa

$y^+ = 2.5$

$$y_{\max(v.s)} = \frac{y^+ \cdot \mu}{\sqrt{\rho \cdot \tau_w}} = 3.8 \cdot 10^{-3}\,\text{m} = 3.8\ \text{mm}$$

The height of the first cell, growth rate and total number of the layers of the boundary layer mesh around the heated surfaces are shown in Tab. 5.1. The described mesh was used in all the cases with detailed numerical models of the thermal manikin.

The computational mesh was refined also in the close vicinity of the walls of the room, as described in Tab. 5.1. After the convergence of the simulation, it was checked that the value of y^+ was in the order of 10^0 for all the cells on all the walls of the room. In fact, there were at least three computational cells in the region of viscous sublayer near the walls of the room, with exception of a small area in the centre of the ceiling, above the heat source, where the rising thermal plume impacts the wall. There was only one cell in the viscous sublayer at this region.

Tab. 5.1 – Boundary layer mesh

Surface	Number of layers	Height of the 1st layer	Growth rate	y^+ of the first cell	Nr. of cells in viscous subl.
Manikin	20	0.21 mm	1.16	0.2	13
Room walls	7	3.50 mm	1.20	0.9	3

All the models were meshed with orthogonal grid, only the regions with more complex geometry (close to the thermal manikins) were meshed by tetrahedral and prismatic cells.

Maximal dimension of the cells in the computational domain was 50 mm, following the recommendations found in the literature, see Chapter 2.4.4. These cells were filling most of the space of the modelled room. The numerical mesh was refined around the thermal manikin, which was surrounded by cells with edge dimensions 12.5 mm (12.5mm cells), followed by 25mm cells. The region of the raising thermal plume (above the heat source) was also meshed with smaller, 25mm cells.

Considering the fact that the parameters of the computational mesh were based on the previously proved recommendations found in the literature, it was assumed that the results of the CFD simulations were grid independent. A simple grid dependence study was performed in order to prove this assumption. Two numerical models of a sitting thermal manikin placed in the middle of a room were meshed in two ways. The model with fine mesh was meshed using the above described procedure, i.e. the thermal manikin was surrounded by 12.5mm cells. In the model with a coarse mesh, the thermal manikin was surrounded by cells twice bigger, i.e. 25mm cells. The results of CFD simulations with both models were compared and found to be identical, which indicates grid independence. To ensure high quality of obtained results, the finer mesh was used for all the reference simulations.

Vertical (*x*-*y*) and horizontal (*x*-*z*) cross sections of the thermal manikin surrounding are shown in the following page in Fig. 5.*1* and Fig. 5.*2*, respectively. It is possible to see individual layers of the hexagonal grid, including the finer boundary mesh around the thermal manikin surface. Fig. 5.3 shows the deformation of the hexagonal volume mesh between the cylindrical legs of the thermal manikin, which was caused during the generation of the fine boundary layer close to the surface of the heat source.

Fig. AII.1 and Fig. AII.2 in Annex II present vertical cross sections of the simulated experimental chamber cut by planes *x*-*y* and *y*-*z*; it is possible to see the finer mesh around the thermal manikin and in the region of the rising thermal plume.

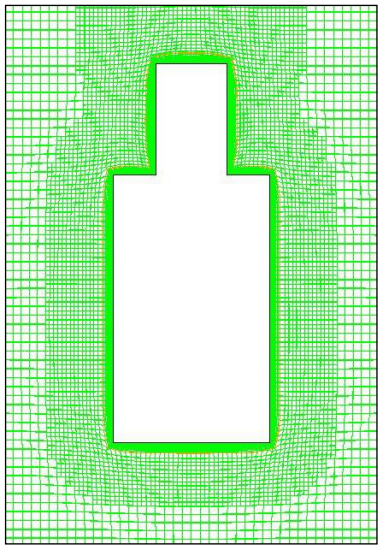

Fig. 5.1 – Cross section x-z (front view)

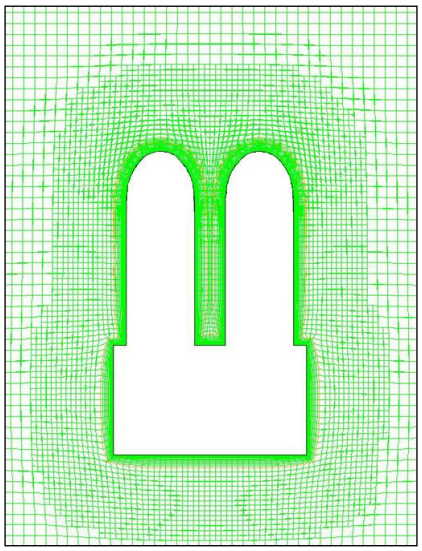

Fig. 5.2 – Cross section x-y (top view)

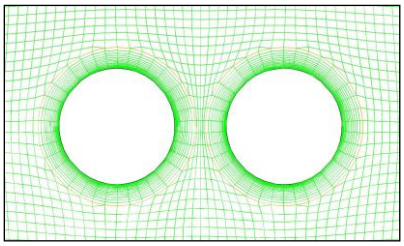

Fig. 5.3 – Cross section of the thermal manikin's leg

5.2 Influence of turbulence model on simulations of natural convection

Two-equation turbulence models, such as *k-ε* and *k-ω,* are the most frequently used for CFD simulations in the field of indoor air flow. The performance of four two-equation models (*k-ε Standard*, *k-ε RNG*, *k-ε Realizable* and *k-ω Standard)* in the thermal plume simulation was assessed in the study elaborated by Zelenský et al. (2013), which focused on the influence of the turbulence models on the formation of thermal plumes in CFD simulations. The results from several simulations with different models of turbulence were compared mutually, as discussed in this chapter, and also with experimentally obtained temperature profiles, as discussed in Chapter 5.4. The outcomes of the study were taken into account for further CFD simulations.

The model of a sitting thermal manikin placed in the middle of a room was used as an example of heat source generating thermal plume in indoor environment, as described in Chapter 4.2. The same geometry of the manikin was used for the numerical part of the study and for the experiment. The properties of the numerical mesh are described in Chapter 5.1.

Comparison of the numerical results

Velocity and temperature profiles of the thermal plume above the thermal manikin, simulated with different turbulence models are compared in Fig. 5.4 and Fig. 5.5. The profiles are presented at two different heights ΔH above the manikin in the vertical plane *x-y* (front view) intersecting the centre of thermal manikin.

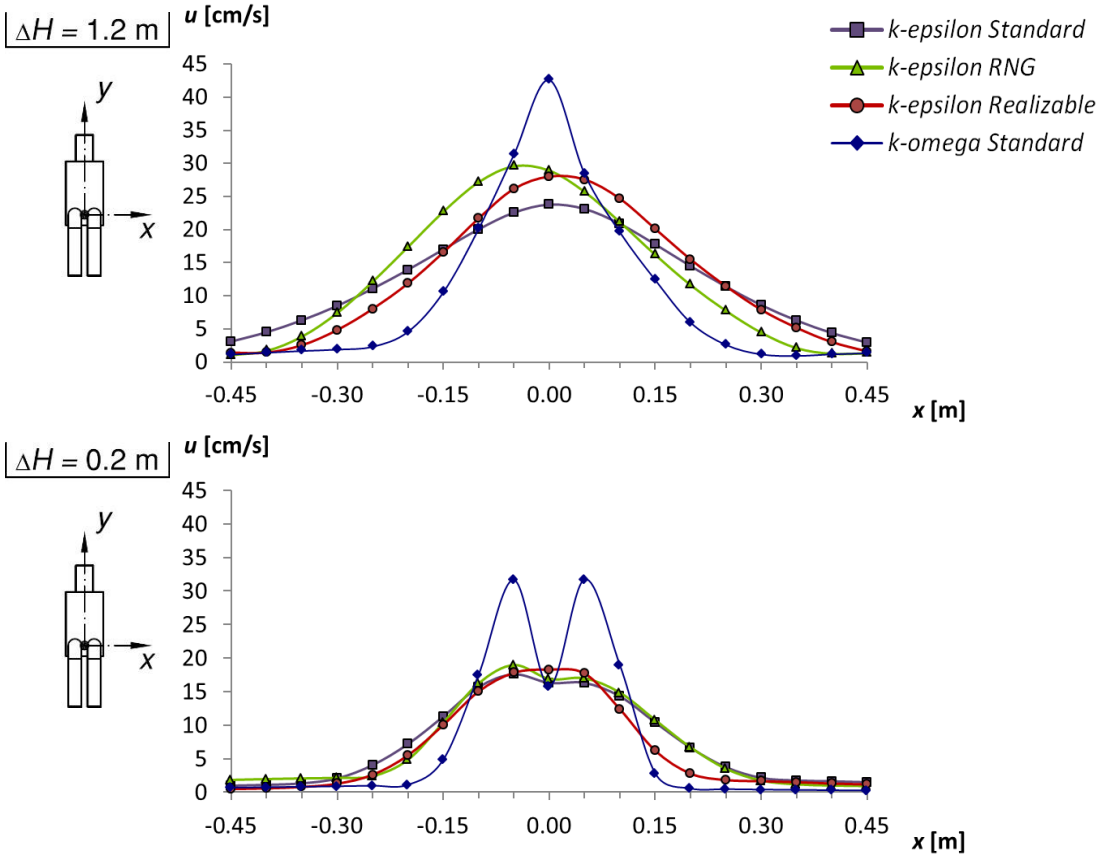

Fig. 5.4 – Velocity profiles in vertical plane x-y, at two different heights ΔH above the manikin

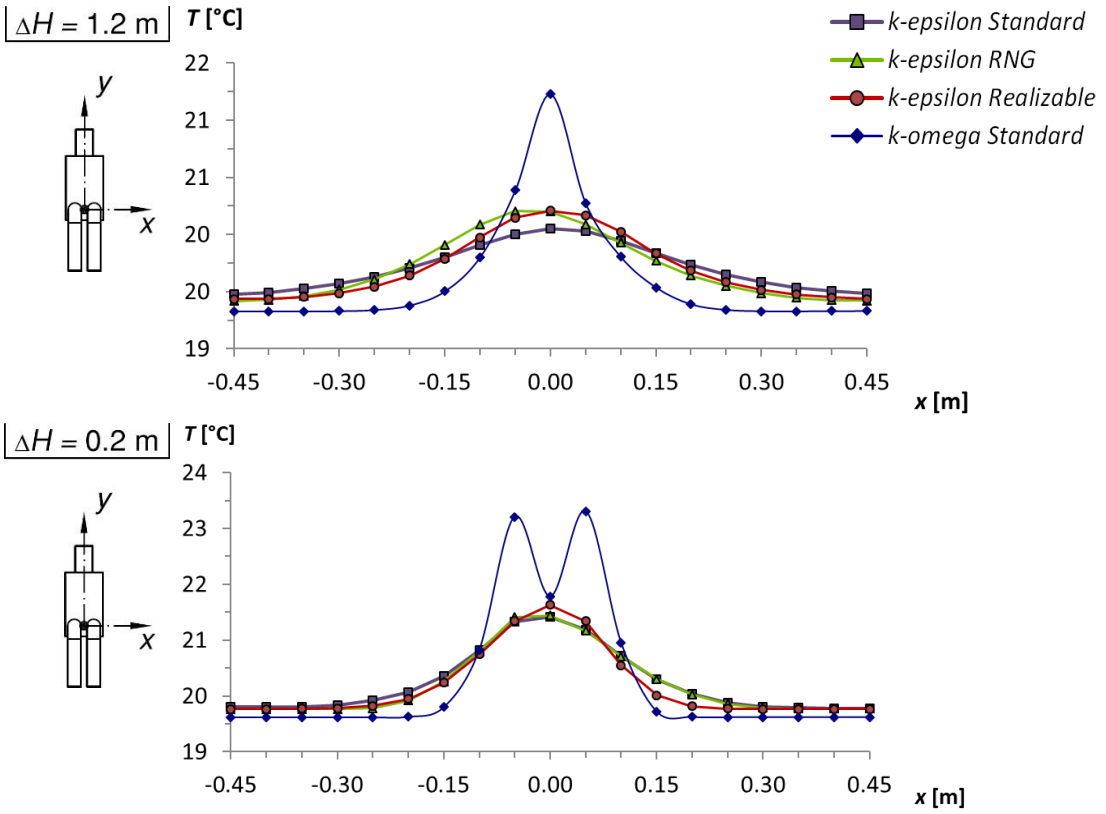

Fig. 5.5 – Temperature profiles in vertical plane x-y, at two different heights ΔH above the manikin

The velocity and temperature profiles obtained from the simulations with all three tested *k-ε* turbulence models are very close to each other. On the other hand, they are very different from the outputs of simulation with the *k-ω Standard* model, which predicts much higher velocities and temperatures in the thermal plume axis; their magnitudes also decrease with the increasing height slower than in the case of the *k-ε* turbulence models.

Although the simulation results based on the three compared *k-ε* turbulence models are very similar, they are not identical. The results obtained using the *k-ε Standard* model were differing considerably from the result with the other two *k-ε* turbulence models, in particular at higher regions above the heat source. The thermal plume in this case spreads more rapidly and its maximum velocity at higher regions is lower than in the other two cases.

The velocity profile simulated with the *k-ε RNG* model shows asymmetry for reasons that are not clear, see Fig. 5.4 (ΔH = 1.2 m). One of the reasons could be slower oscillation or bigger amplitude of thermal plume wandering in the simulation with the *k-ε RNG* model. Another possible reason could be the tendency of thermal plume to permanently deviate from its axis to one side. These asymmetries have been noticed also in experiments published by other authors (Zukowska et al. 2007).

Fig. 5.6 compares the profiles of turbulence kinetic energy *k* obtained from the simulations with all the four turbulence models. It indicates possible reasons for different behaviour of the thermal plume when using different turbulence models. The higher the turbulence kinetic energy *k* is, the higher the intensity of turbulent mixing in air flow and the higher the spreading rate of the thermal plume.

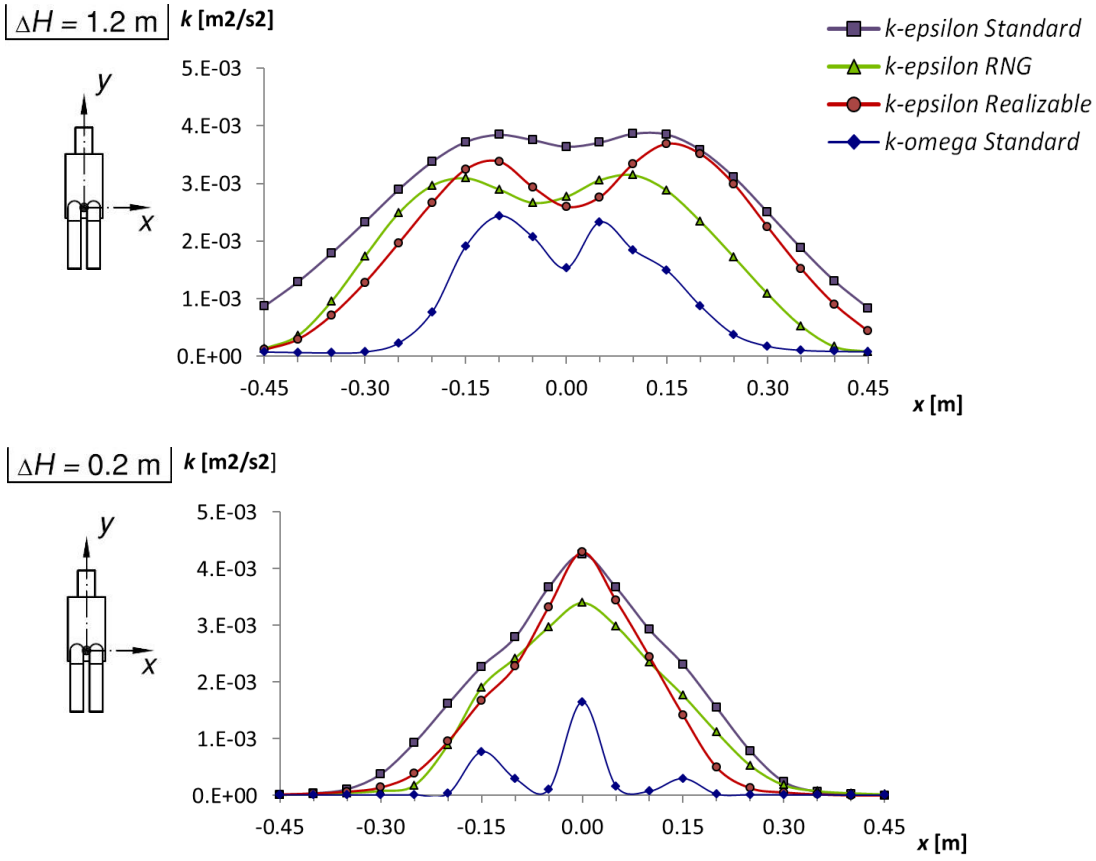

Fig. 5.6 – Turbulence kinetic energy profiles in the plane x-y, at two different heights ΔH above the manikin

It is obvious that the *k-ε Standard* model produces thermal plume with the highest turbulence intensity, and thus with the highest spreading rate. On the other hand, the *k-ω Standard* model shows the lowest values of *k* among the four turbulence models. Thermal plume in this case is therefore much narrower and spreads slower than in the simulations with *k-ε* models.

5.3 Influence of ambient temperature conditions on thermal plume

The effect of the ambient air temperature on thermal plume development is one of the important factors for modelling and simulation of heat sources. The influence of the ambient air temperature on the thermal plume was initially studied on the basis of analytical solutions describing convective flows discussed in Chapter 2.2.2. Basic quantities of analytically predicted convective flow above the point, line and horizontal-surface heat sources, as well as above various objects of more complex geometries (sphere, cylinder of $H/d = 2.7 \div 8.0$, radiator) are influenced only by the heat output of the source. They do not reflect temperature conditions in the surrounding air. See for example formulae (2.1) to (2.4) indicating volume flow rate of thermal plumes formed at an arbitrary height y above the heat sources with various geometries and heat output P_c. The mentioned formulae indicate that the change of the ambient temperature conditions should not affect the formation of thermal plumes above heat sources, providing that their heat output remains constant. The same applies also for the maximum velocity in the plume v_{y0} (axis velocity) and temperature difference ΔT_{y0} at the plume centre, as demonstrated on the example of analytical solutions of the point heat source. See formula (2.5) and formula (2.6).

The analytical solution of the volume flow rate above a vertical surface reflects the temperature difference between the heat source and the ambient air, as describes formula (2.7). However, the temperature difference should remain constant if the heat output of a heat source does not change.

It was expected that the velocity profile in the thermal plume does not depend on the ambient air temperature, providing that the heat output of a heat source is constant. Nevertheless, the ambient air temperature may influence the temperature profile. To prove this, the velocity and temperature profiles obtained from two CFD simulations of an experimental room with a model of one thermal manikin placed in its centre and exposed to different air temperatures 19 °C and 24 °C were compared (Zelenský, Barták & Hensen 2013). See Fig. 5.7 and Fig. 5.8.

It is obvious that the air temperature profiles, which are compared in Fig. 5.7, reflect the difference in the ambient temperature. The higher is the ambient temperature, the higher is the air temperature in the thermal plume. On the other hand, the velocity profiles in the simulations with different ambient air temperature are almost identical, see Fig. 5.8.

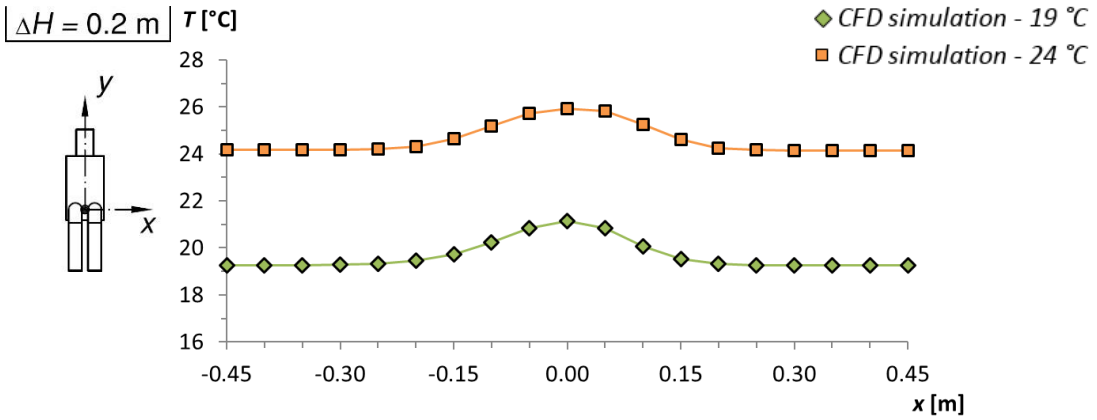

Fig. 5.7 – Temperature profiles in vertical plane x-y, for 2 different temperatures of ambient air

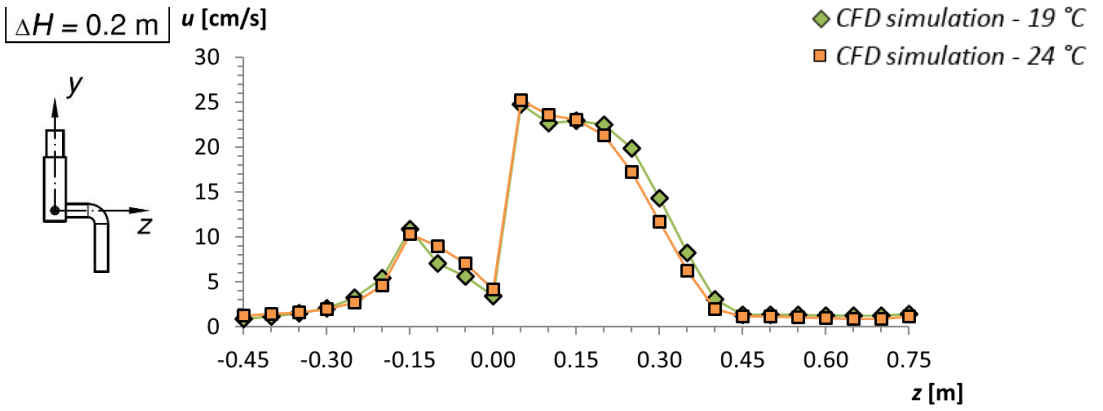

Fig. 5.8 – Velocity profiles in vertical plane y-z, for 2 different temperatures of ambient air

To make the new modelling approach universal with respect to different ambient thermal conditions, the temperature conditions of the thermal plume can be defined independently of different thermal environments by using a non-dimensional form defined using the following formula:

$$\frac{\Delta T}{\Delta T_{max}} = \frac{T(x) - T_{amb}}{T_{max} - T_{amb}} \tag{5.1}$$

where: $T(x)$ is the temperature at the distance x from the vertical axis y;
T_{max} is the maximum temperature in the plume at the given height;
T_{amb} is the ambient air temperature.

Fig. 5.9 shows the non-dimensional profiles of air temperature evaluated at the height of 0.2 m above the heat source according to formula (5.1). It was concluded that the non-dimensional temperature profiles are not significantly influenced by the ambient air temperature, as the temperature profiles obtained from the simulation with two temperatures of the ambient air (19 °C and 24 °C) are close to each other.

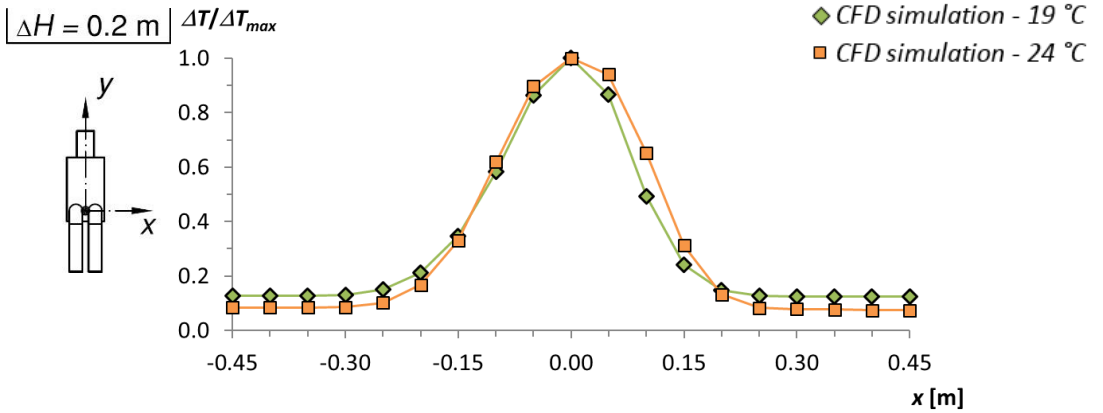

Fig. 5.9 – Non-dimensional temperature profiles in vertical plane x-y, for 2 different temperatures of ambient air

5.4 Comparison of simulations with detailed model with measurement

Temperature profiles obtained from the simulations described in Chapter 5.2 and Chapter 5.3 were compared with an experimental measurement by a thermal imaging camera, described in detail in Chapter 4.2.1. As the ambient temperatures in the experiment and in the CFD simulations were different, it was necessary to use non-dimensional temperature profiles for this comparison, as defined by the formula (5.1). Results of this study were used both to choose the most suitable model of turbulence for further simulations and to prove the correctness of the simulated results.

Fig. 5.10 presents the non-dimensional profiles of air temperature evaluated at two heights above the heat source in the experiment and in the simulations with different turbulence models. From their comparison, it follows that the results of simulations with all kinds of *k-ε* turbulence models are in a reasonable agreement with the measurements, although at higher positions above the heat source, all the simulated temperature profiles are less flat (i.e. less spread) than the measured ones.

The temperature profile closest to the experimental data is the one simulated with the *k-ε Standard* model of turbulence, which was used for all the following simulations. On the other hand, the temperature profile simulated with the *k-ω Standard* turbulence model was the most different from the measured one, being significantly narrower.

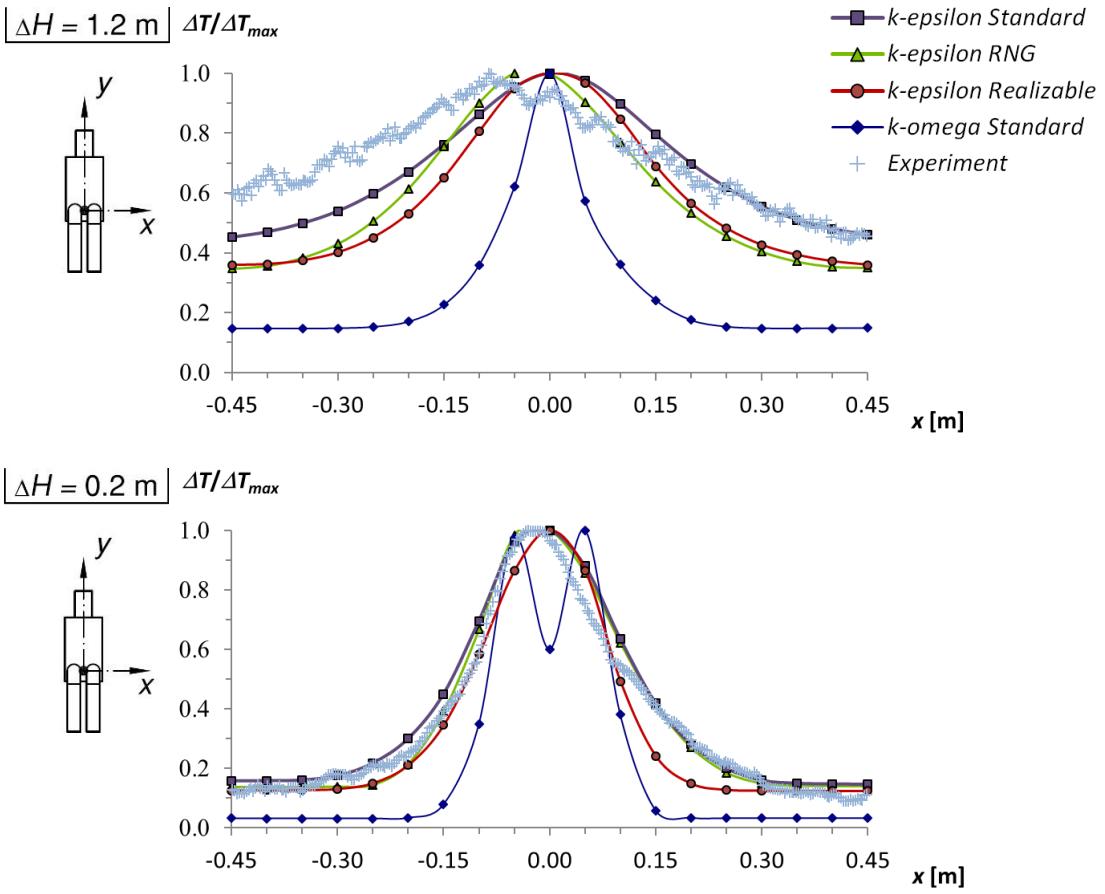

Fig. 5.10 – Non-dimensional temperature profiles in vertical plane x-y, at two different heights ΔH above the manikin

Fig. 5.11 shows the comparison of the non-dimensional profiles of air temperature of the thermal plume from the experiment with the simulations at the ambient air temperatures 19 °C and 24 °C, respectively. It is possible to see that all the profiles show a good correspondence. The thermal plume in the experiment is slightly deflected to the left, which could have been caused by an instability of the rising convective flow that was affected by non-uniformities of boundary conditions in the real environment. More details are described in Chapter 2.2.1.

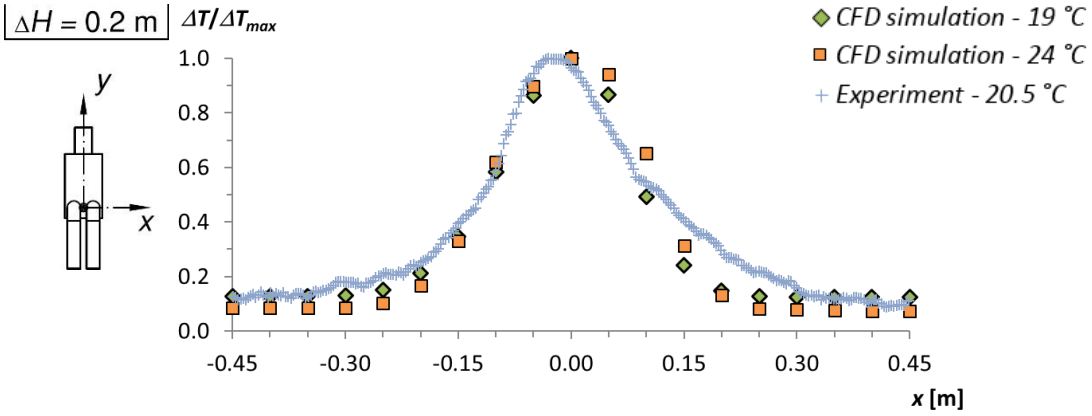

Fig. 5.11 – Non-dimensional temperature profiles in vertical plane x-y, 0.2 m above the manikin

6 RESULTS

This chapter of the thesis describes the key outcome of the research, i.e. the proposition of a new modelling method to represent heat sources in indoor air flow simulations (Zelenský et al. 2012). It also presents results of several studies which were performed in order to test the proposed method and reveal its limitations.

The proposed modelling method to represent heat sources in CFD simulations was inspired by the box method used for modelling of air supply diffusers (Nielsen 1997). It is based on the replacement of a heat source by one or more appropriately positioned simplified boundary conditions inducing a thermal plume potentially identical to that rising above the real heat source, see for example Fig. 6.1. Each of the boundary conditions substituting the heat source prescribes velocity, temperature and turbulence of the induced flow. These characteristics are determined in advance on the basis of reference CFD simulation with detailed representation of the heat source. The work-flow of the method is described in Tab. 6.1.

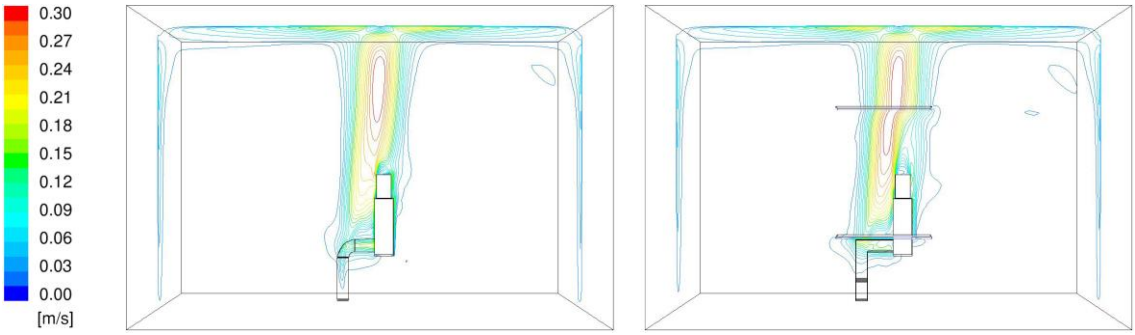

Fig. 6.1 – Thermal plume above a detailed and substitute model of heat source (velocity isolines) (Zelenský et al. 2012)

The method reflects the issues that are not addressed by the current ways of modelling heat sources for CFD simulations, as mentioned in Chapter 3. Faster CFD simulation was achieved, enabling both more effective simulation of spaces with a large number of heat sources and variant CFD studies of places with high variability of heat sources occurrence, such as different occupancy patterns. Once the reference simulation is finished and the simplified model of a heat source is prepared, it can be used as a multiple object in one simulation (in the case of a large number of the same heat sources), or repeatedly in different simulations (for example in the case of variant studies). Although in the current research the method was applied to models of occupants, it can be used to represent any heat source in general.

To ensure the correctness of the proposed method, all the factors affecting development and physical behaviour of the rising thermal plume and its simulation had to be taken into account. This concerns both the design phase of the detailed numerical model and the computational phase of the reference and simplified CFD simulations.

Tab. 6.1 – Work-flow of the new modelling method to represent heat sources

Step	Description
1	**Preparation of the numerical model for reference simulation** **→ detailed representation of a heat source:** - current best practice methods of numerical modelling for CFD simulations should be followed; - the numerical model of a heat source should be modelled in detail, without any significant simplification.
2	**Reference CFD simulation with a detailed model of the heat source:** - the best practice of CFD simulations should be followed; - heat and momentum transfer near the heat source surface is modelled using a fine boundary layer mesh (i.e. with integration of governing equations in the viscous sublayer); - turbulence can be modelled using RANS-based turbulence models – it can be advised to used the *k-ω Standard* model, see Chapter 5 ; - CFD simulation is performed to obtain velocity and temperature fields around the heat source, with focus on the generated thermal plume rising around the heat source.
3	**Determination of simplified boundary condition(s):** - air flow velocity, temperature and turbulent quantities are recorded from the reference CFD simulation in the rising thermal plume, using a grid of measuring points; - the obtained values should be time-averaged.
4	**Creation of a numerical model with simplified representation of heat source(s):** - the heat source body is substituted by a simplified geometrical object with adiabatic surface, acting solely as an obstacle to the ambient flow (there is no heat transfer from the surface of the object); - the thermal plume is induced artificially, by boundary condition(s) prescribed in the place of each heat source.
5	**Real scenario simulation with simplified model(s) of heat source(s):** - one simulation with multiple simplified heat sources (i.e. large number of models created in the Step 4); - several simulations with repeated use of the simplified model (i.e. variant numerical studies using the model created in the Step 4).

During the preparation of a numerical model for the reference simulation (i.e. Step 1), the current methods of heat sources modelling can be followed, as discussed in Chapter 2.4. Although the reference model should be as realistic as possible, it is for example feasible to neglect some details of the geometry, non-uniformities of the boundary conditions on the surface of the heat source, respiration process and small localized body movements in the case of occupants, as they do not have significant influence on the results of simulations.

The numerical mesh of the reference computational case should be prepared according to the best practice of meshing for CFD simulations, see Chapter 2.4.4. The maximum and minimum size of the computational cells in the domain have to be chosen correctly. In addition, the differences in the contiguous cells dimensions have to be considered. For CFD simulation of natural convection, the height of the first cell near the heated surface and correct meshing of the near-wall regions is very important. The appropriate numerical mesh for the CFD simulation of the selected heat source was already discussed in Chapter 5.1

The process of the simplified boundary condition determination (i.e. Step 3) has to reflect also the oscillation of the flow, as discussed in Chapter 2.2.1. The instability of thermal plumes must be taken into account both during the experimental measurements and during the evaluating of the reference CFD simulations with a detailed model. The prescribed quantities should be time averaged.

Following Chapter 6.1 describes in detail the way to simplify a model of heat source using the proposed method. The numerical mesh used for the simplified simulations is introduced as well. Optimal positioning of the simplified boundary condition and combination of two boundary conditions is discussed in the following Chapters 6.2 and 6.3, respectively.

The phenomenon of thermal plumes merging should be considered in the case of more heat sources placed near to each other. In such cases, it can significantly affect the development of thermal plumes rising above individual heat sources. A computational study was performed to address this issue, see Chapter 6.4

6.1 Substitution of heat sources by simple boundary conditions

This chapter describes the way to simplify a model of a heat source using the proposed method. The procedure will be demonstrated on the example of a sitting thermal manikin, as described in Chapter 4.2. The rising thermal plume is, in the simplified case, induced by the velocity and temperature profiles set as the boundary conditions at subsidiary zones created at chosen heights in the place of the original thermal manikin model, see Fig. 6.2. The subsidiary zone with the prescribed simple boundary condition is, for better clarity, hereinafter referred to as *SBC*.

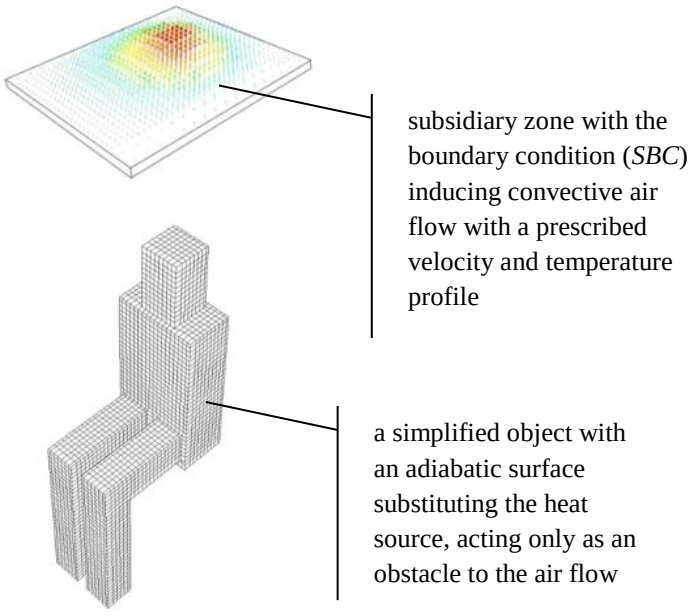

Fig. 6.2 – Simplified model of the sitting occupant

The original model of the heat source (i.e. model of the thermal manikin) is substituted by a significantly simplified object with an adiabatic surface. Cylindrical legs and head are replaced by rectangular blocks. The object acts only as an obstacle to the indoor air flow and it does not release heat to the surroundings. This brings lots of advantages, especially in the process of meshing. It is not necessary to generate fine mesh in the boundary layer region surrounding the object's surface and the computational cells in the vicinity of the object can be bigger. Neglecting the cylindrical parts of the model makes meshing easier as well. For detailed geometry of the simplified model used in the following studies, see Annex I, drawing D2 / DT-PZ-2018.

The velocity and temperature profiles imposed on the *SBCs* are determined from the reference simulation with detailed model of the heat source. In the described example of the sitting thermal manikin, horizontal grids of 156 measuring points covering the area 700 x 600 mm are set at six heights: at the level of calves, waist and four heights above the head of the manikin (35 mm, 200 mm, 450 mm and 700 mm).

Each of the velocity components u_x, u_y, u_z, temperature T and turbulence quantities k and ε are obtained in each measuring point as an average of 120 values acquired during 120 s of computational time. The averaged profiles of velocity components, temperature, k and ε are imported into the simplified computational cases and set as boundary conditions on each *SBC*. The file with the obtained time-averaged values of each quantity is included in the Annex V. The induced thermal plume leaves the *SBC* from its top (see Fig. 6.3) and equivalent flow rate is drawn through its bottom from the domain.

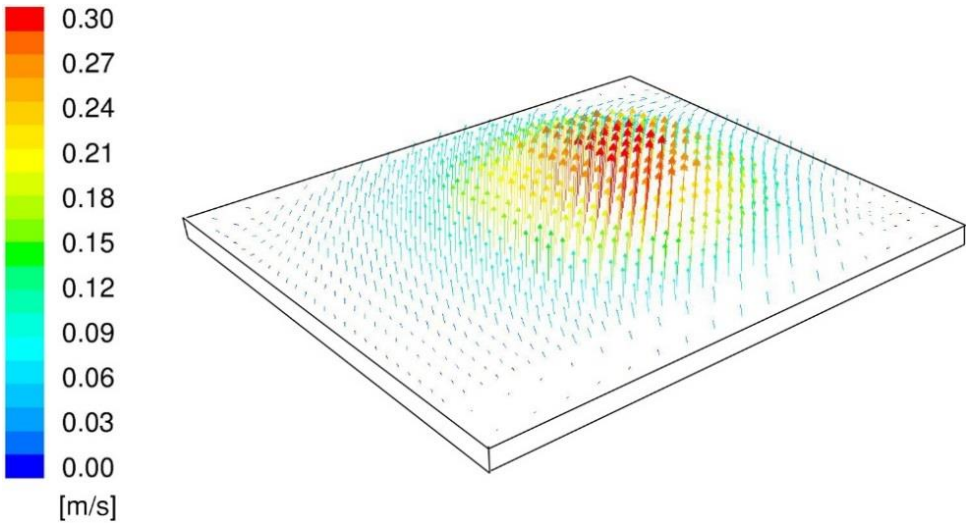

Fig. 6.3 – Velocity profile on the top surface of the SBC, displayed as velocity vectors

Computational mesh in simulations with simplified models

The computational domain was meshed with orthogonal grid taking into account the size of the computational cells in the reference detailed simulation described in Chapter 5.1. The model of a simplified object substituting the thermal manikin was surrounded by cells with edge dimension of 25 mm (25mm cells). Cells with the same dimension were filling also the area of the rising thermal plume above the heat source. The 25mm cells were followed up by 50mm cells, which filled the remaining volume of the modelled room. The computational mesh was refined only in the close vicinity of the walls of the room in the same way as in the case of the reference simulation, see Tab. 5.1.

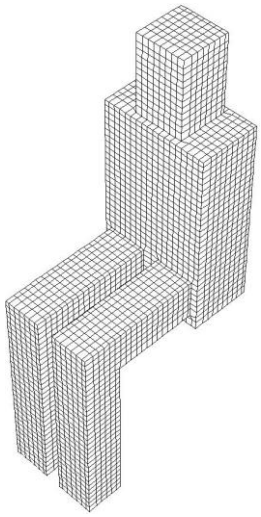

Fig. 6.4 – Simplified model surface mesh

The surface mesh on the simplified object substituting the heat source is displayed in Fig. 6.4. Vertical (*x-y*) and horizontal (*x-z*) cross section of the object's surroundings is shown in Fig. 6.5 and Fig. 6.6, respectively. Fig. 6.7 shows the mesh around the simplified legs. Annex II presents vertical cross sections of the simulated experimental chamber cut by planes *x-y* and *x–z*, where it is possible to see the finer mesh around the simplified model of the heat source and in the region of the rising thermal plume. See Fig. AII.3 and Fig. AII.4

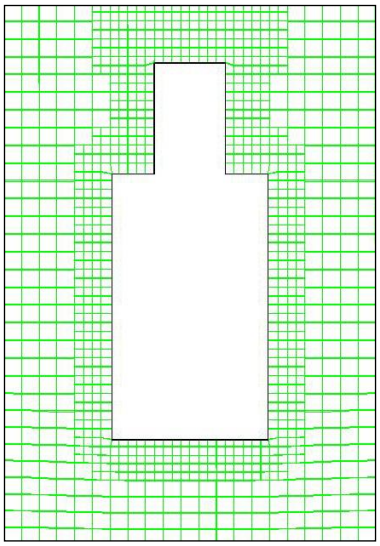

Fig. 6.5 – Cross section x-y (front view) Simulations with the SBCs

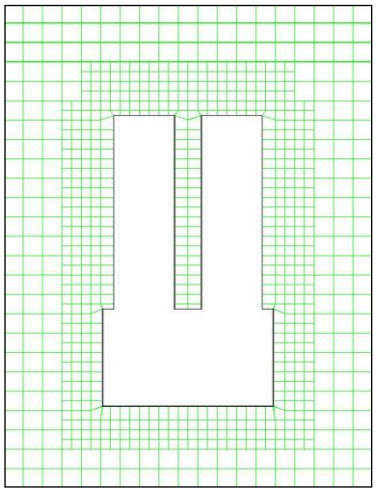

Fig. 6.6 – Cross section x-z (top view) Simulations with the SBCs

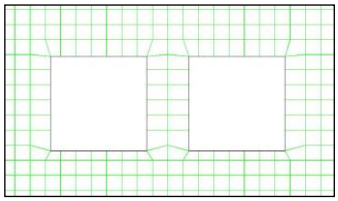

Fig. 6.7 – Cross section of the thermal manikin's leg Simulations with the SBCs

6.2 Vertical position of substituting boundary condition

The positioning of the *SBC(s)* depends both on the features of the heat source (especially geometrical shape) and on the properties of the thermal plume. It is very important to understand the process of the convective flow forming, the factors influencing its properties and affecting the final form of the thermal plume (see Chapter 2.2.1). The *SBC* position should be optimized in order to induce convective flow pattern which is close to the substituted reference case.

The optimal position of the *SBC* above the heat source was studied by Zelenský et al. (2017) in the case of thermal manikin situated in the middle of a room, as described in Chapter 4.2. Four computational cases with different vertical positions of the *SBC* were solved and compared. The tested vertical positions were in the range from 35 mm to 700 mm above the head of the thermal manikin as shown in Fig. 6.8.

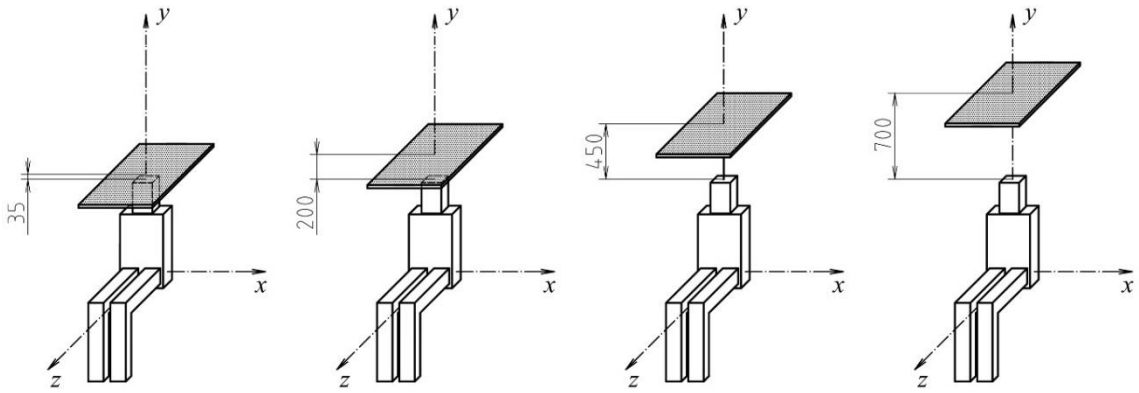

Fig. 6.8 – Vertical positions of the SBC above the manikin's head

The isolines of velocity magnitude in the vertical plane *x-y* (front view) and *z-y* (side view) intersecting the centre of the thermal manikin's head are displayed in Fig. 6.9. The simulations with the simplified heat source were compared to the simulation with the detailed model of thermal manikin (Fig. 6.9, case A), which is considered to be the reference case (all the simplified boundary conditions were determined from this case).

The thermal plume patterns are close to each other in all the computational cases at the region above the *SBCs*. The thermal plumes adhere to the ceiling of the room and spread further towards the vertical walls in a very similar way in all the simulations. There is no convective flow formed around the manikins in the simplified simulations. The lower the vertical position of the *SBC*, the closer the simulated velocity field is to the reference simulation, as the thermal plume is induced nearer to the manikin's head.

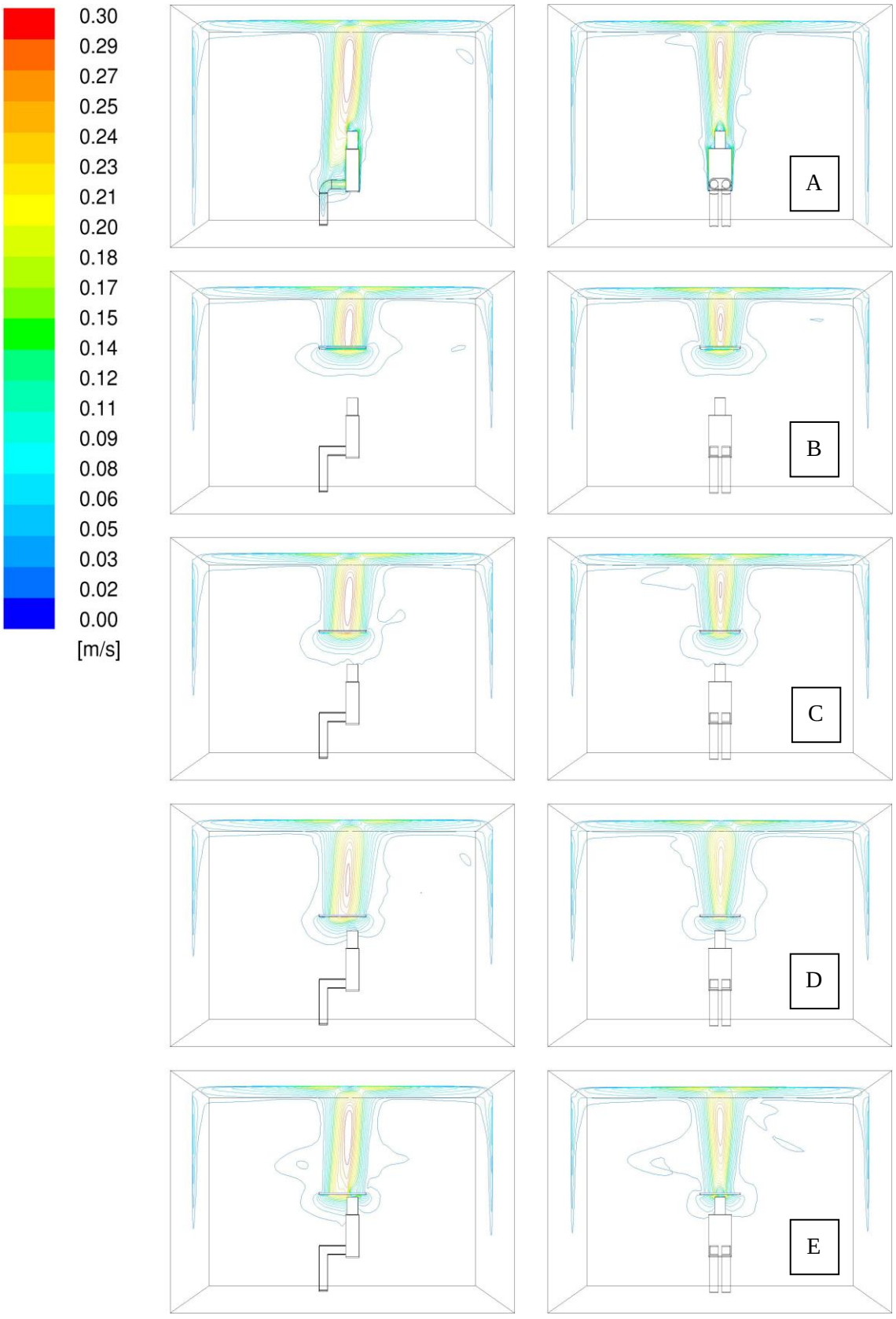

Fig. 6.9 – Velocity magnitude isolines in thermal plume above detailed and substitute model of heat source: A – detailed model; B to E – simplified models with various SBC positions

Velocity profiles

The velocity fields presented in Fig. 6.9 give a good preview of the simulation results. However, for more exact evaluation of the thermal plumes, it is necessary to compare velocity and temperature profiles. They were determined for every computational case at several heights above the manikin. The results at the heights ΔH = 0.4 and ΔH = 1.2 m above the thermal manikin in the vertical plane *x-y* (front view) intersecting the centre of the manikin's head are displayed in Fig. 6.10.

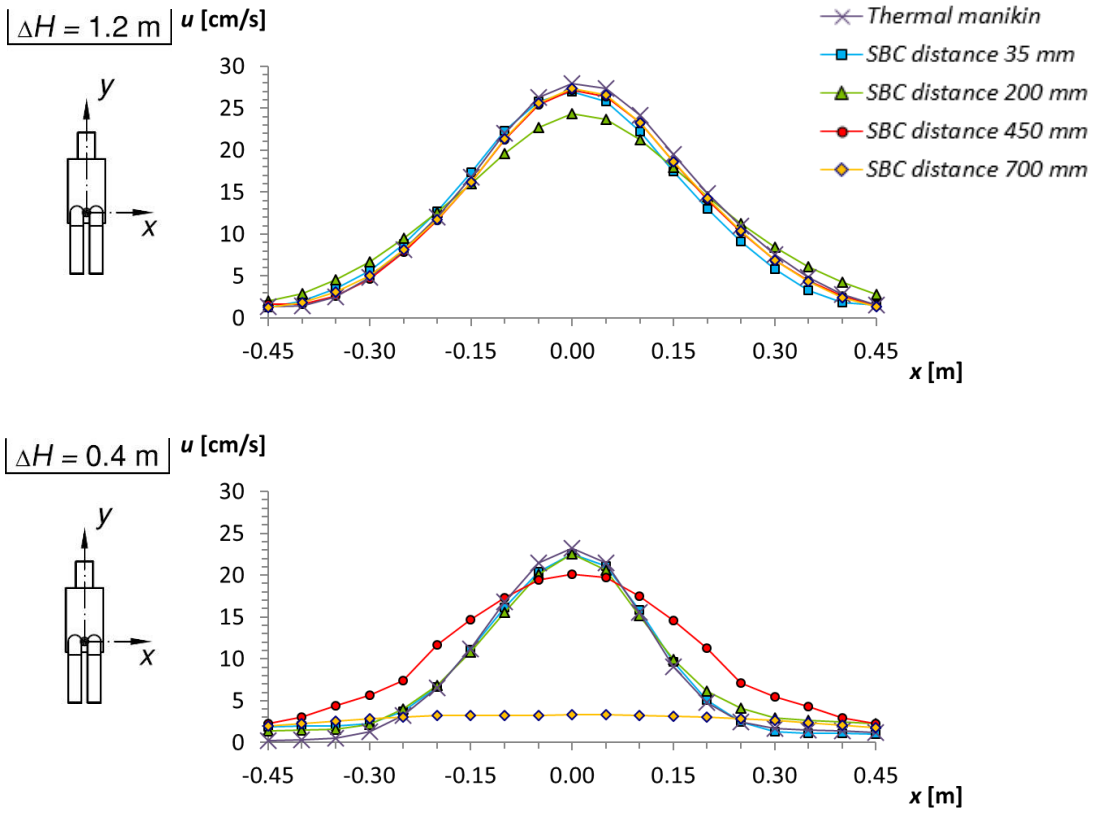

Fig. 6.10 – Velocity profiles in vertical plane x-y, at two different heights ΔH above the manikin

The velocity profiles determined for the simulations with simplified models are close to the reference case especially at higher regions of the room, i.e. above the *SBCs*, see Fig. 6.10 (ΔH = 1.2 m). The most similar cases corresponding to the reference simulation are the simulations with the *SBCs* in the heights 450 and 700 mm above the manikin's head. The case with the *SBC* positioned 35 mm above the manikin is reasonably corresponding to the reference simulation as well. The exception is the case with the *SBC* positioned 200 mm above the manikin's head, where the comparison shows a lower velocity in the centre of the convective flow above the manikin than in the reference simulation. The simulation with this simplified model was repeated twice, to check whether it was fully converged and if the deficiency was not caused by an instability of the convective flow in the simplified simulation. As the results of the two simulations were identical, the deficiency must have been caused by an instability of the thermal plume in the reference case, at the height where the simple boundary condition for the simplified simulation was determined.

There are bigger differences in the locations closer to the manikin, see for example Fig. 6.10 (ΔH = 0.4 m). It shows velocity profiles of the thermal plumes 400 mm above the manikin's head, i.e. in the region under the *SBC* in the two cases with *SBCs* positioned 450 mm and 700 mm above the manikins and in the region above the *SBCs* in the remaining two cases with *SBCs* positioned 35 mm and 200 mm above the manikins. It is possible to see that in the region under the *SBC* the results of the simplified simulation do not correspond to the reference case.

Temperature profiles

The temperature profiles in the simulations with simplified models show good correspondence to the reference case at the heights above the *SBCs*, see Fig. 6.11 (ΔH = 1.2 m). The exception is the simulation with the *SBC* placed 200 mm above the head of the thermal manikin. In this case, the thermal plume in the simulation with a simplified model has slightly lower maximal temperature than in the reference case. The difference is approximately 0.2 K. Below the *SBCs* the temperature profiles in the simplified simulations do not correspond to the reference case, see for example Fig. 6.11 (ΔH = 0.4 m).

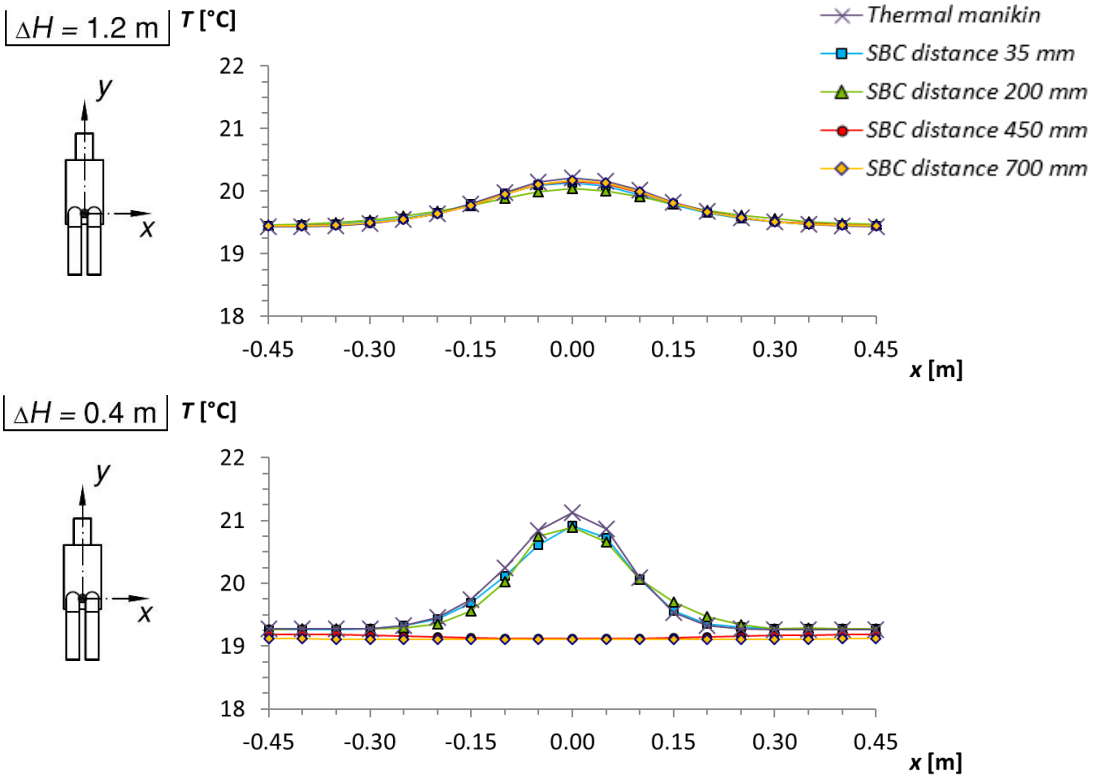

Fig. 6.11 – Temperature profiles in vertical plane x-y, at two different heights ΔH above the manikin

6.3 Multiple SBCs

Considering the problem on hand, the main (upper) *SBC* can be accompanied by another one positioned lower above the floor. The influence of the combination of two *SBCs* inducing the thermal flow was studied by Zelenský et al. (2012). Three computational cases with different configurations of the *SBCs* were solved and compared, see Fig. 6.12.

In the simplest case, only one *SBC* was used at the height 700 mm above the head of the model, in the region where the thermal plume is considered to be fully developed (Zukowska et al. 2010b). In the other two cases the velocity and temperature profiles were assigned to the surfaces of two *SBCs*. The upper one was created at the height of 700 mm above the model's head for the reasons mentioned above. The lower one was defined either at the height of calves of the thermal manikin or at the height of its waist, in order to assist the upper *SBC* in creating the convective current around the manikin's body. The aim was to study the importance of the lower *SBC* position.

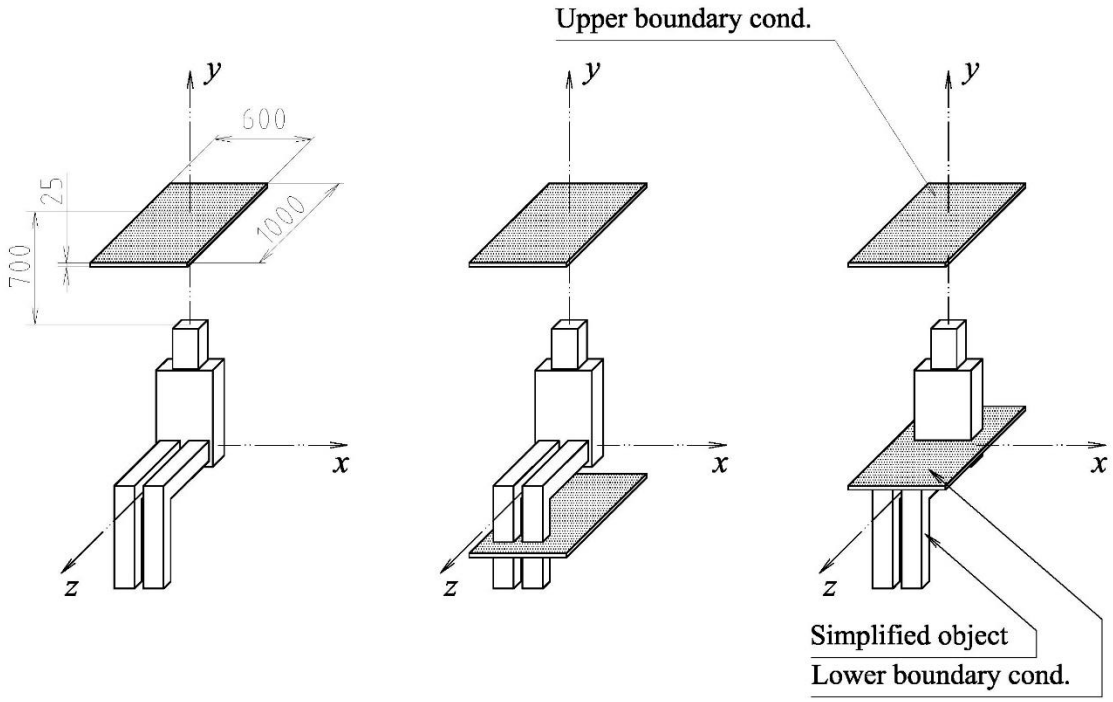

Fig. 6.12 – Substitution of the heat source by two SBCs (Zelenský et al. 2012)

The isolines of velocity magnitude in the vertical plane *z-y* (side view) intersecting the centre of the thermal manikin's head are displayed in Fig. 6.13. The simulations with the simplified heat source were compared to the simulation with the detailed model of thermal manikin, i.e. with the reference case (denoted as side view A).

The thermal plume patterns are close to each other in all the computational cases at the height above the upper *SBC*. The plumes adhere to the ceiling of the room and spread further to the vertical walls in a very similar way in all the simulations.

The formation of the thermal plumes under the upper *SBCs* differs more significantly in the individual simulations. There is no convective flow formed around the manikin in the simulation with just one *SBC* (Fig. 6.13, side view B). This deficiency was addressed by placing another *SBC* to the lower height above the floor. The convective current generated by the lower *SBC* flows around the object substituting the thermal manikin and enters the upper *SBC*, which generates the plume rising towards the room ceiling.

The air flow in the computational case with the second *SBC* positioned at the height of calves (Fig. 6.13, side view C) is being formed also in the area under the higher *SBC*. However, this flow is significantly different from the reference one (Fig. 6.13, side view A). The thermal plume induced by the simplified boundary condition rises only above the knees of the manikin and partly adheres to its front. There is a very weak flow above the head under the upper *SBC* and no flow along the back of the model.

The flow in the case with the second *SBC* positioned at the level of waist (Fig. 6.13, side view D) is the closest to the reference case. The generated thermal plume rises above the thighs and appropriately adheres to the manikin. The flow above thighs significantly influences the rising thermal plume, which is in accordance with the findings of Zukowska et al. (2007). The imperfection in this case is caused by the insufficient flow along the back of the manikin, which would, after merging with the flow above the legs, bend the resulting thermal plume more behind the manikin.

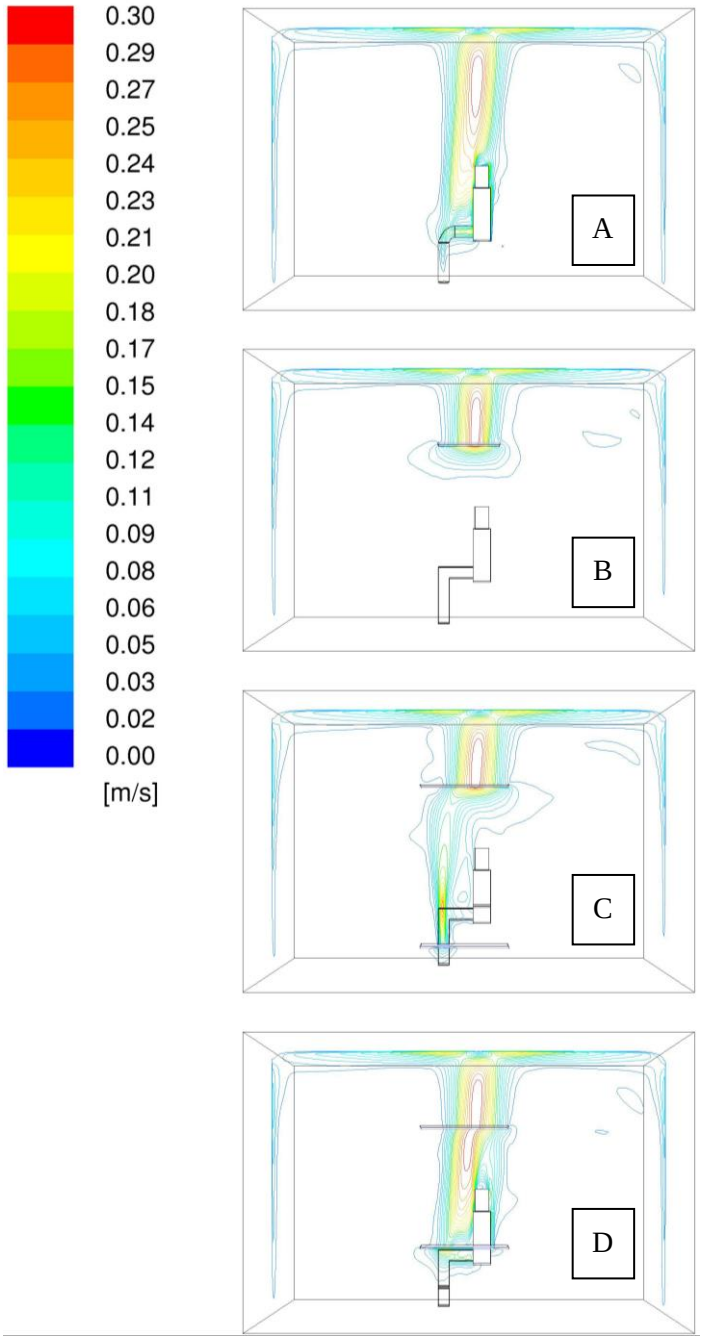

Fig. 6.13 – Velocity magnitude isolines of thermal plume around detailed and substitute model of heat source (Zelenský et al. 2012): A – detailed model; B to D – simplified models with various combinations of SBCs

Velocity profiles

Velocity profiles were determined for every computational case at several heights above the manikin. The results at the heights of 0.2 m and 1.2 m above the thermal manikin in the vertical plane *y-z* (side view) intersecting the centre of the manikin's head are displayed in Fig. 6.14.

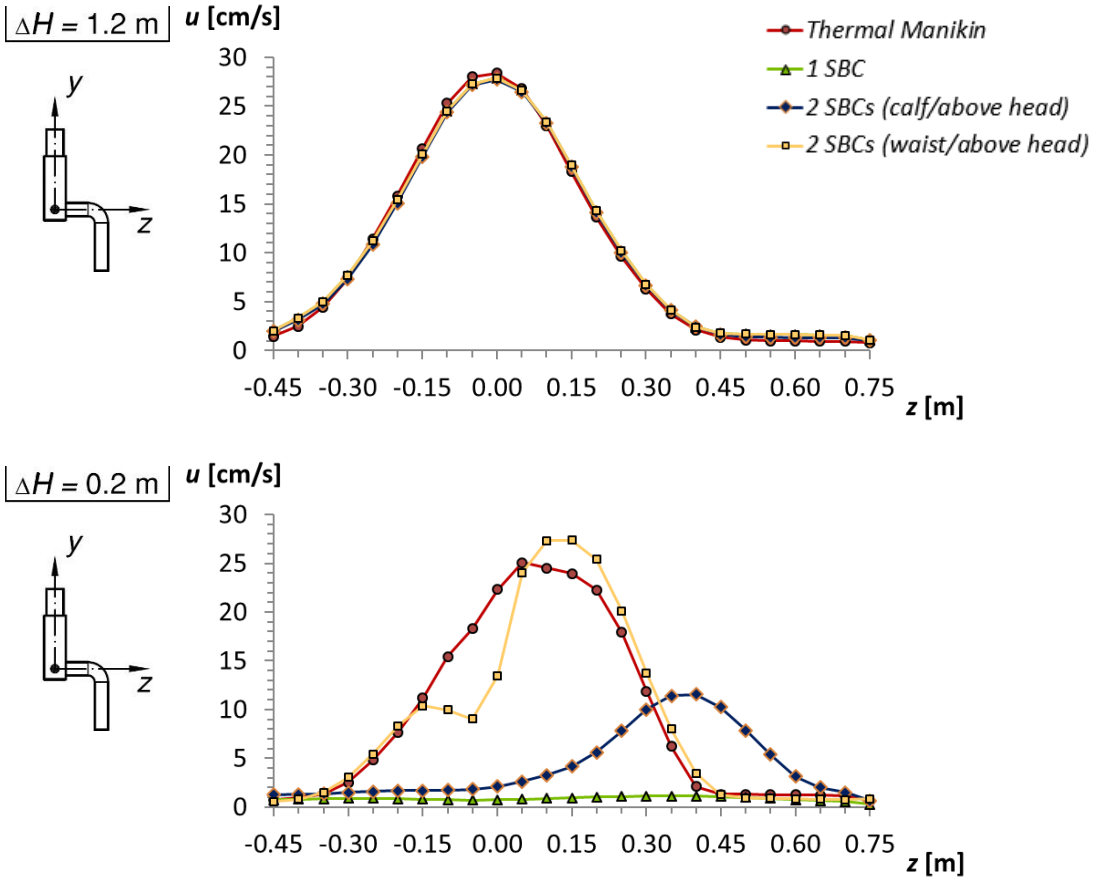

Fig. 6.14 – Velocity profiles in vertical plane y-z, at two different heights ΔH above the manikin

The velocity profiles determined for each simulation are corresponding to each other especially at the higher regions of the room, see Fig. 6.14 (ΔH = 1.2 m). There are apparent differences between individual simulations at lower heights (around the thermal manikin and under the upper *SBC*). The simulation with two *SBCs*, where the lower *SBC* is positioned at the waist level, is the one most corresponding to the reference case. However, the thermal plume is still influenced by insufficient flow along the back of the manikin. The flow velocity is too high above the legs of the manikin and, on the other hand, too low above its head.

Temperature profiles

Temperature profiles of thermal plumes at the higher regions correspond to each other in all the simulations, see Fig. 6.15 (ΔH = 1.2 m). However, there is again some deficiency of induced thermal flow at lower heights. The thermal plume induced by two *SBCs*, where the lower *SBC* is positioned at the waist level, is the one closest to the reference case.

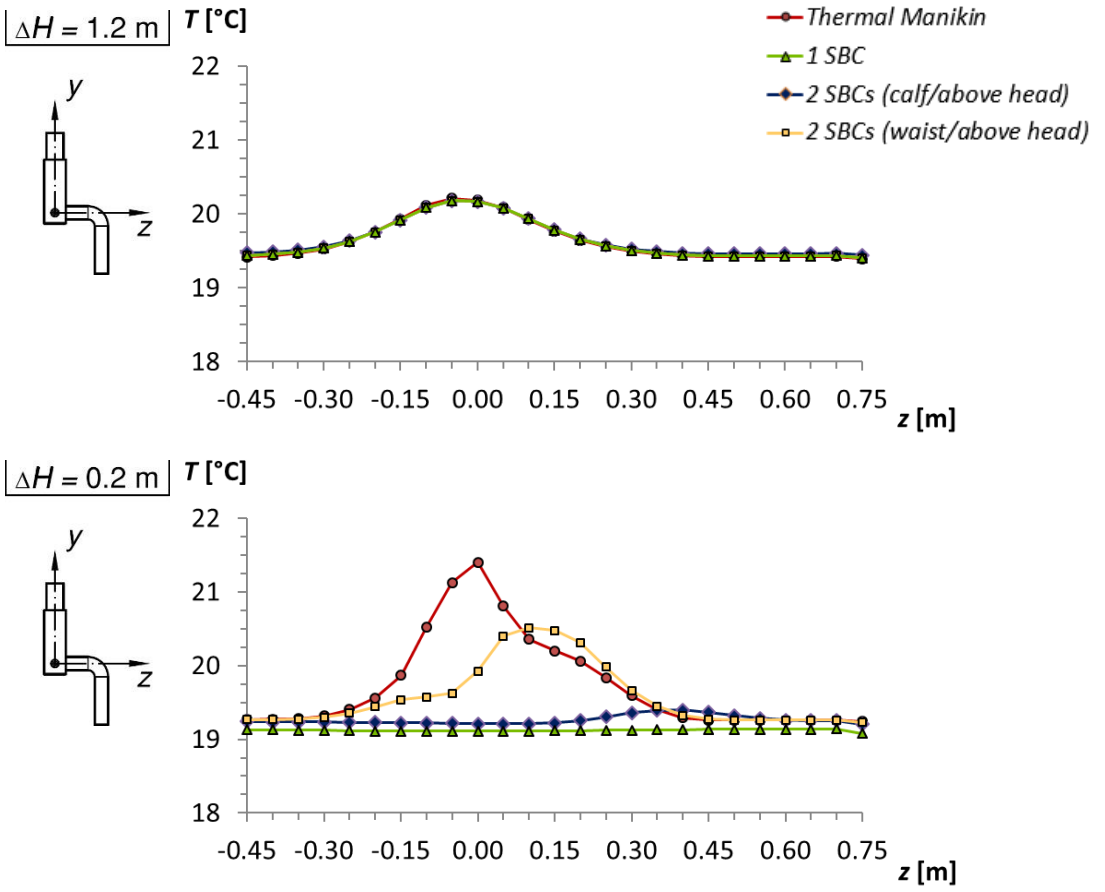

Fig. 6.15 – Temperature profiles in vertical plane y-z, at two different heights ΔH above the manikin

6.4 Merging of thermal plumes

Simulations with multiple heat sources should reflect the merging of individual thermal plumes in higher regions. There was a concern about how the developed method influences this physical process, especially as it is targeting simulations of spaces with a large number of heat sources possibly positioned close to each other.

A numerical study was elaborated upon with the focus on thermal plumes merging above multiple heat sources (Zelenský et al. 2016). It compares a set of simulations with numerical models of four sitting thermal manikins placed inside an enclosed room. The manikins were modelled either in detail (see Chapter 4.2), or simplified, using the developed method, with one *SBC* 700 mm above each thermal manikin. For the geometry of the numerical models see Annex I. The target was to assess the usability of the previously developed modelling method to represent indoor heat sources in CFD simulations of more complex real scenarios.

The reference simulation was performed with detailed models of the manikin positioned in the middle of an enclosed room with dimensions (width x length x height) 5 x 5 x 5.6 m, see Fig. 6.16 (left). Heat and momentum transfer near the manikin's surface was modelled using fine mesh in the region of the boundary layer, i.e. by integration of the governing equations within the viscous sublayer. The boundary conditions on the surface of the manikins and on the walls are described in Chapter 4.2.2. The room dimensions and no obstacles around and above the manikins provided enough space for the thermal plumes to sufficiently develop and merge.

The results of the simulation with detailed models were compared to the results obtained with the simplified models of thermal manikins. Both numerical models were meshed in a similar manner as described in Chapter 5.1 for the reference simulation and in Chapter 6.1 for the simulation with simplified models. The simulations were performed and evaluated according to Chapter 4.1. Air flow patterns in the room (velocity magnitude isolines) were recorded for every computational case at the last time step (i.e. termination of the simulation, when the flow can be considered as fully developed). The isolines were recorded in the planes *x-y* (front view) and *z-y* (side view) intersecting the centre of the front left thermal manikin's head, as illustrated by the coordinate cross in Fig. 6.16 (left).

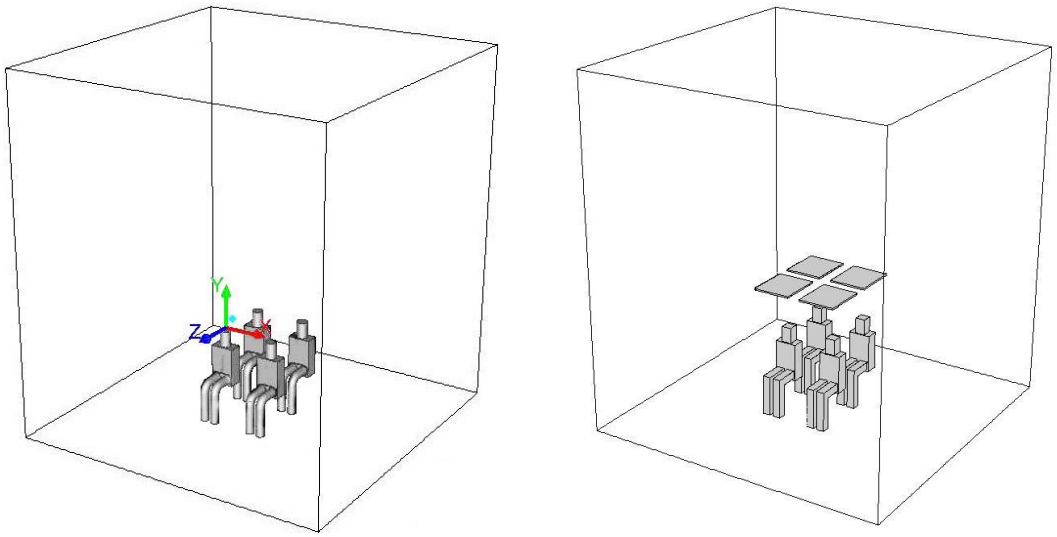

Fig. 6.16 – Simulation setup with detailed (left) and simplified (right) models

Fig. 6.17 presents the isolines of velocity magnitude in the room for both computational cases in the vertical planes *x-y* (front view) and *z-y* (side view). The reference simulation with the detailed models of thermal manikins was compared to the simulation with the simplified models.

The thermal plumes patterns are resembling each other in both computational cases at the region above the SBCs, especially close to the ceiling. Merging of the four thermal plumes is obvious in both cases, although it is more noticeable above the detailed models due to the lower merging height in this reference simulation. Especially in the side view, it is possible to see that the thermal plume above the front seated manikin rises in a slightly different way when comparing the simulations with detailed and simplified models. In the case with the detailed models, it is deflected more from the vertical direction and rises more towards the rear manikin than in the case with the simplified models. However, in the higher region, the thermal plumes merge completely in both simulations and adhere to the ceiling of the room and spread further to the vertical walls in a very similar way.

The formation of thermal plumes under the *SBC* differs significantly in the two cases. There is no convective flow formed around the manikins in the simulation with the simplified models. This deficiency could be solved by placing another *SBC* to the lower height above the floor of the room, see Chapter 6.3. However, the study was targeting the merging of thermal plumes above the heat sources and the air flow nearby the ceiling, therefore the mentioned deficiency could be neglected.

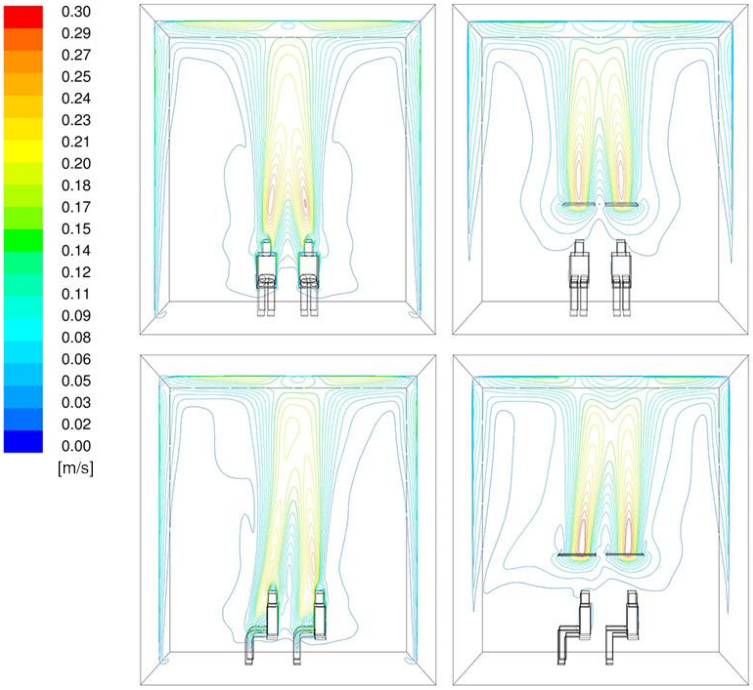

Fig. 6.17 – Velocity magnitude isolines, detailed (left) and simplified (right) models (top – front view; bottom – side view)

Velocity profiles

For a more detailed comparison of the results, it is better to evaluate velocity profiles of the rising thermal plumes. They were determined for both simulations at 10 heights above the manikins. See Annex I for the positioning of data acquisition points. The results are displayed in Fig. 6.18 and Fig. 6.19 for the heights 1.0 m and 3.6 m above the head of the thermal manikins, in the vertical planes *x*-*y* (front view) and *y*-*z* (side view), intersecting the centre of the head of the front left manikin.

There are obvious differences in the velocity profiles determined for each simulation at the height 1.0 m, see Fig. 6.18 (ΔH = 1.0 m) and Fig. 6.19 (ΔH = 1.0 m). For the two simulated cases, the reference one with the detailed models of thermal manikins provides narrower flow with lower maximal velocity at the corresponding height and individual thermal plumes adhering more to each other. It is possible to see that the thermal plume above the front manikin is deflected from the vertical direction towards the rear manikin, see Fig. 6.19 (ΔH = 1.0 m). In the case of simplified models, the thermal plumes above the front and rear thermal manikins remain less influenced by each other.

The higher above the manikins, the more the thermal plumes resemble each other in the two simulated cases, see Fig. 6.18 (ΔH = 3.6 m) and Fig. 6.19 (ΔH = 3.6 m) for example, presenting the velocity profiles nearby the room's ceiling. Although the plumes in the simulation with the simplified models are not fully merged yet, they are very close to the plumes in the simulation with the reference models. The absolute velocities, in both cases, are comparable and it can be expected that the full merging in the simplified case would be achieved if the space was higher. This deficiency could be solved by placing the prescribed *SBC* lower above the thermal manikins' heads, so the merging would be achieved sooner in the case with the simplified models too. However, depending on the problem on hand, this may not be necessary (for example, when the primary interest is to simulate air flow in the higher regions above the floor).

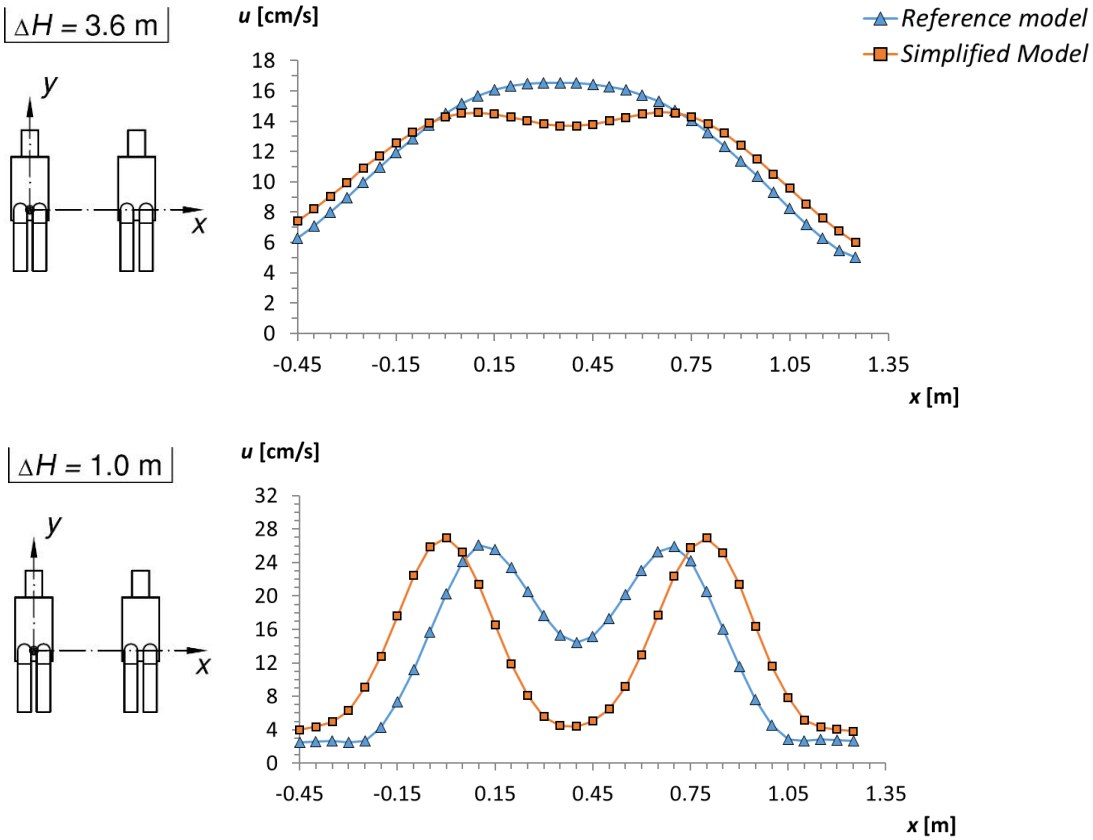

Fig. 6.18 – Velocity profiles in the vertical plane x-y, at two different heights ΔH above the manikins

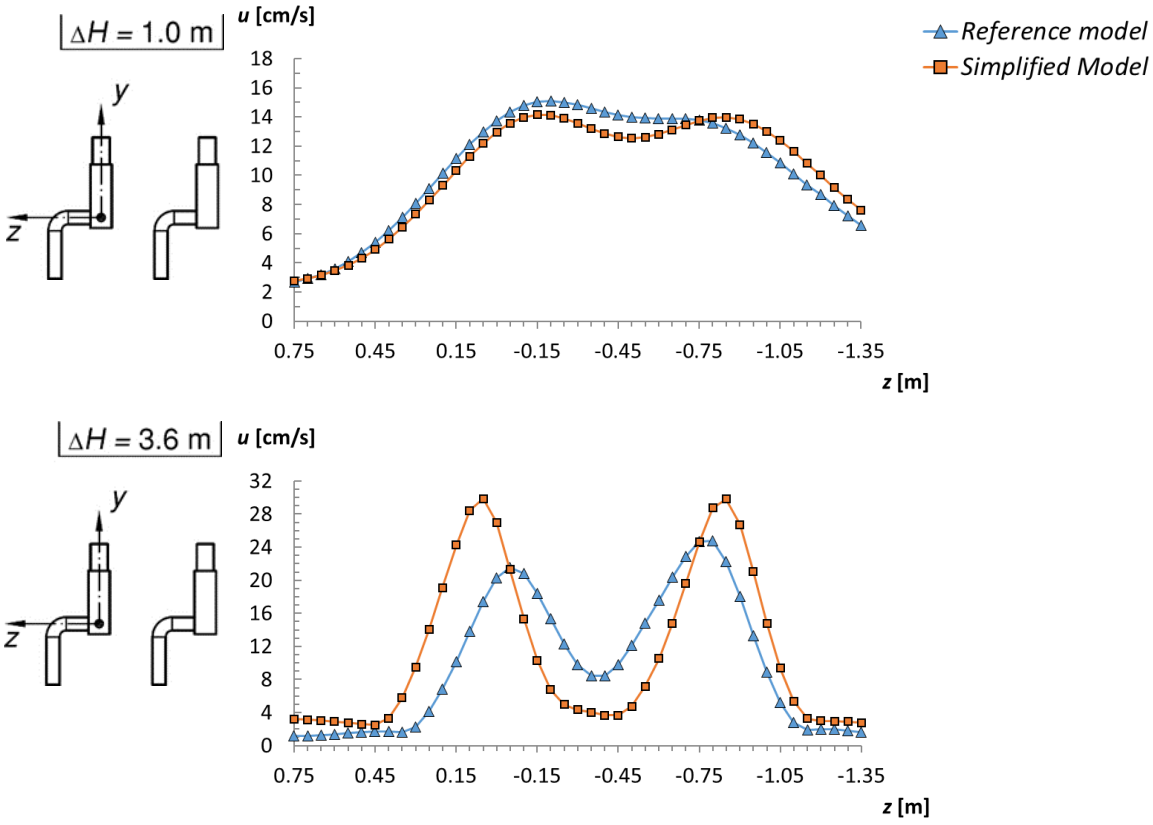

Fig. 6.19 – Velocity profiles in the vertical plane y-z, at two different heights ΔH above the manikins

Temperature profiles

The non-dimensional temperature profiles were evaluated according to the formula (5.1) at 10 heights above the manikins for both simulated cases. Such profiles may be used to prescribe boundary conditions inducing the thermal plumes above the simplified models of heat sources in more complex cases.

The non-dimensional temperature profiles are influenced by the simplification of the heat sources in a way similar to velocity profiles, see Fig. 6.20. The results are displayed for the heights 1.0 m and 3.6 m above the thermal manikins in the vertical plane *x-y* (front view).

Slower merging of the individual plumes above the heat sources in the simulation with the simplified models causes deficiency of the results. Although in the higher regions the thermal plumes from reference and simplified simulation resemble each other closely, it is possible to see that the merging of the plumes in the simulation with the simplified models is not completed yet.

The maximum temperature difference between the two profiles at the corresponding height was 0.3 K. The temperature in the case with the simplified models was lower in almost all the points and it was more varying than in the reference simulation. See for example Fig. 6.21 showing the temperature profile at the height 1.0 m above the manikins.

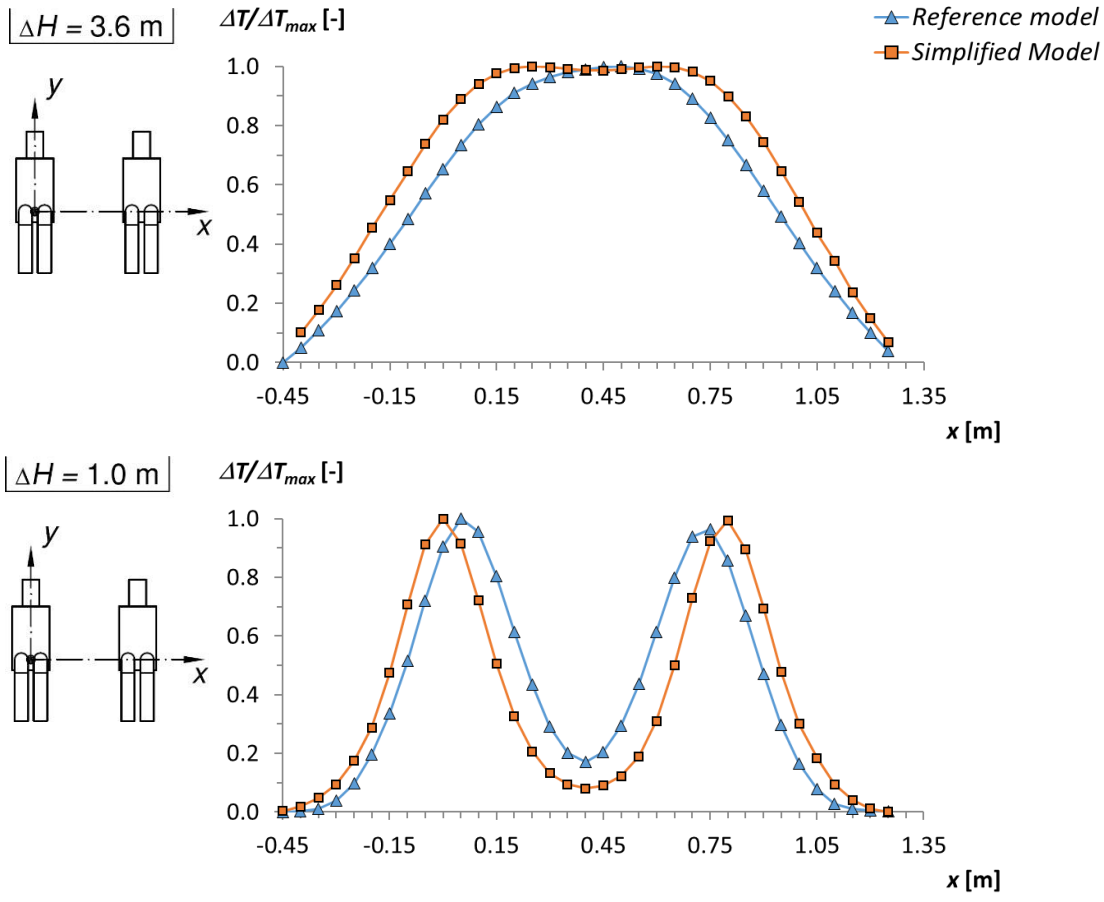

Fig. 6.20 – Non-dimensional air temperature profiles in vertical plane x-y, at two different heights ΔH above the manikin

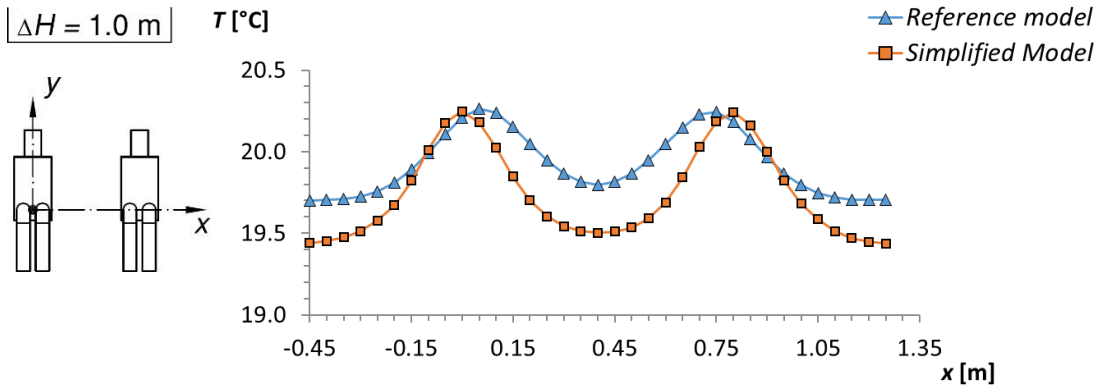

Fig. 6.21 – Air temperature profile in vertical plane x-y, 1.0 m above the manikin

Momentum of the thermal plumes

Momentum transfer rate of the raising thermal plumes was evaluated and compared for both simulations in order to assess the influence of the simplification. The momentum flux was calculated as an integral over a rectangular region with dimensions 2.2 x 2.5 m, intersecting the raising thermal plumes at the height 2.4 m above the heads of the thermal manikins. Custom field function programmed in ANSYS Fluent was used to enable the calculation following the formula (6.4), where $\dot{I}$ is the momentum transfer rate, u_y is vertical velocity of the air flow and ρ is air density.

$$\dot{I} = \int_A u_y^2 \rho \cdot dA \tag{6.4}$$

The momentum transfer rate of the raising thermal plume was 0.057 kg·m/s^2 in the simulation with the reference models and 0.052 kg·m/s^2 in the case with the simplified models, which is lower by 9 %. This indicates that the proposed simplification of heat sources can slightly underestimate the momentum of the rising thermal plumes and their potential influence on the air flow in the simulated spaces.

6.5 Computational demands

Four computational cases with sitting thermal manikin placed in the middle of an enclosed room were simulated in order to show the effect of the simplification on the speed of simulations. The thermal manikin was modelled in detail in the first case and in the other three cases, it was simplified according to the proposed method. The simplification setups were identical to the ones described in Chapter 6.3.

Tab. 6.2. summarizes the total number of computational cells in all the compared cases and computational time necessary for 10 iterations. All the simulations were calculated in the same way and with identical set-up during the testing calculations. The flow was considered as unsteady and 10 iterations were calculated for each time step of 0.1 s. This test was performed on the computer with 8 CPUs AMD Opteron 8378 (frequency 2.4 GHz) and 128 GB of operational memory. From the summarized values, it is possible to see the advantage of substituting the heat source by a simplified boundary condition. The size of the computational case as well as the computing time necessary for simulation are less than half of the case with the detailed model of the thermal manikin.

Tab. 6.2 – Comparison of mesh cell number and computing time

Computational case	Mesh cells	Computational time	
Thermal manikin	3 569 984	130 s	100 %
1 *SBC*	1 469 837	45 s	35 %
2 *SBCs* (calf/above head)	1 548 459	51 s	40 %
2 *SBCs* (waist/above head)	1 538 362	51 s	40 %

6.6 Development of UDF for practical use

The usability of the proposed method for more complex cases with higher number of heat sources can be enhanced by using the User Defined Function (UDF) tool which is available in ANSYS Fluent. The velocity and turbulent quantities of the induced flow can be prescribed in absolute values. The temperature of the convective flow may be prescribed as relative to the reference ambient temperature. The workflow of the programmed UDF which was used by Zelenský et al. (2015) in the performed study targeting air flow simulation in a large cultural space is described below. For more details see Annex IV.

1. set the local coordinate system with the origin in the geometrical centre of the *SBC*;
2. get the reference temperature in the vicinity of the *SBC*;
3. calculate the temperature profile of the convective flow on the basis of the reference temperature;
4. prescribe the boundary condition for the temperature;
5. prescribe the boundary condition for the vertical velocity;
6. prescribe the boundary conditions for the turbulent quantities k and ε.

6.7 Results summary

A new modelling method to represent heat sources in CFD simulations of indoor air flow was proposed enabling faster CFD simulation of indoor air flow. It is based on the substitution of heat source model by simplified boundary condition(s). The method was tested by several numerical studies.

Four CFD simulations with simplified model of one thermal manikin with four different vertical positions of the *SBC* (35 mm, 200 mm, 450 mm and 700 mm above the manikin) were compared mutually and with a detailed reference case. From the obtained velocity fields, velocity profiles and temperature profiles, it is obvious that the results of simulations with the simplified models correspond well to the detailed reference case in the regions above the *SBC* in most of the simulations. The best results were obtained in the simulations with the *SBC* positioned 450 mm and 700 mm above the head of the thermal manikin, where the rising thermal plume is considered to be fully developed. The case with the *SBC* in the close vicinity of the manikin's head (35 mm above it) showed reasonable correspondence with the reference simulation as well. However, the results of the simulation in the case with the *SBC* positioned 200 mm above the thermal manikin differed noticeably from the reference case. The induced thermal plume in the simplified simulation was slower with lower air temperature. Thus, it can be advised to position the *SBC* at a reasonable height above the heat source, where the thermal plume is fully developed, if the problem on hand allows it (i.e. in the simulation of a room with sufficient space above the heat sources). If it is for some reason necessary to position the *SBC* in a closer vicinity to the heat sources (for example, rooms with a low ceiling), a CFD study should be performed, in order to

test the correctness of the boundary condition defined on the basis of the reference detailed simulation.

In the regions below the *SBC*, the results with the simplified models did not correspond to the reference case. This issue was addressed by adding another *SBC* in a lower height. Three CFD simulations with simplified model of one thermal manikin in three different configurations of the *SBCs* were compared mutually and with the reference case. From the obtained velocity fields it is obvious that the combination of *SBCs* has a significant influence on the simulation results. Thermal plumes from individual computational cases differ from each other especially at lower regions (under the upper *SBC* and around the object substituting the heat source). The thermal plume in the model with two *SBCs*, when the lower *SBC* is placed in the level of the thermal manikin's waist, is the most corresponding to the reference case, even though that it is still partly deficient.

The effect of the simplification on the merging phenomenon of individual thermal plumes rising above multiple heat sources was demonstrated in a study with four thermal manikins sitting close to each other. Although the thermal plume above the simplified models differs from the thermal plume in the simulation with the reference models, the difference decreases with the increasing height above the heat sources. In both simplified and detailed simulations, the thermal plumes are merging in a similar way nearby the ceiling of the modelled room, although in the simplified case they do not merge completely. For room with high ceilings, it can be expected that the thermal plumes would merge completely also in the case with the simplified models and rise further in the same manner as in the simulation with the detailed models.

The comparison of the thermal plumes momentum transfer rate in the two performed simulations with multiple heat sources indicates 9% underestimation in the case with the simplified models. This should be taken into account during further use of the method.

The simplification in the described arrangements of *SBCs* could be suitable especially for the evaluation of the air flow in higher regions, where the thermal plumes in simplified cases correspond very well to the reference flow above the detailed model of the heat source. Lower demand for computing time has been demonstrated by a numerical study with one heat source modelled in different levels of simplification. It was found that even in such a simple case the reduction of the computational time can be up to 65 %. Additionally, an UDF for ANSYS Fluent was developed in order to further facilitate the use of the method for practical applications.

7 CASE STUDY – CONCERT HALL HOUSED IN A FORMER CHURCH

The previously developed modelling approach to represent heat sources in CFD simulations was applied in a real scenario of the former church of St. Anna, a 14th century gothic building located in the Old Town of Prague (hereinafter referred to as *the church)*. It was desecrated at the end of the 18th century, recently completely reconstructed and it now serves as a community centre and universal space suitable for events such as concerts, conferences, etc., with the total capacity of up to 350 visitors staying for different time periods during a day. The eastern part of *the church* interior after reconstruction is displayed in Fig. 7.1. A study based on the results of CFD simulations with simplified models of visitors acting as heat sources under two different occupancy scenarios was elaborated by Zelenský et al. (2015).

Fig. 7.1 – Interior of the church after reconstruction

Adaptation of historical buildings to a new function always brings a question about the influence of the indoor environment change on the building structures. This question arose also during the restoration works in 2001. It was presumed that the large number of visitors could have a crucial effect on the environment inside *the church*. It was possible to use only natural ventilation through window openings on the street level and the windows in the roof, so that the original look of the building was preserved.

The main impact of occupants on the air flow is caused by convective currents generated by human bodies. Warm air is driven upwards by buoyancy forces and forms a rising thermal plume above each heat source. The biggest concerns were indoor air flow velocities and air temperature distribution in the vicinity of the internal wall surfaces (Barták, Drkal, Lain, et al. 2001). The design team had to assess the possible negative effects of the changes in the indoor environment of *the church* on the original stucco decorations on its walls and the original wooden roof trusses.

Building energy simulation (BES) and simple CFD study were used to tackle this uneasy task (Barták, Drkal, Hensen, et al. 2001). Detailed CFD modelling and simulations of natural convective flows generated in ventilated and air-conditioned spaces are quite demanding for computing power and time. Therefore, the original CFD simulation used by the design team in 2001 did not contain explicitly modelled indoor heat sources. The natural ventilation of the indoor space was emulated by prescribed pressure difference between the internal space of *the church* and the surrounding environment, which was pre-calculated using BES. The floor of the model was heated in order to mimic the thermal gain from the occupants. Yet, the explicit modelling of heat sources is important, as they can be important for the appropriate air change (Xing et al.

2001; Skistad et al. 2002) and they can significantly influence air flow distribution indoors as well as the indoor environment quality (Awbi 2003; Zbořil et al. 2007; Zukowska 2011).

The following case study elaborates on the CFD simulations of the indoor air flow inside *the church* with two different occupancy scenarios: 65 and 304 visitors. The models of the visitors were represented according to the previously developed method based on the replacement of each heat source by a simple boundary condition of convective flow, which was determined in advance from a detailed simulation of a thermal plume above a comprehensive model of the heat source. The influence of each heat source on the overall air flow pattern is preserved, while the computational demands of the simulation are lowered, enabling e.g. variant studies.

The target was to investigate the influence of the visitors acting as heat sources on the air flow near the stucco decorations and the wooden roof trusses of *the church*. The results of the simulations with 65 and 304 visitors are compared mutually and also with the simulation without the explicitly modelled visitors. The effect of the heat sources on the indoor air flow, temperature stratification and ventilation rates are studied. The study also demonstrates the usability of the previously developed modelling method to represent indoor heat sources in complex real situations.

7.1 Numerical model of the church

The modelled building is a former single-nave church with the main enclosure of approx. 9,630 m^3 total volume and the basic external dimensions (width x length x height) of approx. 11.4 x 43.5 x 29.2 m. The western half of the nave is divided by a gallery located 6 m above the ground floor, see Fig. 7.2.

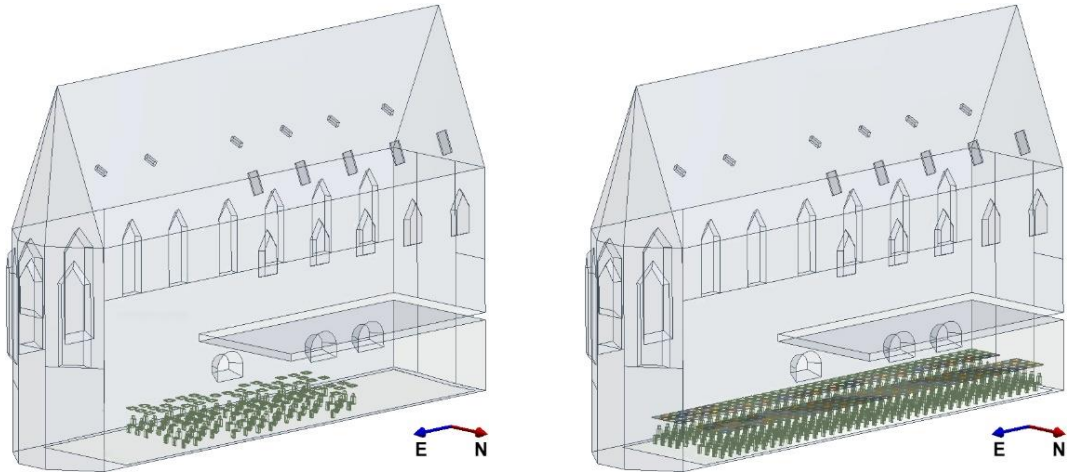

Fig. 7.2 – Models of the church, 65 (left) and 304 (right) seated visitors

The church has three large window openings on the street level and eleven small window openings in the roof, six of them on the south-facing side and five of them on the north-facing side. Only natural ventilation through these openings is possible to use.

Two numerical models of *the church* with a different number of seated visitors were created in the ANSYS Design Modeller. Both models include a 1.5 m wide region of external space surrounding *the church*, in order to simulate the process of natural ventilation, see Fig. 7.3. The first model represents almost fully occupied space with 304 seated visitors distributed in two rows, the second model represents lowly occupied space with 65 seated visitors. Both cases are shown in Fig. 7.2.

The individual occupants were considered in the CFD simulation. However, their models had to be simplified, in order to lower computational demands of the simulation. All the visitors were considered to be identical (with the same geometry and heat output) and substituted by a repeatedly used simplified model based on the previously developed method. The *SBC* was placed 0.7 m above each visitor, considering sufficient space above the auditorium in *the church* (the gallery is 6 m above the ground floor).

The building interior and the external space surrounding the building was divided by an unstructured tetrahedral grid. In the model with 65 visitors there were more than 17.9×10^6 control volumes and in the model with 304 visitors more than 28.6×10^6 control volumes. The minimum size of a cell was in both cases 25 mm and the maximum was 250 mm. A fine mesh was created especially in the space of the auditorium and near the walls.

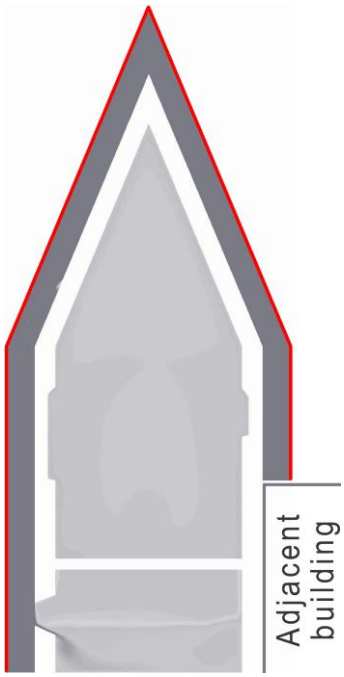

Fig. 7.3 – Boundaries facing the surrounding env. (in red)

The boundary conditions of the surfaces facing the surrounding environment (Fig. 7.3, in red) were specified as a free boundary with zero pressure gradient. The boundary conditions of the internal surfaces of *the church* were defined in two different ways. At first, constant temperature of the internal constructions were prescribed on the basis of the previous multi-zonal BES simulation, performed during the first stage of the project preparation (Barták, Drkal, Lain, et al. 2001). Results with this approach were presented in Zelenský et al. (2015). The initial study was extended by additional simulations with the composition of the building constructions prescribed in the model and the temperature of the internal surfaces calculated by the solver, i.e. the thermal conduction through walls was taken into account.

The external air temperature was set to –7 °C, as winter conditions were considered. From two sides, *the church* is partially surrounded by other occupied buildings, with the indoor temperature being considered as 20 °C. The temperature of the ground under the floor was considered to be 5 °C. See Annex IV for the composition of the individual constructions of *the church* as shown in Fig. 7.4. All the walls of *the church* are from marlstone and the windows are single glazed. Results of the extended study considering the thermal conduction through the building constructions are presented below.

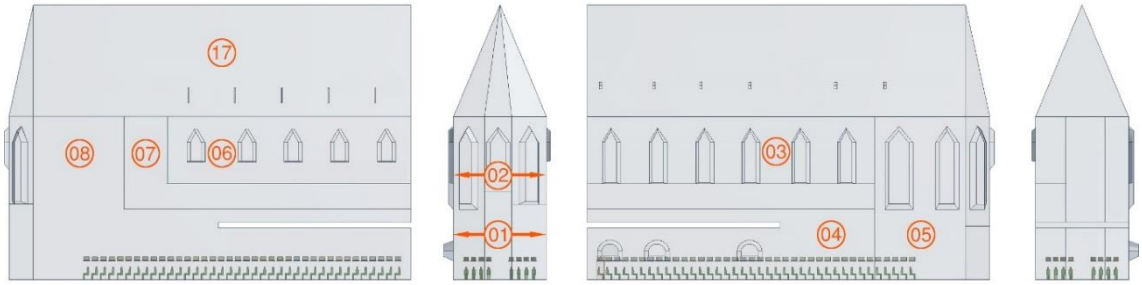

Fig. 7.4 – Constructions of the church – for more detail see Annex IV

7.2 CFD Simulations

The CFD simulations were solved in the software ANSYS Fluent 16.0 as a non-isothermal flow of incompressible ideal gas (air). The flow in the proximity of the walls was solved using wall functions. The two-equation turbulence model by Launder and Spalding (1974) – so called *k-ε Standard* – was used, extended with respect to the influence of temperature and buoyancy on the turbulence.

The Body Force Weighted scheme was chosen for the discretisation of the pressure term as it is recommended for buoyancy driven flows (ANSYS 2013). The convective terms were solved using a second order upwind scheme. A coupled and steady-state solver was used to obtain the pressure and velocity fields.

The evaluation of the results targeted at the influence of heat source on the indoor environment inside *the church*, especially on the air flow patterns, temperature stratification and air change rates.

CFD simulations of the indoor air flow with a prevailing effect of natural convection caused by low temperature differences are always challenging and the calculation tends to be slow and unstable. The convergence criteria were achieved after more than 4,000 iteration in the case of the simulation with 65 visitors and more than 5,000 iterations in the case of 304 visitors. However, both simulations were run for additional 5,000 iterations. All the residuals reached the order of 10^{-4} or less, excluding the residuals of continuity equation, which reached the order of 10^{-3}. This could have been caused by the instability of the convective flow. The convergence was proved on the basis of the total mass flux balance in the whole computational domain, which reached approx. $4 \cdot 10^{-2}$ kg/s in both simulated cases. This is reasonable, considering that it is approximately 1 % of the absolute value of the mass flow rate in the computational case. The imbalance occurred on the boundary facing the surrounding environment.

7.3 Results analysis and discussion

Images of the velocity and temperature fields in *the church* were evaluated. The velocity vectors, the isolines of velocity magnitude and the contours of temperature were evaluated in one vertical plane *y-z* (side view) intersecting the geometrical centre of the building and five vertical planes *x-y* (front view) intersecting *the church* with a spacing of 7 m.

Velocity fields

The velocity vectors in the vertical plane *y-z* intersecting the centre of *the church* (side view) for the case with no explicitly modelled heat sources from the simulation performed during the study of Barták et al. (2001) are displayed in Fig. 7.5; Fig. 7.6 shows the velocity vectors and isolines of the velocity magnitude of two simulated cases with the models of visitors represented using the previously developed method.

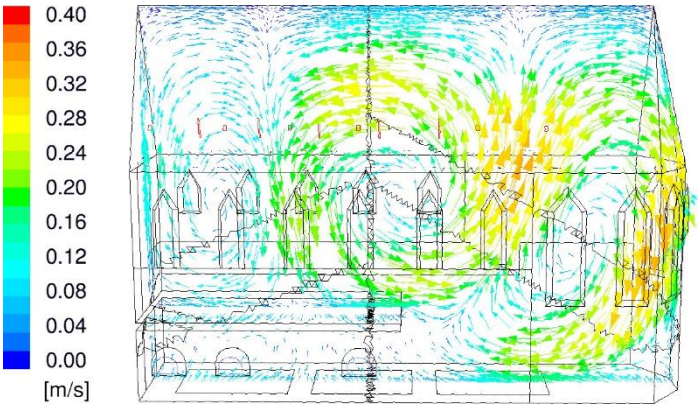

Fig. 7.5 – Velocity field in the case without explicitly modelled heat sources (velocity vectors) (Barták, Drkal, Lain, et al. 2001)

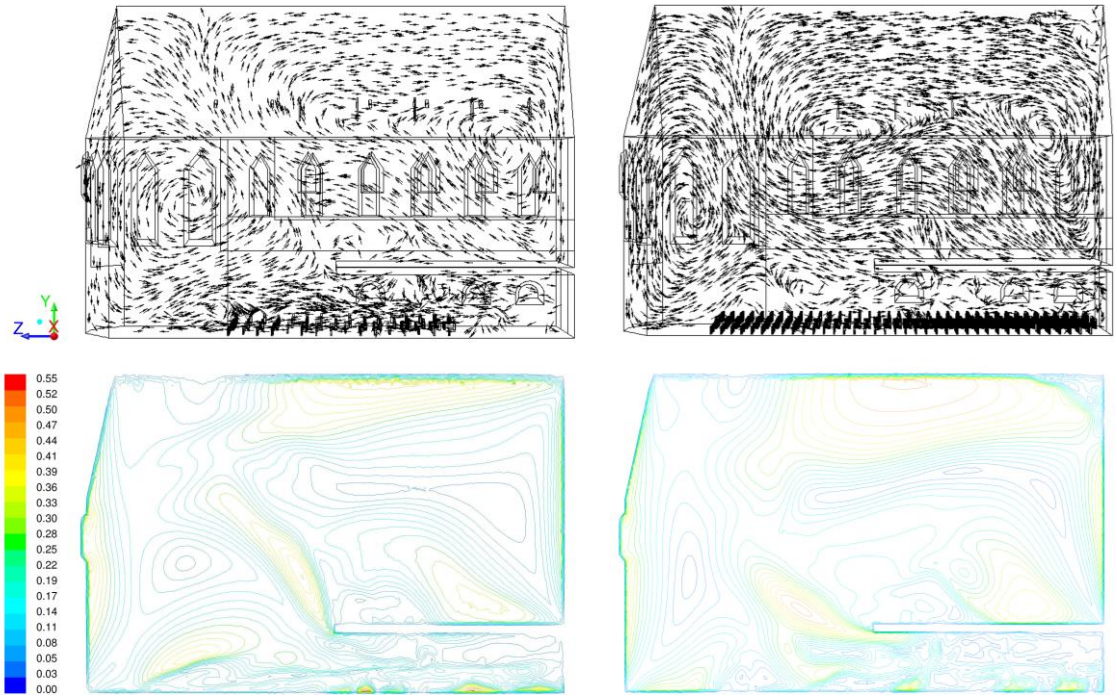

Fig. 7.6 – Velocity fields in the case with 65 visitors (left) and 304 visitors (right)
- Upper: velocity vectors
- Lower: velocity magnitude isolines

Comparison of the velocity fields in the three presented simulations shows that the explicit modelling of the visitors acting as heat sources significantly affects the results of the simulation. In the case without the explicit models of visitors (Fig. 7.5) there are two large vortices above the raised gallery in the western part of *the church* and one large vortex in the eastern part of the building. However, in both cases with the models of visitors (Fig. 7.6), the vortices above the gallery merge in one large circulation flow. This may have been caused by a strong thermal plume, which is formed above the models of visitors and rises from the space under the gallery, see Fig. 7.8, showing a velocity field 21 m from the east-facing wall of *the church*. Also, it is possible to see that in the case with 304 visitors there is a stronger air circulation in the space of *the church* than in the case with 65 visitors, although the flow trajectories resemble each other.

The visitors have a significant influence also on the environment in their close vicinity. There is a very low air circulation under the gallery in the simulation without the explicitly modelled visitors. The presence of the visitors in the space causes a strong mixing of the air flow in the other two cases, as shown in Fig. 7.7.

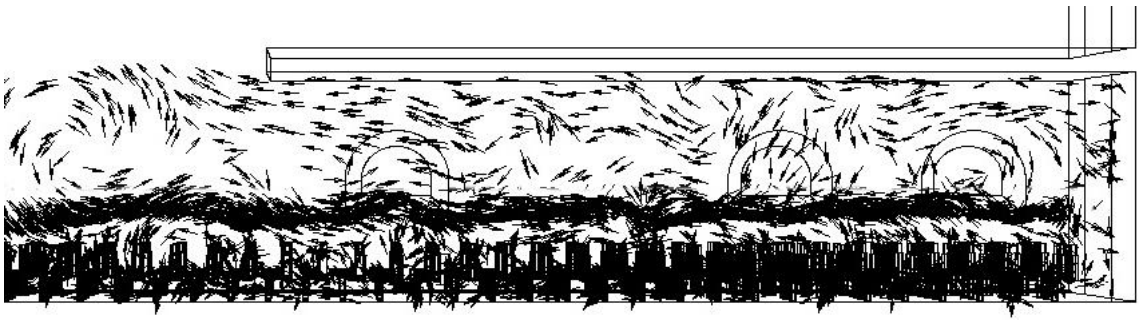

Fig. 7.7 – Air circulation in the space under the gallery

The large windows on the east facing side of the building (on the left side of the displayed intersections in Fig. 7.5 and Fig. 7.6) have a strong influence on the air flow in *the church* as well. The air is cooled down on the glazed surface and falls down towards the floor. The falling flow does not fully reach the auditorium in the two simulations with the visitors, as it is turned upward by the convective flow rising from the space under the gallery. This is different from the case without the explicitly modelled heat sources.

The maximal air flow velocity was below 0.65 m/s in all of the three simulated cases. The maximum velocities in both simulations with the models of visitors are in the space under the gallery, where the ventilation air enters the building through the three window openings on the street level. This may be the main concern, as the fast cold flow directly enters the space with the sitting visitors and it could cause their discomfort. The visitors acting as heat sources consequently influence the distribution of this flow in the rest of the space. Nearby the walls, the air flow velocity does not exceed 0.45 m/s.

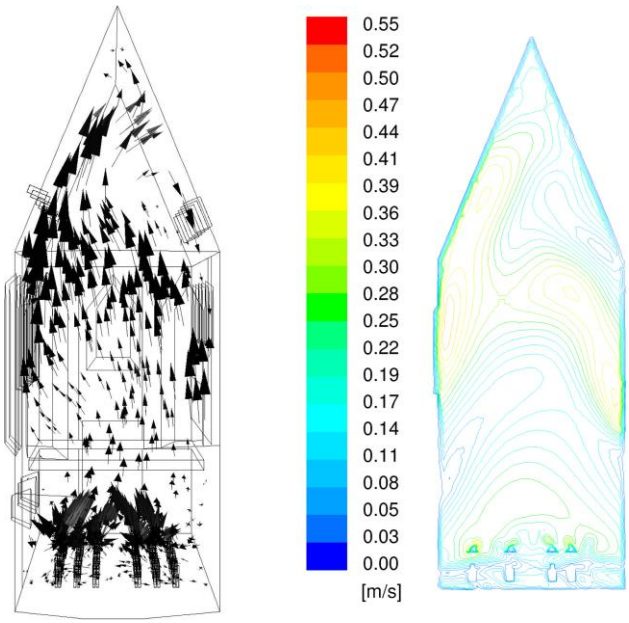

Fig. 7.8 – Velocity field in the case with 65 visitors
- Left: velocity vectors
- Right: velocity magnitude isolines

Temperature fields

The temperature distribution in *the church* was evaluated on the basis of the temperature contours in one vertical plane *y-z* (side view) and five vertical planes *x-y* (front view). The selected cross-sections for the cases with 65 and 304 visitors are displayed in Fig. 7.9 and Fig. 7.10.

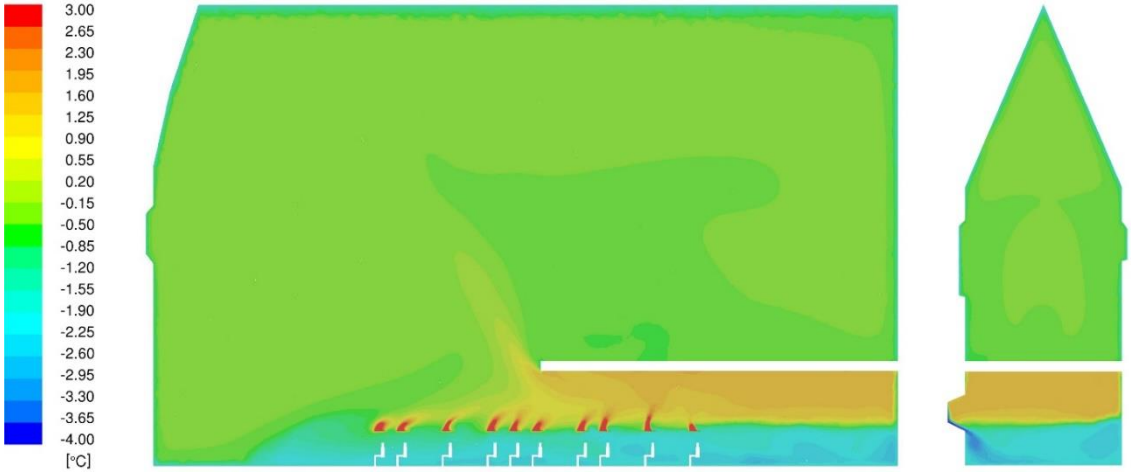

Fig. 7.9 – Temperature field, simulation with 65 visitors (isosurfaces of temperature)

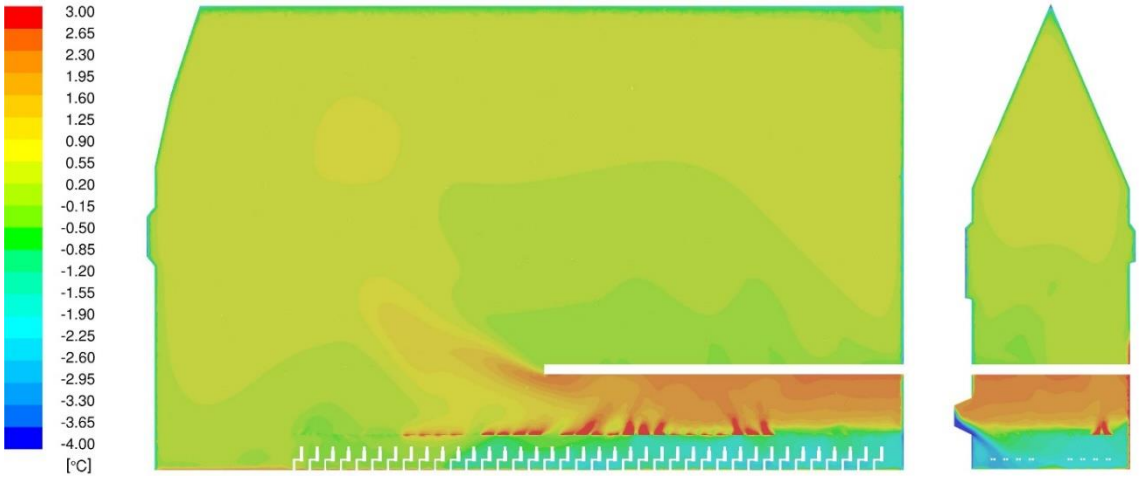

Fig. 7.10 – Temperature field, simulation with 304 visitors (isosurfaces of temperature)

The influence of the visitors acting as heat sources is obvious. In the case with 65 visitors, the space below the gallery in the western part of *the church* is colder with more gradual stratification. In the case with more visitors, the supplied air is heated up faster and the influence of the cold air flow from the low window openings is decreased.

While the lower regions of *the church* are strongly influenced by the visitors, the remaining space shows better thermal stability. The temperature fields in the higher regions are almost uniform in both simulations, without any significant stratification. The only disturbances are the warmer plumes rising from the space below the gallery, with the temperature higher by approx. 0.5 K than the surrounding air.

The average temperature in *the church* increased by 1.1 K due to the increase in the number of visitors from 65 to 304. This relatively small temperature change should not have a negative effect on the preserved internal constructions of the building. The main concern may be very low temperatures in the space of auditorium, caused by the cold air supply from the low window

openings. The temperatures in both simulations are in this region below 0 °C, which is unacceptable considering the thermal comfort of visitors. It should be considered that the methodology used to simplify indoor heat source models does not perform well in the low regions above the ground and it can be expected that the temperature above the ground (up to a height of approx. 2 m) would be higher in reality, with a more gradual thermal stratification. However, some heating system should be used during winter days.

Ventilation flow rates

In both simulated cases, where the visitors were modelled using the developed method to represent heat sources, the ventilation flow rates have been evaluated by summing up the volume flow rates through the low window openings, see Tab. 7.1. The supplied volume per visitor was calculated.

Tab. 7.1 – Ventilation rates

Simulated occupancy	Ventilation flow rate	Flow rate per visitor
65 visitors	1.07 m^3/s	16.5 L/s
304 visitors	1.35 m^3/s	4.4 L/s

The supplied volume of fresh air is more than sufficient for this type of space in both simulated cases. The recommended value of the volume flow rates for the auditorium seating area is 2.7 L/s per person (ASHRAE 2003). The volume of fresh air per visitor in both simulated cases exceeds this minimal rate and the natural ventilation should be sufficient for the case of *the church*. However, according to Czech standards, the minimal recommended volume flow rate for occupied spaces is 5 L/s per person (ÚNMZ ČR 2010), so the case with 304 visitors would not comply with the recommendation. Although this recommendation is indicated for forced ventilation systems only, it should be taken into account.

In situations with less visitors in *the church*, it can be advised to reduce the opened area of the window openings and reduce the air flow rates. In the simulated cases with fully opened windows, the cold air flow supply enters the space of the seated visitors with the velocity reaching 0.65 m/s, which could cause discomfort. Partial closing of the window openings may reduce the risk of draught in the auditorium. In addition, the internal air temperature will increase. In the situation with 304 visitors the partial closing of the windows should be accompanied by the installation of a heating system in *the church*, so the driving force of the natural ventilation will increase and the minimal fresh air flow rate per visitor will be met.

7.4 Case study outcomes

Two CFD models of *the church* with two different occupancy scenarios (65 and 304 visitors) were created in order to study the influence of the indoor heat sources (visitors) on the environment inside the building. The models of the heat sources were represented by simple boundary conditions generating thermal plumes. The CFD simulations were, aside of the mutual comparison, compared also to the simulation without explicitly modelled heat sources (Barták, Drkal, Lain, et al. 2001).

It was shown that the presence of the visitors influences velocity patterns in the whole space and the temperature fields, especially in the regions close to the floor. The higher regions of *the church* show a good thermal stability.

The indoor air velocities in the close vicinity of these structures do not exceed 0.45 m/s. The building's thermal environment shows good resistance to the occupancy fluctuation as well, especially in the higher regions, at the location of the preserved building structures and the original wooden roof trusses. The increase in the number of visitors from 65 to 304 caused an increase in the average temperature in the space of only 1.1 °C, with only a small change in the temperature fields in the higher regions. The ventilation flow rate of *the church* increased from the 1.07 m^3/s in the case of 65 visitors to the 1.35 m^3/s in the case of 304 visitors.

It has been shown that natural ventilation of the building in the winter period is a feasible option, as it effectively removes heat gains from the visitors and provides enough fresh air. It can be recommended to use a heating system during winter, as the indoor air temperature is very low even in the case with 304 visitors, which would have a negative effect on the comfort of the visitors. Another concern may be the cold air supply from the low window openings that directly enters the space of auditorium, with the velocity reaching 0.65 m/s. A partial blocking of the windows could reduce this fast cold air flow.

In addition, it has been shown that the previously developed modelling method to represent indoor heat sources in CFD simulations is suitable for this type of study. The proposed method enabled the simplification of both heat sources' geometry and computational mesh around them, but it preserved the rising thermal plumes patterns. Thus, the possibility of the variant CFD simulation study was enhanced and the obtained results were more realistic in comparison with the simulation without the explicitly modelled heat sources.

8 RESEARCH ACHIEVEMENTS AND CONTRIBUTIONS

8.1 Theoretical contributions

The main theoretical contribution of the current research is the new modelling method to represent heat sources for numerical studies of indoor air flow by CFD simulations. It is based on the replacement of a heat source by one or more appropriately positioned simplified boundary conditions (in this study referred to as *SBCs*) inducing a thermal plume potentially identical to the one rising above the real heat source. It enables simplification of the heat source model geometry and reduces the requirements on the computational mesh around it, while it preserves the thermal plume pattern above the heat source in the simulation. Although in the current research the method was applied to models of occupants, it can be in general used to represent any other indoor heat source.

The method was validated, tested and described in detail for further use or adaptation. In order to make the new modelling approach universal with respect to different ambient thermal conditions, the boundary condition inducing the thermal plume was derived using a non-dimensional temperature profile.

Aside of the new modelling method to represent heat sources, the following two contributions for theory can be mentioned.

Thermal plumes development in different ambient air temperatures

The current research brings a better understanding of the behaviour of thermal plumes rising above heat sources under different ambient air temperature conditions. The issue was initially studied on the basis of a semi-empirical formulae available in the literature. However, the influence of the ambient air temperature is not fully described in the available publications. Therefore, an additional numerical study targeting thermal plume development around a thermal manikin under different temperature conditions was conducted.

It was demonstrated that the velocity profile of the thermal plume does not depend on the ambient air temperature, providing that the heat output of the heat source is constant. On the other hand, the ambient air temperature influences the absolute values of air temperature in the thermal plume, while non-dimensional temperature profile of the thermal plume is not significantly influenced.

Modelling of turbulence in CFD simulations of thermal plumes generated by people indoors

Another contribution to theory is the discussion of the optimum turbulence model for CFD simulations of thermal plumes rising above heat sources indoors. A numerical study was conducted targeting the performance of the k-ε and k-ω two-equation turbulence models that are the most frequently used for CFD simulations in the field of indoor air flow.

It was shown that the choice of a particular turbulence model affects the turbulent mixing and consequently the spreading rate of the thermal plume and its velocity and temperature profiles. The velocity and the temperature decay of the thermal plume along the vertical distance from the heat source is influenced as well.

The turbulence models of k-ε type have been found more appropriate for the simulation of thermal plumes caused by natural convection than the k-ω model, which significantly underestimated turbulent mixing in the thermal plume and produced results that were too different from the measurements. The k-ε *Standard* turbulence model, proposed by Launder and Spalding (1974),

produced results which showed the best agreement with the experiment. The use of this turbulent model was recommended for CFD simulations of thermal plumes above heat sources.

8.2 Practical contributions

The proposed method to represent heat sources in CFD simulations of indoor air flow enables faster preparation of numerical models, easier and faster meshing, it decreases the number of computational cells in the domain and consequently reduces the computational time. It facilitates simulations of large spaces with large numbers of heat sources and/or variable occupancy patterns, such as various entertainment facilities, industrial premises, lecture halls, etc., which would otherwise be very challenging. The possibility of numerical variant studies of such places is enhanced as well. It is possible to easier prepare a numerical model, solve the simulation faster and reach relevant results more rapidly. Thus, the presented method enables CFD simulations to be more effective part of practical design process.

A lower demand for computing time has been demonstrated by the numerical study with one heat source modelled in different levels of simplification. It was found that even in such a simple case the reduction of the computational time can be up to 65 %.

A user defined function (UDF) for ANSYS Fluent inducing the artificial thermal plume above a simplified model of heat source was proposed in order to facilitate the use of the developed method for practical applications. Based on the previous studies, the velocity and turbulent quantities of the induced flow were prescribed as absolute values and the temperature was defined as relative to the ambient air temperature. The UDF enables easier setup of the simulation with the heat sources represented by numerical models prepared according to the proposed method.

9 CONCLUSION

The main goal of the dissertation work was to identify the current methods of indoor heat sources modelling, ascertain their limitations and propose a new modelling method to represent indoor heat sources in numerical models for CFD simulations. It was targeting better design of large indoor spaces with high number of heat sources and/or variable occupancy patterns. The aim was to enhance the effective use of CFD simulation for practical applications in HVAC Engineering.

ANSYS Fluent software was used as the main simulation tool, together with the related ANSYS tools for the preparation of geometry and numerical mesh. Various cases of three-dimensional convective flow in the indoor environment were simulated. The results of the experiment in the experimental room were used for validation of the proposed modelling method to represent heat sources in CFD simulations of indoor air flow, together with inter-model comparative testing.

- The current methods of modelling and simplified representation of indoor heat sources in numerical models for CFD simulations were summarized. It has been found that the common approaches to simplify the models based on simplification of shape, boundary conditions and/or operational characteristics are not sufficient in every case. For example, it can be problematic to simulate an environment with high number of heat sources and/or high variability of heat sources distribution, which demands a complex variant studies.

- A modelling method to represent indoor heat source in numerical models for CFD simulations was developed in order to address the limitations of the currently used ways of modelling. The method is based on the substitution of heat source model by one or multiple simplified boundary conditions, which are set at zones (*SBCs*) in the area of the original thermal plume rising around the heat source. The thermal plume is thus induced artificially, i.e. without the need to calculate heat transfer from the heated surface. Although in the current research the method was applied to model a sitting thermal manikin resembling a human body, it can be used to represent any heat source in general.

- The simplification method was tested by several numerical studies targeting the following issues:
  - optimal positioning of the *SBC(s)* inducing the rising thermal plume around the heat source was discussed;
  - the effect of the surrounding air temperature on the rising thermal plume was addressed by the use of a non-dimensional temperature profile prescribed to the *SBC*, since it was proved that the non-dimensional temperature profiles are not influenced by the ambient air temperature;
  - the effect of the simplification on the merging of thermal plumes above the multiple heat sources was studied. It was found that the merging is affected by the simplification. However, the deficiency decreases with the increasing height above the heat sources. In both simplified and detailed simulations, the thermal plumes merged in a similar way nearby the ceiling of the modelled room.

- The testing of the modelling method to represent heat sources showed its suitability for simulation of convective flows in regions above the heat sources. It can be used to simulate the effect of heat sources on the surrounding environment as a whole. It would not be appropriate to use the method for a simulation of air flow in the close vicinity of heat sources, as the generated artificial thermal plume shows a deficiency in this region. It was demonstrated that the method can save time for preparation of numerical models with large number of heat sources and also computational time. It should be taken into account that the

proposed simplification can slightly underestimate the momentum of the rising thermal plumes and thus their potential influence on the air flow in the simulated spaces

- Another target was to assess the influence of the turbulence model selection on the simulated convection flow. A numerical study was performed in order to test various two-equation turbulence models that are the most frequently used in CFD simulations for HVAC engineering. It was found that the choice of a particular model of turbulence affects the thermal plume spreading rate and consequently the axial velocity magnitude and the axial velocity decay with increasing height above the heat source. The main outcome of the study was that turbulence models of *k-ε* type are appropriate for the simulation of thermal plumes. The *k-ε Standard* turbulence model, proposed by Launder and Spalding (1974), produced results which showed the best agreement with the experiment.
- The proposition and testing of the modelling method was followed up by a numerical case study of the former church of St. Anna, a building that nowadays serves as a community centre and universal space suitable for cultural events. Two computational models of the building with two different occupancy scenarios (65 and 304 visitors) were created in order to study the influence of the indoor heat sources (visitors) on the environment inside the building. It was shown that the developed modelling method to represent indoor heat sources is suitable for CFD simulation of the building. The proposed method enabled simplification of the heat sources' geometry and computational mesh around them, but it reasonably preserved the pattern and influence of the rising thermal plumes on the surrounding environment as a whole. Thus the possibility of a variant CFD simulation study was enhanced.

The proposed method can be used especially for CFD simulations of environments with high quantity of indoor heat sources and/or numerical studies of environments with high variability of heat sources' distribution, where it is problematic to model each heat source in detail. Various entertainment facilities, industrial premises, lecture halls, atriums, etc. can be mentioned as possible applications. The detailed models of occupants and other heat sources can be effectively simplified and the computational burden of CFD simulations is lowered. The method is intended to be applied for simulations of overall air flow in the indoor environment. The method is not appropriate for simulating air flow in the vicinity of the heat source. In such case a very detailed computational model should be used.

The goals of the dissertation thesis have been met; nevertheless, there are issues that could be further investigated. The presented method could be adapted in order to simulate emission of contaminants and water vapour by the source (as heat sources often release also other substances). The *SBC* can be extended by a boundary condition of contaminant and/or water vapour emission. This adaptation, after its validation, would increase the usability of the method for numerical case studies targeting, for example, indoor contaminants spreading and distribution, condensation on the room surfaces, ventilation efficiency etc.

In order to make simulations of large groups of heat sources more accurate, the interaction of thermal plumes rising above individual heat sources can be taken into account already during the preparation of the simplified models, following the proposed method. A set of heat source models with different *SBCs* could be created, considering the heat source position in the group, i.e. create different models with *SBCs* adapted for heat sources positioned in the front row, back row, left row, right row and heat sources positioned in the middle of the group. Thus, the phenomena of thermal plume merging could be addressed in a more precise way. However, this approach makes the preparation of the simplified model more complicated. This could be addressed by creation of

the database of heat sources that are the most commonly present in the indoor environment, as discussed in the following paragraph.

To enhance the use of the developed method itself, a database of simplified models of heat sources that are the most commonly present in indoor environments could be created. Thus, the first step of the method would not be necessary, i.e. there would be no need to perform the CFD simulation with a detailed heat source model followed by the creation of its simplified version with *SBC(s)*. The user could take the simplified model directly from the database and use it for further numerical studies. Consequently, the time required for the preparation of a numerical model would be considerably reduced.

REFERENCES

Author's references directly related to the current research

Barták, M. & Zelenský, P. (2011). *Simplified Modeling of Heat Sources for CFD Simulations of Indoor Air Flow - SGS10/053/OHK2/1T/12* [SGS Project]. Czech Technical University in Prague, Faculty of Mechanical Engineering, Department of Environmental Engineering. Prague.

Zelenský, P., Barták, M., Hensen, J. L. M. (2012). Model sedící osoby jako zdroje tepla ve vnitřním prostředí. *Vytápění Větrání Instalace*, *5*, 22–26. [in Czech]

Zelenský, P., Barták, M., Hensen, J. L. M. (2013). Simplified Representation of Indoor Heat Sources in CFD Simulations. In *Proceeding of the 13th International Conference of the International Building Performance Simulation Association* (pp. 3-29). Chambéry, France.

Zelenský, P., Barták, M., Hensen, J. L. M. (2013). Faktory ovlivňující CFD simulaci konvekčního proudu nad zdrojem tepla ve vnitřním prostředí. *Vytápění, Větrání, Instalace*, *22*(5), 214–220. [in Czech]

Zelenský, P., Barták, M., Hensen, J. L. M., Vavřička, R. (2013). Influence of Turbulence Model on Thermal Plume in Indoor Air Flow Simulation. In *Proceeding of the 11th REHVA World Congress „Energy Efficient, Smart and Healthy Buildings" – Clima 2013* (pp. 6755-6764). Prague, Czech Republic.

Zelenský, P., Barták, M., Hensen, J. L. M. (2015). Simulation of Indoor Environment in the Concert Hall housed in a Converted Former Church. In *Proceeding of the 14th International Conference of the International Building Performance Simulation Association* (pp. 1716-1721). Hyderabad, India.

Zelenský, P., Barták, M., Hensen, J. L. M. (2016). Influence of Thermal Plumes Interaction on CFD Simulation of Indoor Heat Sources. In *Sborník 9. národní konference s mezinárodní účastí Simulace budov a techniky prostředí* (pp. 127–132). Brno, Czech Republic.

Zelenský, P., Barták, M., Hensen, J. L. M. (2017). Simulation of Indoor Environment in the Concert Hall Housed in a Former Church. *Vytápění, Větrání, Instalace*, *26*(6), 342–348.

Author's references not related to the current research

Zelenský, P., Hensen, J. L. M., Zavřel, V., Bynum, J., Barták, M. (2014). Air-Flow Modelling in Design and Operation of Data Centers. In *Sborník 8. národní konference s mezinárodní účastí Simulace budov a techniky prostředí* (pp. 71-75). Prague, Czech Republic.

Zelenský, P., Barták, M., Zmrhal, V., Krupa, R. (2017). CFD model ventilátorové komory sestavné klimatizační jednotky. In *Sborník 22. konference Klimatizace a větrání* (pp. 244-251). Prague, Czech Republic.

Other references

ANSYS Inc. (2013). *ANSYS Fluent User's Guide*. USA: ANSYS Inc.

ASHRAE. (2003). Ventilation for Acceptable Indoor Air Quality. *ANSI/ASHRAE Standard 62-2001*.

Awbi, H. B. (2003). *Ventilation of Buildings,* 2nd ed. London: Spon Press. 563 p.

Bäckar, J. A. & Davidson, L. (2017). Evaluation of numerical wall functions on the axisymmetric impinging jet using OpenFOAM. *International Journal of Heat and Fluid Flow*, *67*, 27–42. http://doi.org/10.1016/j.ijheatfluidflow.2017.07.004

Barták, M. (2007). *Numerické modelování turbulentního proudění ve větrané místnosti* [Ph.D. Thesis]. Czech Technical University in Prague, Department of Environmental Engineering. Prague. [in Czech]

Barták, M., Drkal, F., Hensen, J. L. M., Lain, M., Matuška, T., Schwarzer, J., Šourek, B. (2001). Simulation to support sustainable HVAC design. In *Proceeding of The 18th International Conference on Passive and Low Energy Architecture* (pp. 7–9). Floriánopolis, Brazil.

Barták, M., Drkal, F., Lain, M., Schwarzer, J. (2001). *Obrazy proudění v kostele Sv. Anny v Praze 1* [Research report no. 01002]. Czech Technical University in Prague, Department of Environmental Engineering. Prague. [in Czech]

Borges, C. P., Quintela, D. A., Brites, G. N., Gaspar, A. R., Costa, J. J. (2007). Analysis of thermal plumes genereated by a seated person, a thermal manikin and a dummy. In *Proceedings of the 10th International Conference on Air Distribution in Roooms – Roomvent 2007* (pp. 253–256). Helsinky, Finland.

Bradshaw, P., Huang, G. P. (1995). The Law of the Wall in Turbulent Flow. *In Proceedings of the Royal Society A: Mathematical, Physical and Engineering Sciences*, 451 (1941), 165–188. http://doi:10.1098/rspa.1995.0122

Deevy, M., Sinai, Y., Everitt, P., Voigt, L., Gobeau, N. (2008). Modelling the effect of an occupant on displacement ventilation with computational fluid dynamics. *Energy and Buildings*, *40*(3), 255–264. http://doi.org/10.1016/j.enbuild.2007.02.021

Djunaedy, E., Hensen, J. L. M., Loomans, M. G. L. C. (2003). Towards External Coupling of Building Energy and Airflow Modeling Programs. *ASHRAE Transactions*, *109*(2), 771–787.

Fontaine, J. R., Rapp, R., Koskela, H., Niemelä, R. (2005). Evaluation of Air Diffuser Flow Modelling Methods Experiments and CFD Simulation. *Building and Environment*, (40), 601–615.

Gao, N. & Niu, J. (2006). Transient CFD simulation of the respiration process and interperson exposure assessment. *Building and Environment*, *41*(9), 1214–1222. http://doi.org/10.1016/j.buildenv.2005.05.014

Griffith, B. & Chen, Q. (2003). A momentum-zonal model for predicting zone airflow and temperature distributions to enhance building load and energy simulations. *HVAC&R Research*, 9(3), 309–325.

Hensen, J. L. M. (2004). Integrated building airflow simulation. *Advanced building simulation*, 87–118.

Hyldgaard, C. E. (1998). Thermal plume above a person. In *Proceeding of the 6th International Conference on Air Distribution in Roooms – Roomvent 1998* (pp. 407–413). Stockholm, Sweden.

Cho, J., Lim, T., Kim, B.S. (2009). Measurements and predictions of the air distribution systems in high compute density (Internet) data centers. *Energy and Buildings*, 41(10), 1107–1115.

Jančík, L. & Bašta, J. (2011). Termovizní vizualizace teplotního pole neizotermního vzdušného proudu. *TZB Haustechnik, 1,* 11–14. [in Czech]

Karimi, A. (2018). Design Optimization of Active Chilled Beam for an Office Space using Large Eddy Simulation. In *Proceeding of the 2018 ASHRAE Winter Conference*. Chicago, USA.

Karimpour, F., Venayagamoorthy, S.K. (2013). Some insights for the prediction of near-wall turbulence. *Journal of Fluid Mechanics*, 723, 126–139.

Koiš, G. (2009). *Analýza proudů v klimatizovaném prostoru* [MSc. Thesis]. Czech Technical University in Prague, Department of Environmental Engineering. Prague. [in Czech]

Launder, B. E. & Spalding, D. B. (1974). The numerical computation of turbulent flows. *Computer Methods in Applied Mechanics and Energy*, (3), 269–289.

Loomans, M. G. L. C., Huovila, A., Lefebvre, P. H., Porkka, J., Huovila, P., Desmyter, J., Vaturi, A. (2011). Key Performance Indicators For The Indoor Environment. In *Proceeding of the World Sustainable Building Conference SB11* (pp. 1666–1675). Helsinki, Finland.

Loomans, M. G. L. C., van Houdt, W., Lemaire, A., Hensen, J. L. M. (2008). Performance Assessment of an Operating Theatre Design Using CFD Simulation and Tracer Gas Measurements. *Indoor and Built Environment*, *17*(4), 299–312. http://doi.org/10.1177/1420326X08094948

Macdonald, R., Strom, R., Slawson, P. (2002). Water flume study of the enhancement of buoyant rise in pairs of merging plumes. *Atmospheric Environment*, *36*(29), 4603–4615. http://doi.org/10.1016/S1352-2310(02)00464-8

Mao, X. (2005). *Acoustic Techniques for Temperature and Flow Velocity Measurements*. [Ph.D. Thesis]. Eindhoven University of Technology. Eindhove

Matuška, T. (2005). *Experimentální metody v technice prostředí* (1st ed.). Prague: Czech Technical University in Prague. [in Czech]

Méndez, C., San José, J. F., Villafruela, J. M., Castro, F. (2008). Optimization of a hospital room by means of CFD for more efficient ventilation. *Energy and Buildings*, *40*(5), 849–854. http://doi.org/10.1016/j.enbuild.2007.06.003

Mierzwinsky, L. (1980). *Air motion and temperature distribution above a human body in result of natural convection*, A4-serien nr. 45. Stockholm: Faibo Grafiska. 79 p.

Murakami, S., Kato, S., Zeng, J. (2000). Combined simulation of air flow, radiation and moisture transport for heat release from a human body. *Building and Environment, 35*, 489–500.

Nielsen, P. V. (1997). *The Box Method: a practical procedure for introduction of an air terminal device in CFD calculation.* Aalborg University, Department of Building Technology and Structural Engineering, Aalborg, Denmark.

Nielsen, P. V., Allard, F., Awbi, H. B., Davidson, L., Schälin, A. (2007). *Computational Fluid Dynamics in Ventilation Design - REHVA Guidebook No. 10*. Finland: Forssa. 104 p.

Patankar, S. V. (1980). *Numerical Heat Transfer and Fluid Flow*. Washington: Hemisphere Publishing Corp.

Popiolek, Z. (1987). *Testing and modelling of buoyant convective flows in consideration of the formation of ventilation process* [D.Sc. Thesis]. Silesian University of Technology. Gliwice, Poland.

Rim, D. & Novoselac, A. (2009). Transport of particulate and gaseous pollutants in the vicinity of a human body. *Building and Environment*, *44*(9), 1840–1849. http://doi.org/10.1016/j.buildenv.2008.12.009

Schälin, A. (2007). CFD in Design – Where are we Today? In *Proceedings of the 10th International Conference on Air Distribution in Roooms – Roomvent 2007* (pp. 13-26). Helsinky, Finland.

Shih, T., Liou, W., Shabbir, A., Yang, Z., Zhu, J. (1995). A new eddy viscosity model for high reynolds number turbulent flows. *Computers & Fluids*, *24*, 227–238.

Skistad, H., Mundt, E., Nielsen, P. V., Hagstrom, K., Railio, J. (2002). *Displacement ventilation in non-industrial premises. REHVA Guidebook No. 1.* Trondhaim: Tapir. 95 p.

Sodja, J. (2007). *Turbulence models in CFD* [Seminar]. University of Ljubljana, Faculty for Mathematics and Physics, Department of Physics. Ljubljana.

Sørensen, D. N. & Voigt, L. K. (2003). Modelling flow and heat transfer around a seated human body by computational fluid dynamics. *Building and Environment*, *38*(6), 753–762. http://doi.org/10.1016/S0360-1323(03)00027-1

Srebric, J. & Chen, Q. (2002). Simplified Numerical Models for Complex Air Supply Diffusers. *HVAC&R Research*, *8*(3), 277–294.

Srebric, J., Vukovic, V., He, G., Yang, X. (2008). CFD boundary conditions for contaminant dispersion, heat transfer and airflow simulations around human occupants in indoor environments. *Building and Environment*, *43*(3), 294–303. http://doi.org/10.1016/j.buildenv.2006.03.023

Steskens, P. & Loomans, M. G. L. C. (2010a). Performance indicators for health, comfort and safety of the indoor environment. In *Proceedings of Clima 2010 – 10th REHVA World Congress* (on CD). Antalya, Turkey.

Steskens, P. & Loomans, M. G. L. C. (2010b). *PERFECTION – Performance Indicators for Health, Comfort and Safety of the Indoor Environment: T1.3 Performance Indicators for Health and Comfort*. http://www.ca-perfection.eu/media/files/Perfection_D13_final.pdf (available on 6.5.2018)

Topp, C. (2002). Influence of geometry of a computer simulated person on contaminant distribution and personal exposure. In *Proceeding of the 8th Internation conference on air distribution in rooms – Roomvent 2002* (pp. 265–268). Copenhagen, Denmark.

ÚNMZ ČR. (2010). *Větrání nebytových budov - Základní požadavky na větrací a klimatizační systémy - Standard ČSN EN 15 665/Z1*. [in Czech]

Voigt, L. K. (2001). *Navier-Stokes Simulations of Airflow in Rooms and around a Human Body* [Ph.D. Thesis]. Technical University of Denmark, Department of Mechanical Engineering, Fluid Mechanics Section and International Centre for Indoor Environment and Energy. Lyngby.

Wang, L. & Chen, Q. (2007). Analysis on the well-mixing assumptions used in multizone airflow network models. *The 10th International IBPSA Conference - Building Simulation 2007*, (2001), 1485–1490.

Wilcox, D.C., 1988. Reassessment of the scale-determining equation for advanced turbulence models. *AIAA Journal*, 26, pp.1299–1310.

Wikimedia. (2011). *Law of the wall, horizontal velocity near the wall with mixing length model* [Figure]. Wikimedia Commons: Aokomoriuta. https://upload.wikimedia.org/wikipedia/commons/4/4c/Law_of_the_wall_%28English%29.svg (available on 7.5.2018).

Wilcox, D. C. (1988). Reassessment of the scale-determining equation for advanced turbulence models. *AIAA Journal*, *26*, 1299–1310.

Wilcox, D. C. (2006). *Turbulence Modeling for CFD* (3rd ed.). La Canada: DCW Industries.

Xing, H., Hatton, A., Awbi, H. B. (2001). A study of the air quality in the breathing zone in a room with displacement ventilation. *Building and Environment*, *36*(7), 809–820. http://dx.doi.org/10.1016/S0360-1323(01)00006-3

Yakhot, V. & Orszag, S. A. (1986). Renormalization group analysis of turbulence. *Journal of Scientific Computing*, *1*, 3–51.

Yan, W., Yang, X., Shan, M. (2009). How to Simplify Computer Simulated Persons (CSPs) for Modeling Personal Microenvironments: Comparison and Case Studies. *ASHRAE Transactions*, *115*(1), 473–484.

Zbořil, V., Melikov, A., Yordanova, B., Bozhkov, L., Kosonen, R. (2007). Airflow Distribution in Rooms with Active Chilled Beams. In *Proceedings of the 10th International Conference on Air Distribution in Rooms – Roomvent 2007* (pp. 1–7). Helsinki, Finland.

Zbořil, V., Koiš, G., Melikov, A. (2008). Termální figurína k simulaci konvektivních proudů. [Functional Sample]. Czech Technical University in Prague, Department of Environmental Engineering. Prague. [in Czech]

Zhai, Z. J., Zhang, Z., Zhang, W., Chen, Q. Y. (2007). Evaluation of Various Turbulence Models in Predicting Airflow and Turbulence in Enclosed Environments by CFD: Part 1 – Summary of Prevalent Turbulence Models. *HVAC&R Research*, *13*(6), 853–870.

Zhang, T., Lee, K., Chen, Q. (2009). A simplified approach to describe complex diffusers in displacement ventilation for CFD simulations. *Indoor Air*, *19*, 255–267.

Zhang, X., VanGilder, J. W., Iyengar, M., Schmidt, R. R. (2008). Effect of rack modeling detail on the numerical results of a data center test cell. In *Proceeding of the 11th Intersociety Conference on Thermal and Thermomechanical Phenomena in Electronic Systems* (pp.1183–1190). Orlando, USA.

Zoon, W. A. C., Loomans, M. G. L. C., Hensen, J. L. M. (2011). Testing the effectiveness of operating room ventilation with regard to removal of airborne bacteria. *Building and Environment*, *46*(12), 2570–2577. http://doi.org/10.1016/j.buildenv.2011.06.015

Zukowska, D. (2011). *Airflow interactions in rooms - Convective plumes generated by occupants* [Ph.D. Thesis]. Technical University of Denmark, Department of Civil Engineering. Lyngby.

Zukowska, D., Melikov, A., Popiolek, Z. (2007). Thermal plume above a simulated sitting person with different complexity of body geometry. In *Proceedings of the 10th International Conference on Air Distribution in Rooms – Roomvent 2007* (pp. 191–198). Helsinki, Finland.

Zukowska, D., Melikov, A., Popiolek, Z. (2008). Impact of Thermal Plumes Generated by Occupant Simulators with Different Complexity of Body Geometry on Airflow Pattern in Rooms. In *Proceeding of the 7th Internation Thermal Manikin and Modelling Meeting - University of Coimbra* (pp. 3–6). Coimbra, Portugal.

Zukowska, D., Melikov, A., Popiolek, Z. (2010a). Determination of the integral characteristics of an asymmetrical thermal plume from air speed/velocity and temperature measurements. *Experimental Thermal and Fluid Science*, *34*(8), 1205–1216. http://doi.org/10.1016/j.expthermflusci.2010.04.009

Zukowska, D., Melikov, A., Popiolek, Z. (2010b). Impact of boundary conditions on the development of the thermal plume above a sitting human body. In *Proceedings of the 10th REHVA World Congress „Sustainable Energy Use in Buildings" – Clima 2010* (pp. 2–7). Antalya, Turkey.

Zukowska, D., Melikov, A., Popiolek, Z. (2012a). Impact of geometry of a sedentary occupant simulator on the generated thermal plume: Experimental investigation. *HVAC&R Research*, *18*(4), 795–811.

Zukowska, D., Melikov, A., Popiolek, Z. (2012b). Impact of personal factors and furniture arrangement on the thermal plume above a sitting occupant. *Building and Environment*, *49*, 104–116. http://doi.org/10.1016/j.buildenv.2011.09.015

Zuo, W. (2010). *Advanced Simulations of Air Distribution in Buildings*. [Ph.D. Thesis]. Purdue University. West Lafayette.

ANNEX I: Technical drawings

D1 / DT-PZ-2018	–	Thermal manikin
D2 / DT-PZ-2018	–	Thermal manikin, simplified geometry
D3 / DT-PZ-2018	–	Room with single manikin
D4 / DT-PZ-2018	–	Measuring points distribution: x-y (single manikin)
D5 / DT-PZ-2018	–	Measuring points distribution: y-z (single manikin)
D6 / DT-PZ-2018	–	Room with four manikins
D7 / DT-PZ-2018	–	Measuring points distribution: x-y (four manikins)
D8 / DT-PZ-2018	–	Measuring points distribution: y-z (four manikins)

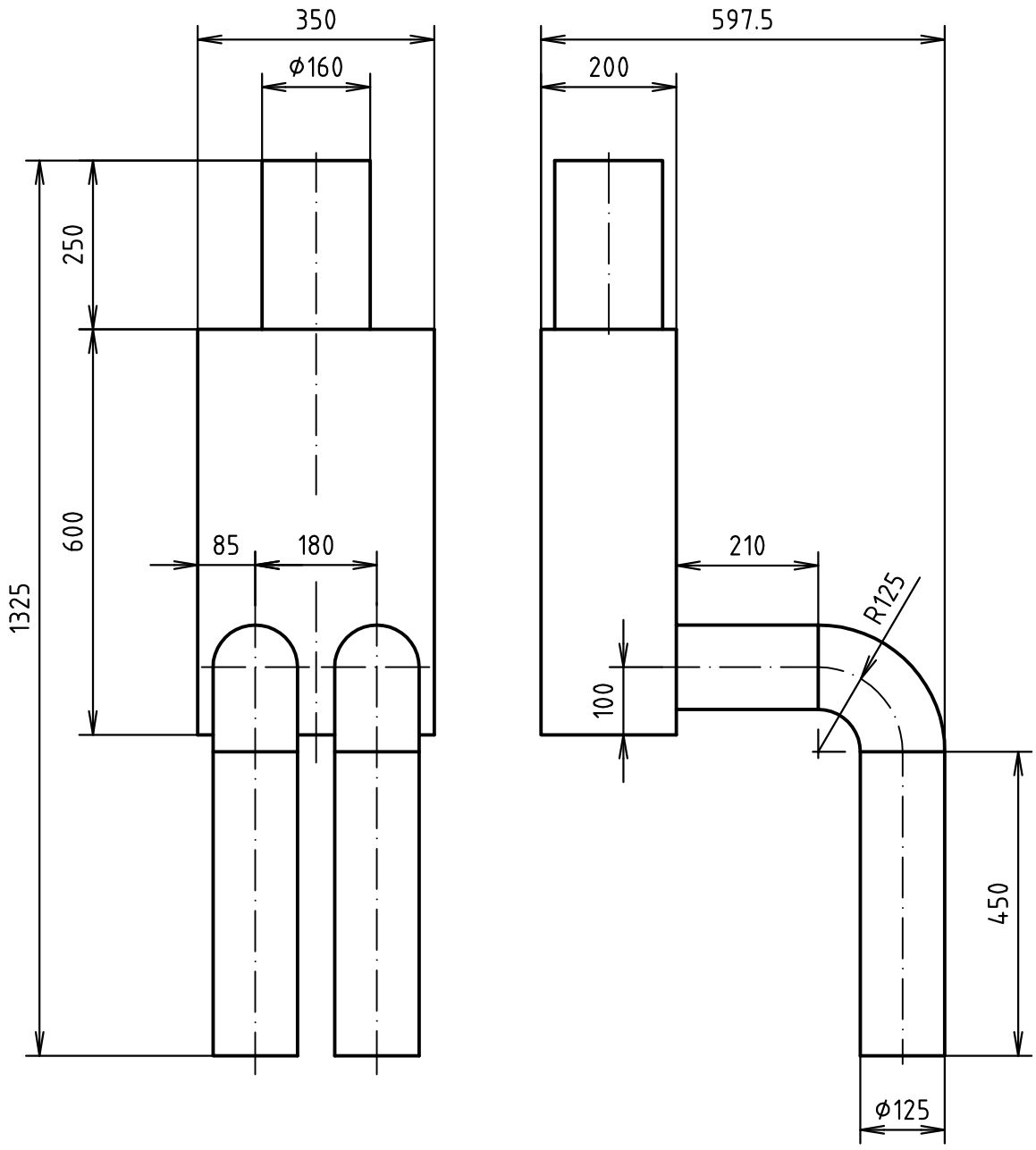

Czech Technical University in Prague Faculty of Mechanical Engineering Department of Environmental Eng.	Author: Zelenský Petr
Drawing: Thermal manikin	Date: 1.4.2018
Drawing nr.: D1 / DT-PZ-2018	Scales: 1:10

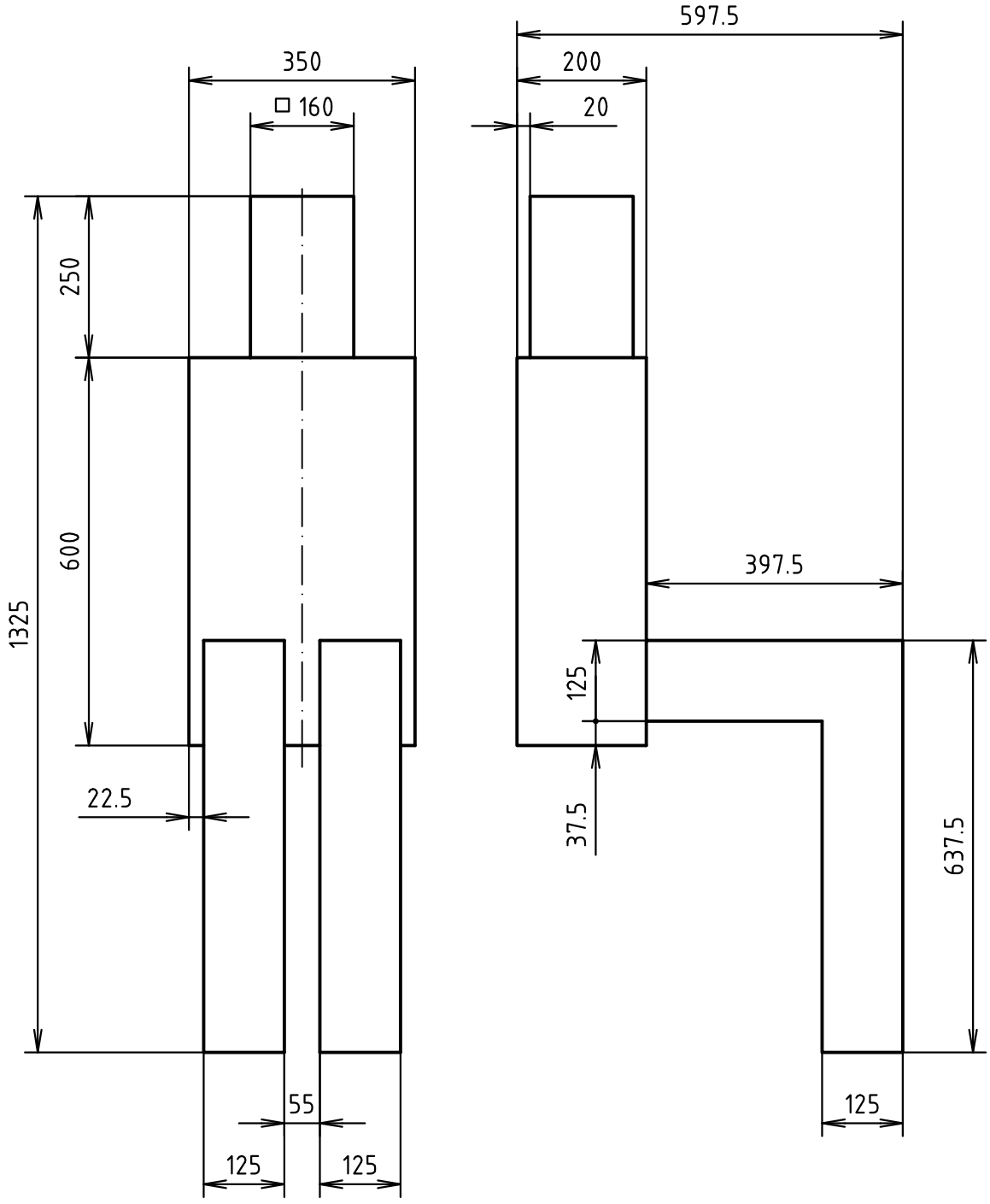

Czech Technical University in Prague Faculty of Mechanical Engineering Department of Environmental Eng.	Author: Zelenský Petr
Drawing: Thermal manikin, simplified geometry	Date: 1.4.2018
Drawing nr.: D2 / DT-PZ-2018	Scales: 1:10

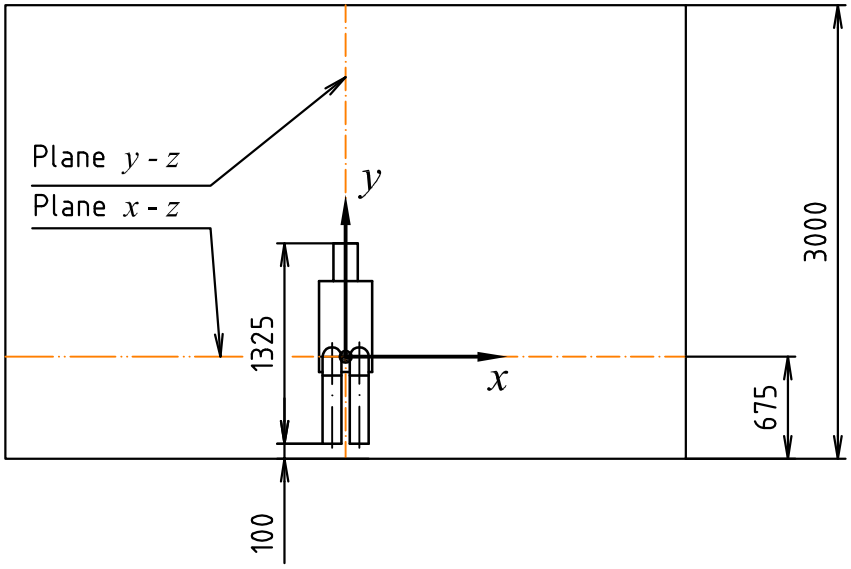

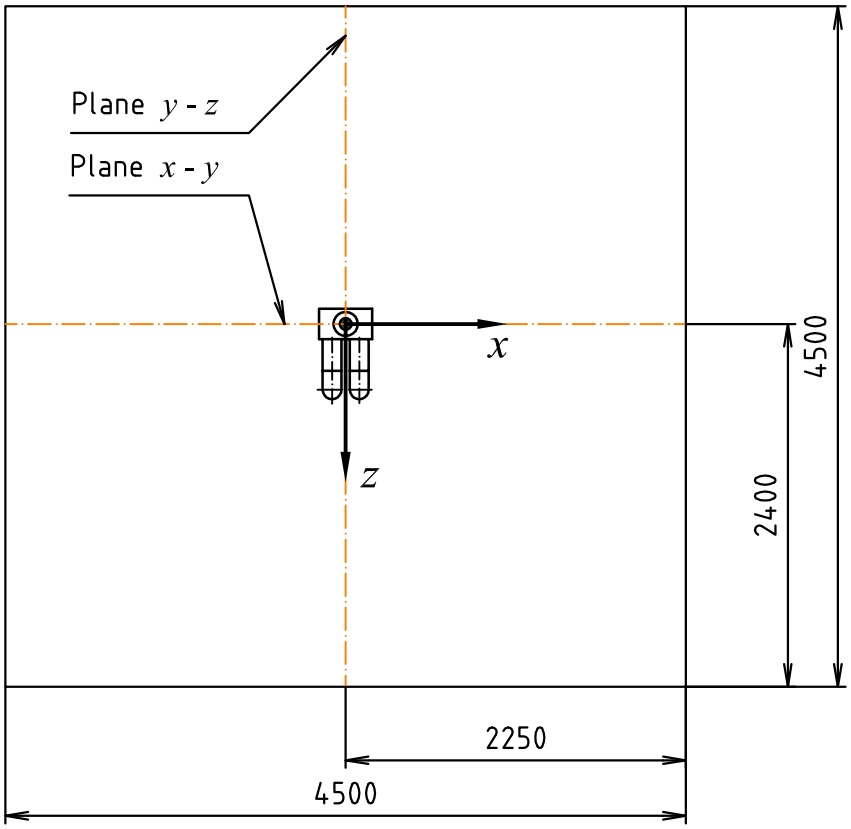

Czech Technical University in Prague Faculty of Mechanical Engineering Department of Environmental Eng.	Author: Zelenský Petr
Drawing: Room with single manikin	Date: 1.4.2018
Drawing nr.: D3 / DT-PZ-2018	Scales: 1:50

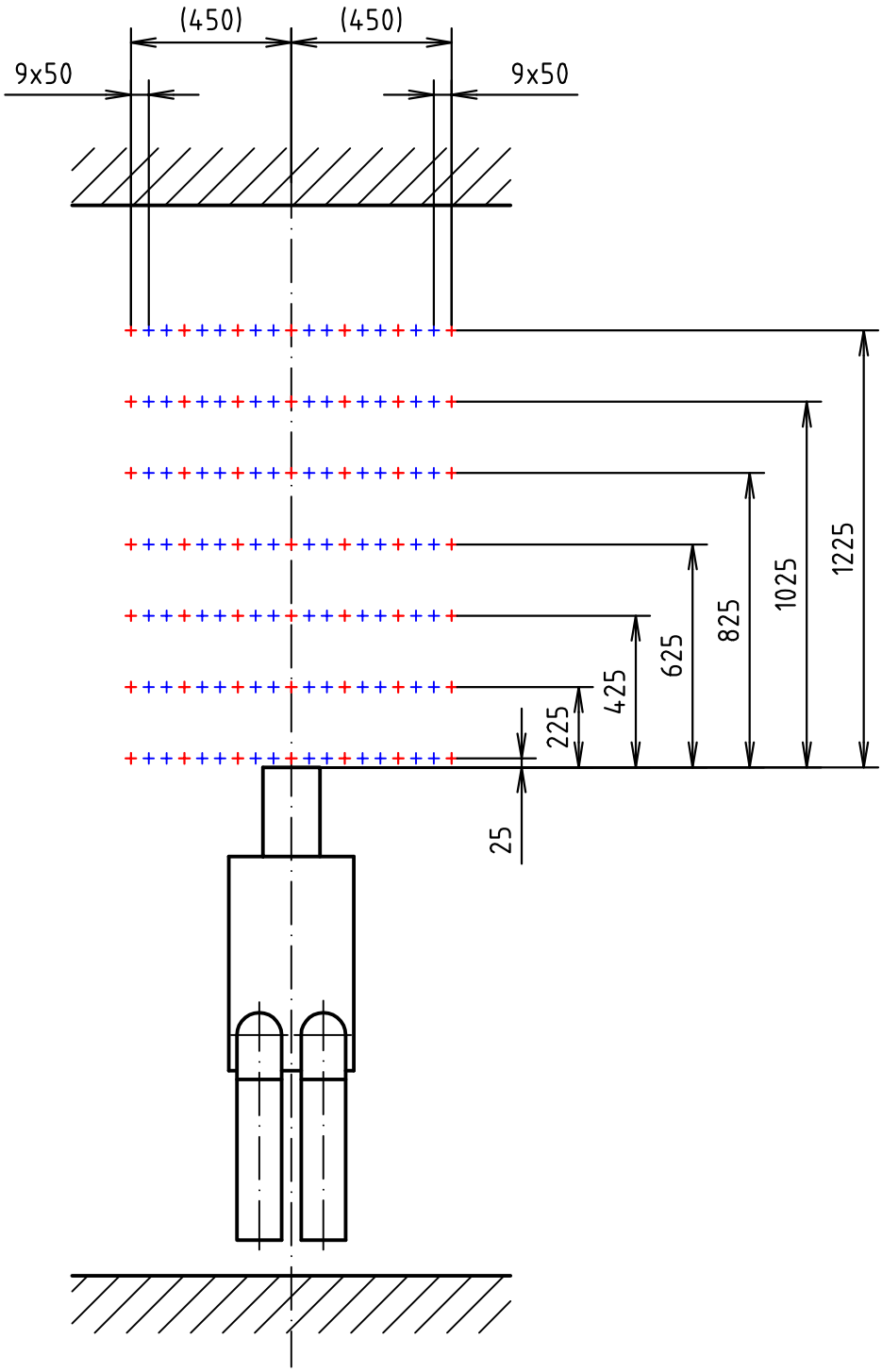

In total 133 measuring points in this plane (7 rows, each with 19 points)
The red points are identical to the points of measurement by Borgese et al. (2007)

Czech Technical University in Prague Faculty of Mechanical Engineering Department of Environmental Eng.	Author: Zelenský Petr
Drawing: Measuring points distribution: x-y	Date: 1.4.2018
Drawing nr.: D4 / DT-PZ-2018	Scales: 1:20

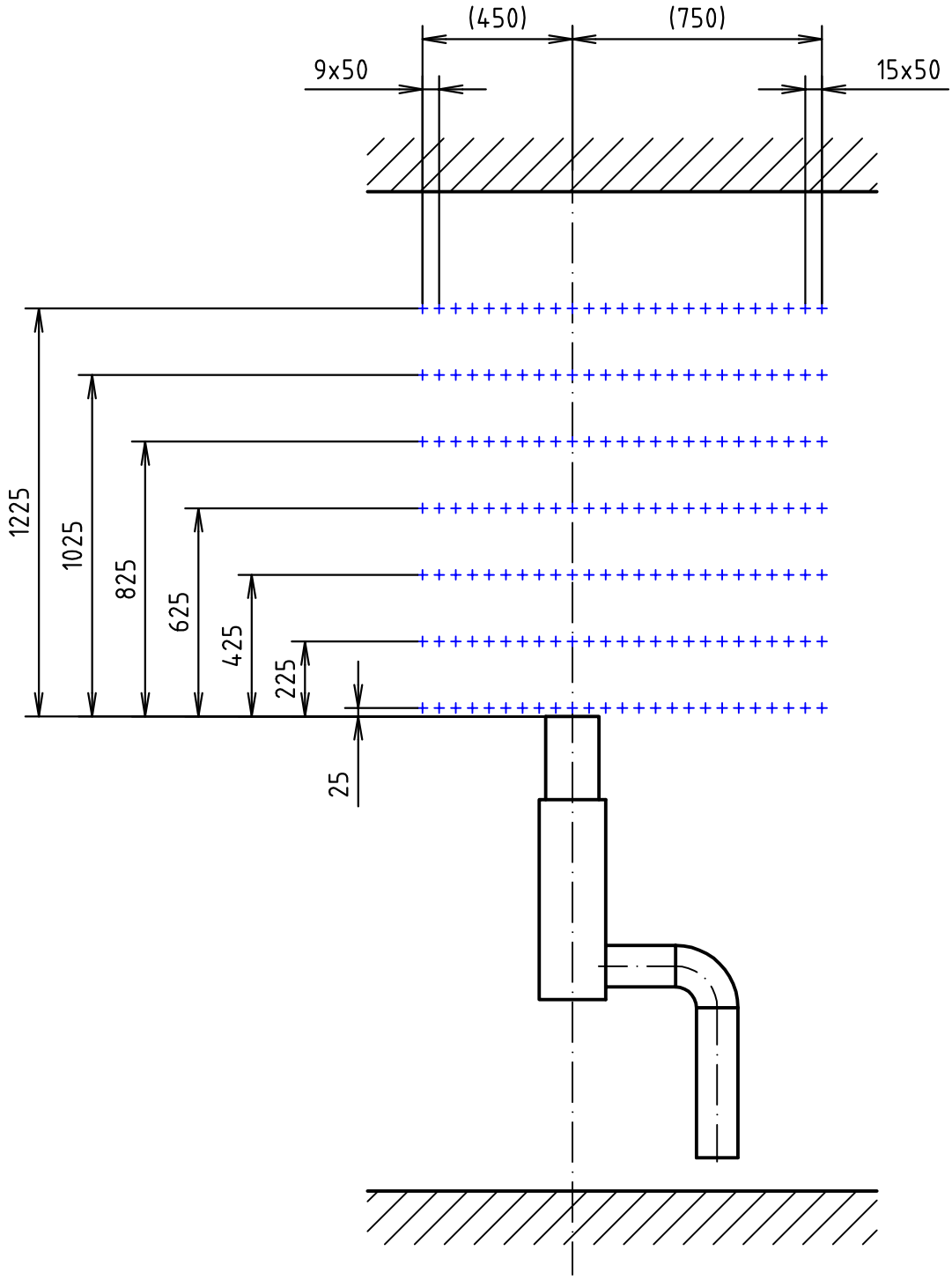

In total 175 measuring points in this plane (7 rows, each with 25 points)

Czech Technical University in Prague Faculty of Mechanical Engineering Department of Environmental Eng.	Author: Zelenský Petr
Drawing: Measuring points distribution: y-z	Date: 1.4.2018
Drawing nr.: D5 / DT-PZ-2018	Scales: 1:20

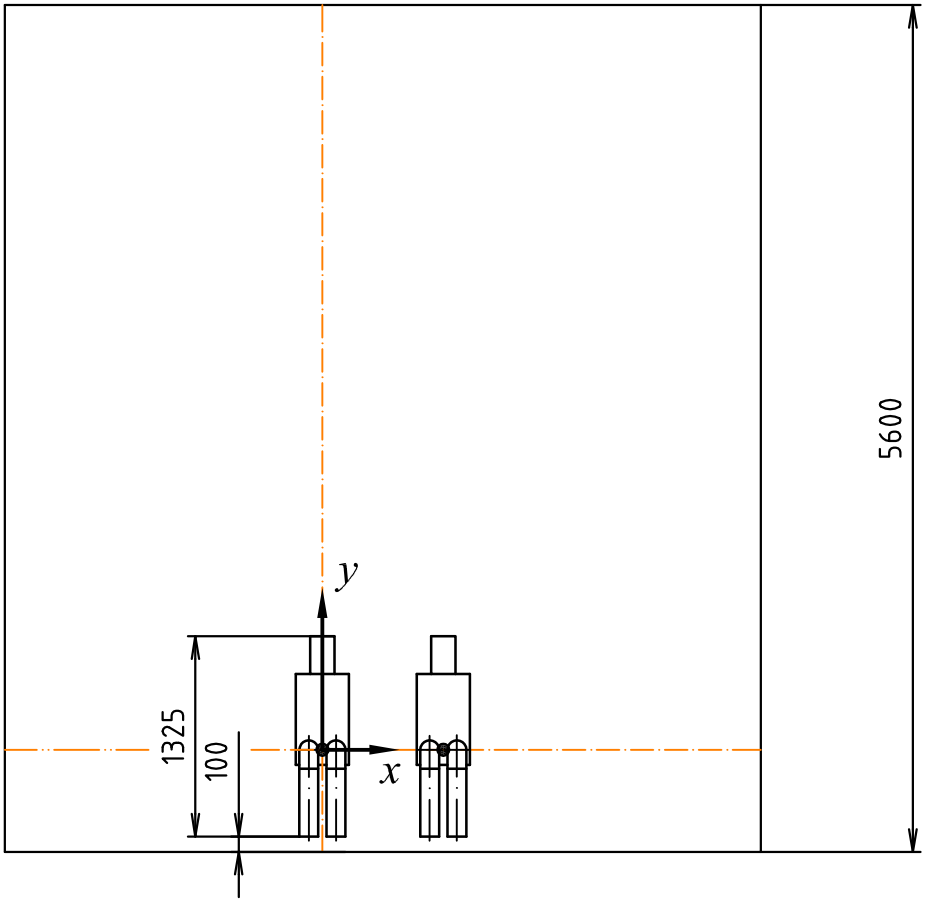

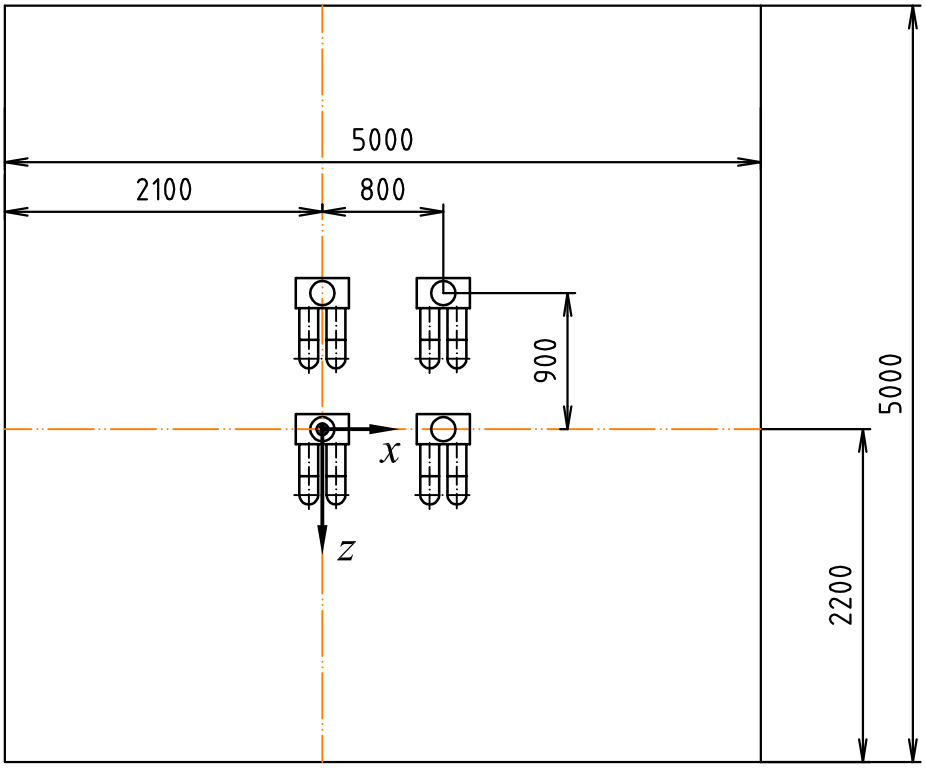

Czech Technical University in Prague Faculty of Mechanical Engineering Department of Environmental Eng.	Author: Zelenský Petr
Drawing: Room with four manikins	Date: 1.4.2018
Drawing nr.: D6 / DT-PZ-2018	Scales: 1:50

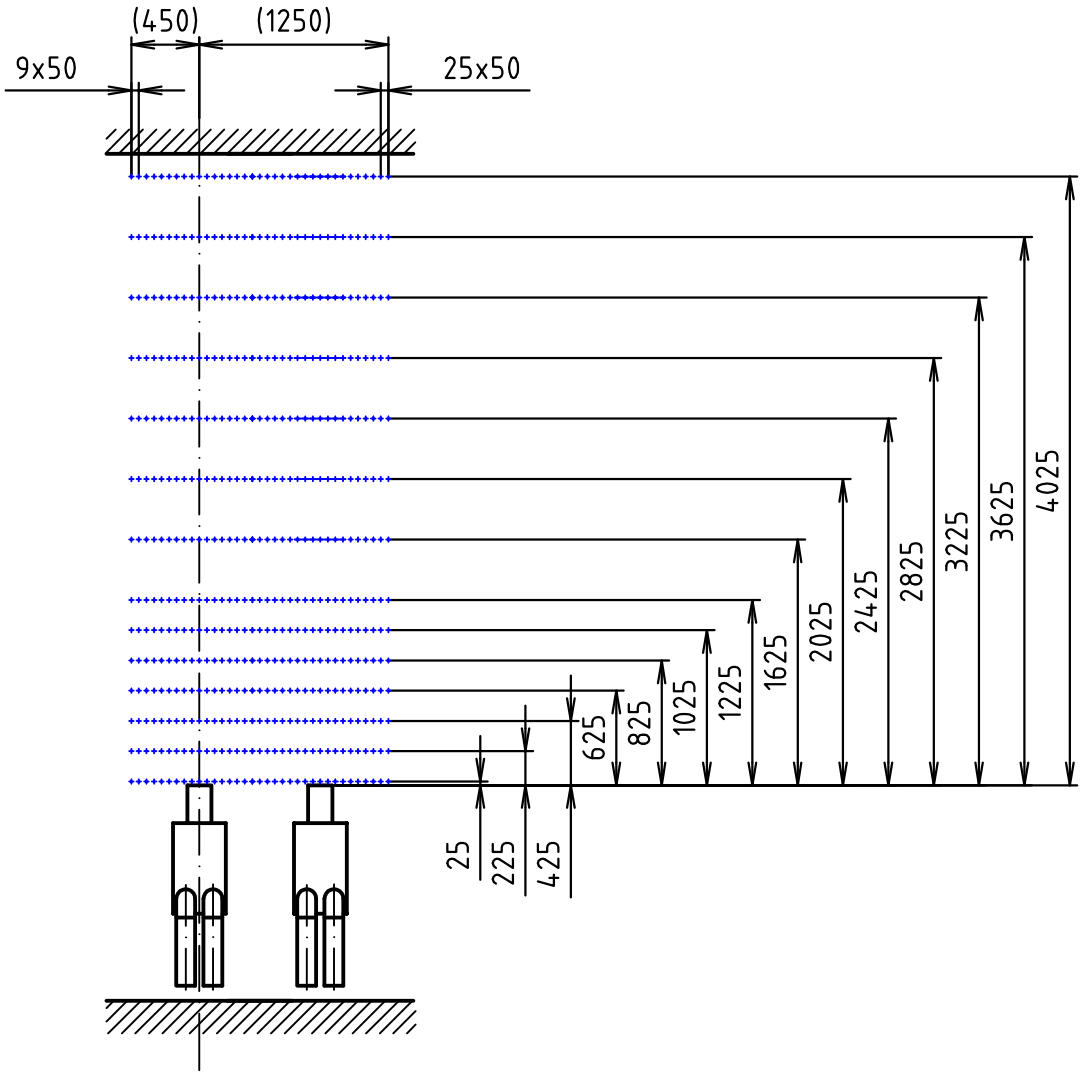

In total 490 measuring points in this plane (14 rows, each with 35 points)

Czech Technical University in Prague Faculty of Mechanical Engineering Department of Environmental Eng.	Author: Zelenský Petr
Drawing: Measuring points distribution: x-y	Date: 1.4.2018
Drawing nr.: D7 / DT-PZ-2018	Scales: 1:50

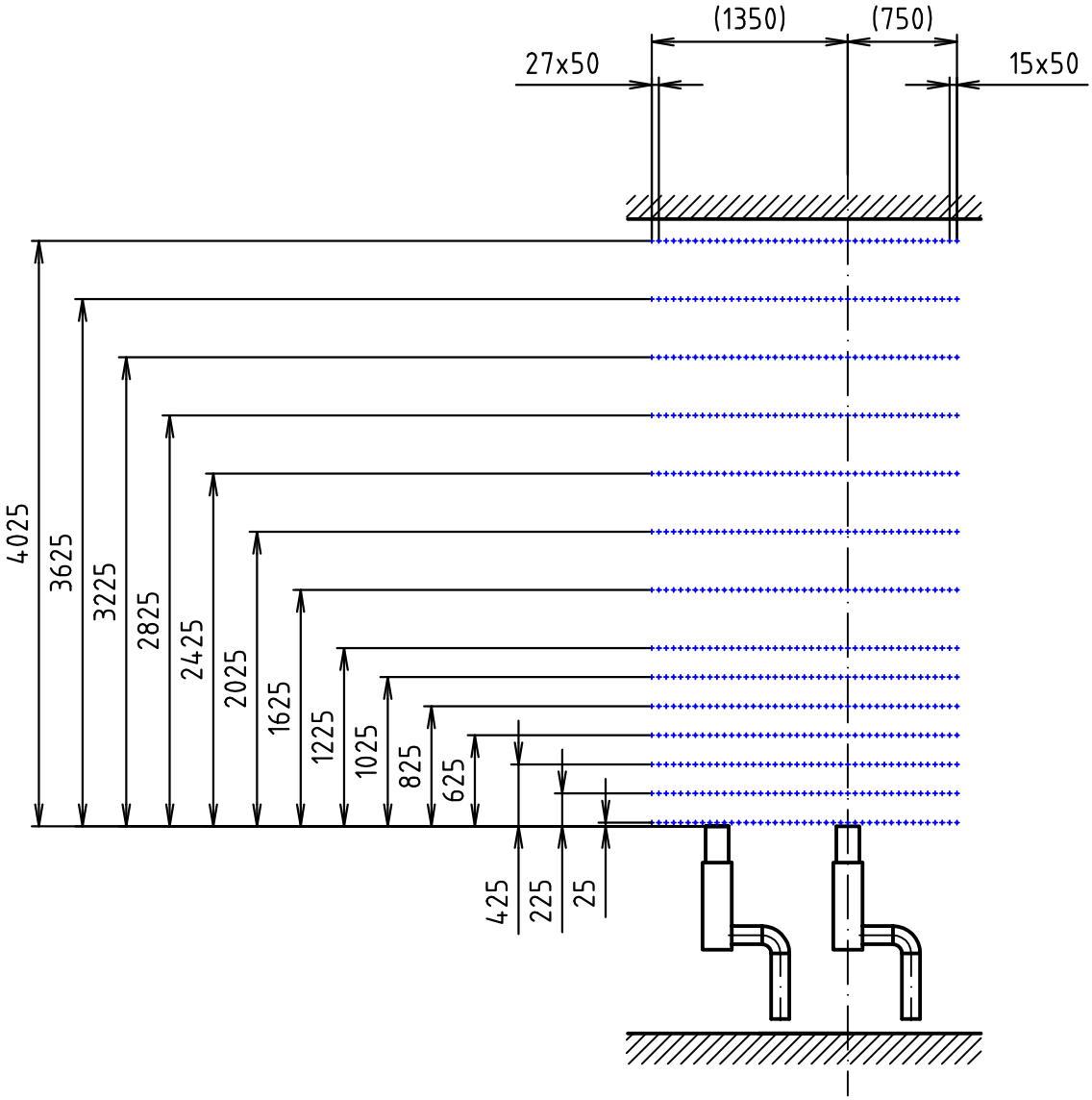

In total 602 measuring points in this plane (14 rows, each with 43 points)

Czech Technical University in Prague Faculty of Mechanical Engineering Department of Environmental Eng.	Author: Zelenský Petr
Drawing: Measuring points distribution: y-z	Date: 1.4.2018
Drawing nr.: D8 / DT-PZ-2018	Scales: 1:50

ANNEX II: Numerical mesh of the simulated rooms

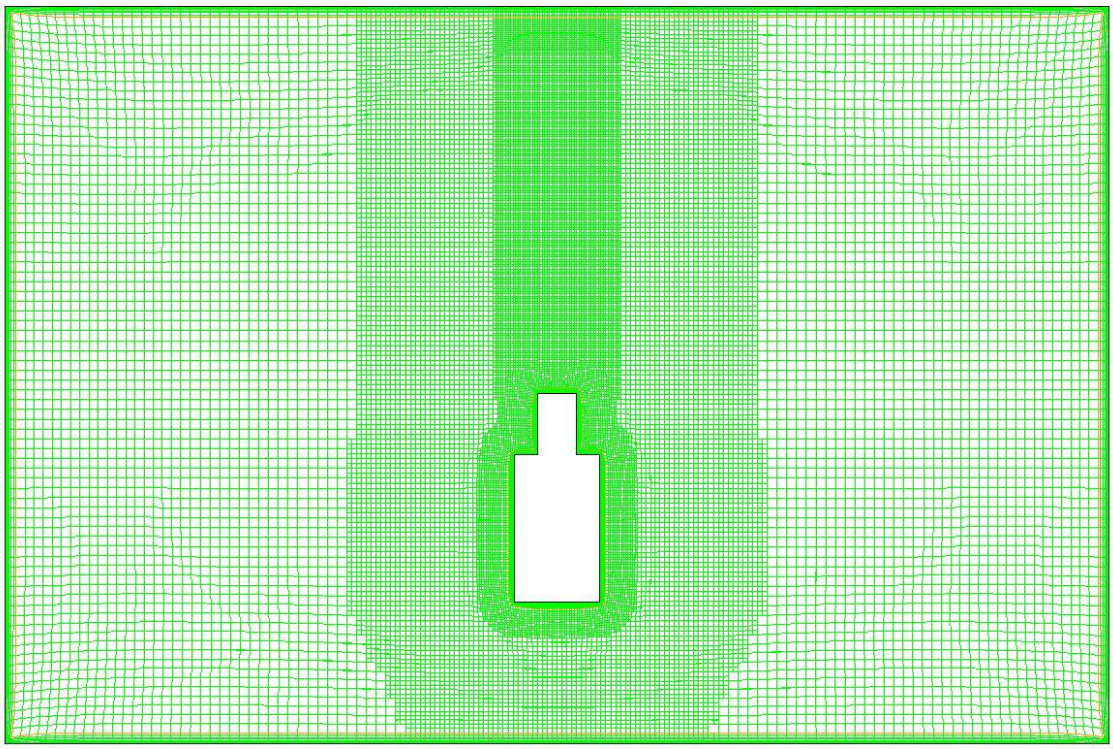

Fig. AII.1 – Room with detailed model of the thermal manikin, cross section x – y

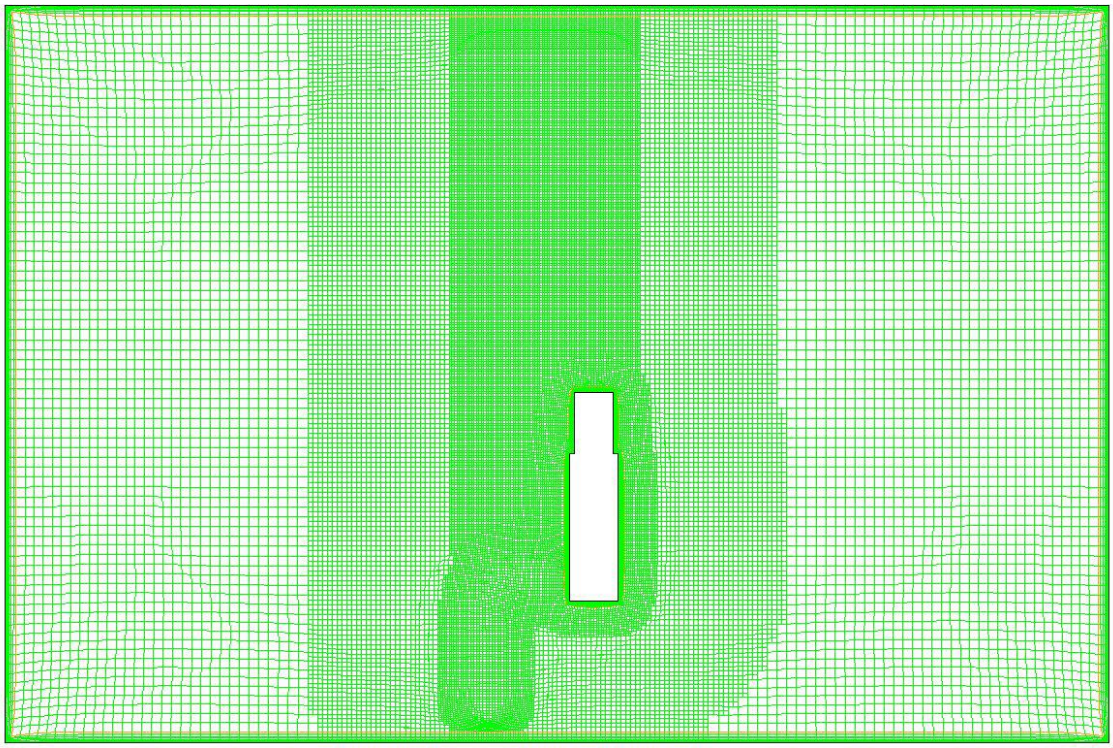

Fig. AII.2 – Room with detailed model of the thermal manikin, cross section y – z

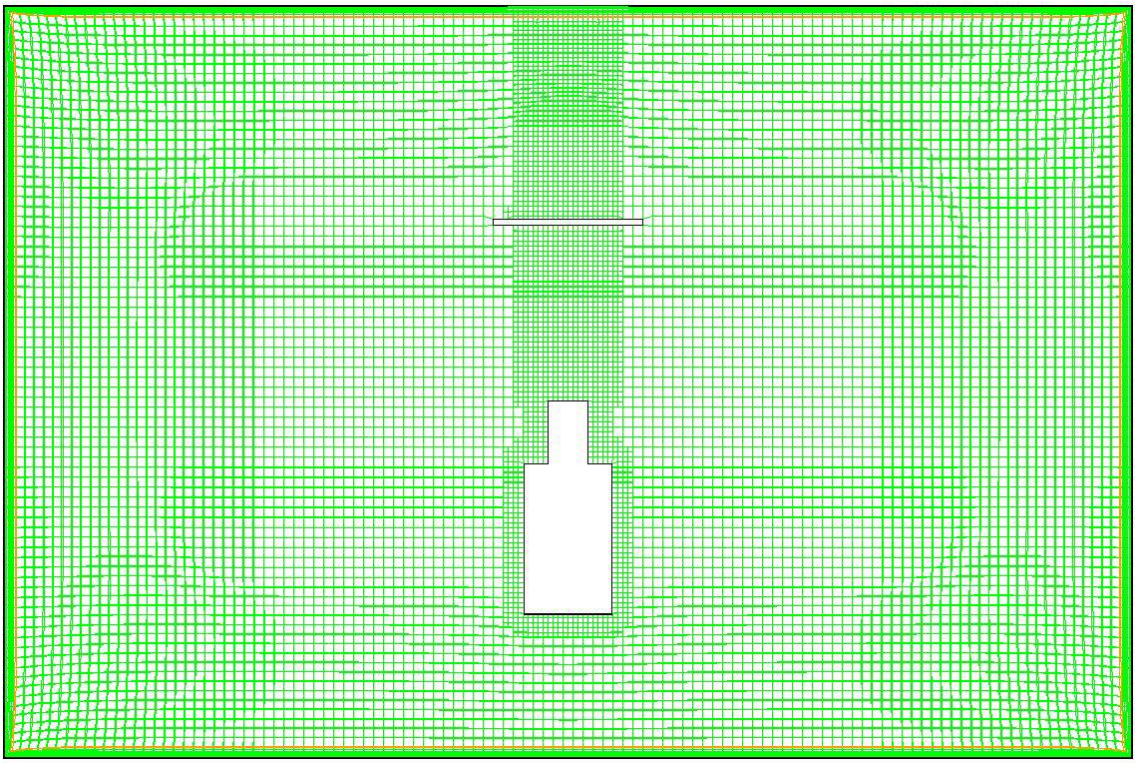

Fig. AII.3 – Room with simplified model of the thermal manikin, cross section x – y

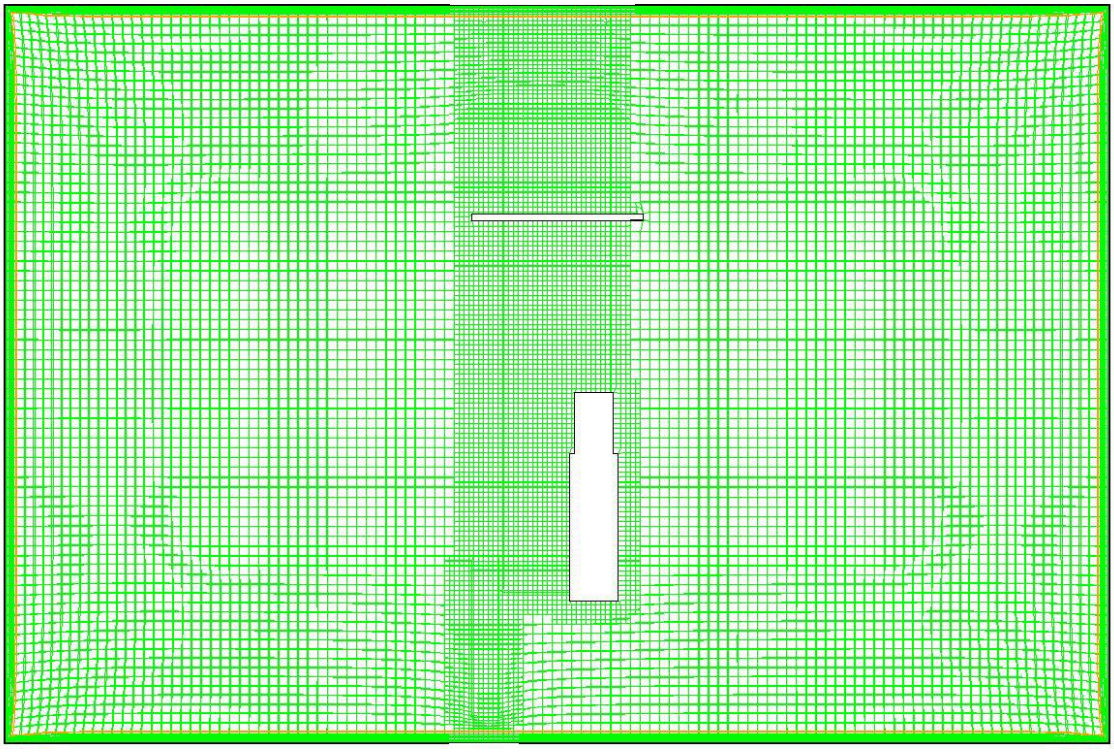

Fig. AII.4 – Room with simplified model of the thermal manikin, cross section y – z

ANNEX III: User Defined Function (UDF)

```
#include "udf.h"
#define t1 1.035374595957496E+02
#define t2 1.002992854968267E-02
#define t3 -1.067417348329309E+00
#define t4 -8.430234999849773E-01
#define t5 9.877100150528142E-01
#define v1 3.14365180149524e+01
#define v2 -3.90817822169181e-02
#define v3 1.36622018851687e+00
#define v4 -5.29828844141097e-01
#define v5 1.36491150708335e+00
#define k1 4.06346885727016e+01
#define k2 -4.22829384588423e-03
#define k3 1.70609744902679e+00
#define k4 -4.25274876334079e-01
#define k5 1.69430628350562e+00
#define eps1 1.04812022241770e+01
#define eps2 1.12493502900831e-02
#define eps3 -1.65270088420495e+00
#define eps4 -6.40034467412009e-01
#define eps5 1.54447637728469e+00

DEFINE_PROFILE(inlet_temperature,t,position)
{
real x[ND_ND];
real thermosensor_temperature;
real xdist;
real ydist;
real zdist;
real xmin;
real xmax;
real ymin;
real ymax;
real zmin;
real zmax;

cell_t c;

xmin= 0.24;
xmax= 0.29;
ymin=-0.015;
ymax= 0.015;
zmin= -0.34;
zmax= -0.31;
xdist= 1000000;
zdist= 1000000;
ydist= 1000000;

/* Begin loops to determine the lowest x,y and z coordinates of the boundary condition zone*/
/* Begin loop to determine the lowest x coordinate of the boundary condition zone*/
        begin_c_loop(c,t)
          {
           C_CENTROID(x,c,t);
           if ((x[0] <= xdist))
            {
            xdist = x[0]; /* get x coordinate */
           }}
        end_c_loop(c,t)
```

```
/* Begin loop to determine the lowest y coordinate of the boundary condition zone - height*/
        begin_c_loop(c,t)
          {
          C_CENTROID(x,c,t);
           if ((x[1] <= ydist))
            {
            ydist = x[1]; /* get y coordinate */
           }}
        end_c_loop(c,t)

 /* Begin loop to determine the lowest z coordinate of the boundary condition zone*/
        begin_c_loop(c,t)
        {
          C_CENTROID(x,c,t);
          if ((x[2] <= zdist))
           {
             zdist = x[2]; /* get z coordinate */
          }}
        end_c_loop(c,t)

/* Begin loop to determine the temperature at the centroid of cells near the thermosensor */
 begin_c_loop(c,t)
 {
  C_CENTROID(x,c,t);
   if (((x[0]-xdist-0.3) >= xmin) && ((x[0]-xdist-0.3) <= xmax))
  {
   if (((x[1]-ydist-0.025) >= ymin) && ((x[1]-ydist-0.025) <= ymax))
   {
    if (((x[2]-zdist-0.35) >= zmin) && ((x[2]-zdist-0.35) <= zmax))
    {
     thermosensor_temperature= C_T(c,t); /* get thermosensor temperature */
  }}}}
 end_c_loop(c,t)

/* Calculate temperature profile for boundary condition */
begin_c_loop(c,t)
 {
   C_CENTROID(x,c,t);
   C_PROFILE(c,t,position) = thermosensor_temperature + 0.01*(t1*exp(-0.5*(pow(((10*(x[0]-xdist-0.3)-
t2)/t3),2)+pow(((10*(x[2]-zdist-0.35-0.1475)-t4/t5)),2))))*(1.184);
 }
end_c_loop(c,t)
}

DEFINE_PROFILE(inlet_velocity,t,position)
{
real x[ND_ND];
real xdist;
real zdist;
cell_t c;
xdist= 1000000;
zdist= 1000000;

/* Begin loops to determine the lowest x and z coordinates of the boundary condition zone*/
/* Begin loop to determine the lowest x coordinate of the boundary condition zone*/
        begin_c_loop(c,t)
          {
           C_CENTROID(x,c,t);
           if ((x[0] <= xdist))
            {
```

```
        xdist = x[0]; /* get x coordinate */
        }}
      end_c_loop(c,t)
```

/* Begin loop to determine the lowest z coordinate of the boundary condition zone*/

```
      begin_c_loop(c,t)
      {
       C_CENTROID(x,c,t);
       if ((x[2] <= zdist))
        {
         zdist = x[2]; /* get z coordinate */
        }}
      end_c_loop(c,t)
```

/* Calculate y-velocity profile for boundary condition */

```
begin_c_loop(c,t)
 {
  C_CENTROID(x,c,t);
  C_PROFILE(c,t,position)                =                0.01*(v1*exp(-0.5*(pow(((10*(x[0]-xdist-0.3)-
v2)/v3),2)+pow((((10*(x[2]-zdist-0.35-0.1475))-v4/v5)),2))));
 }
end_c_loop(c,t)
}

DEFINE_PROFILE(inlet_turbkinen,t,position)
{
real x[ND_ND];
real xdist;
real zdist;
cell_t c;
xdist= 1000000;
zdist= 1000000;
```

/* Begin loops to determine the lowest x and z coordinates of the boundary condition zone*/
/* Begin loop to determine the lowest x coordinate of the boundary condition zone*/

```
      begin_c_loop(c,t)
       {
        C_CENTROID(x,c,t);
        if ((x[0] <= xdist))
         {
         xdist = x[0]; /* get x coordinate */
         }
       }
      end_c_loop(c,t)
```

/* Begin loop to determine the lowest z coordinate of the boundary condition zone*/

```
      begin_c_loop(c,t)
      {
       C_CENTROID(x,c,t);
       if ((x[2] <= zdist))
        {
         zdist = x[2]; /* get z coordinate */
        }
       }
      end_c_loop(c,t)
```

/* Calculate y-velocity profile for boundary condition */

```
begin_c_loop(c,t)
 {
```

```
  C_CENTROID(x,c,t);
  C_PROFILE(c,t,position) = 0.0001*(k1*exp(-0.5*(pow(((10*(x[0]-xdist-0.3)-
k2)/k3),2)+pow((((10*(x[2]-zdist-0.35-0.1475))-k4/k5)),2))));
 }
end_c_loop(c,t)
}

DEFINE_PROFILE(inlet_turbdissipation,t,position)
{
real x[ND_ND];
real xdist;
real zdist;

cell_t c;

xdist= 1000000;
zdist= 1000000;

/* Begin loops to determine the lowest x and z coordinates of the boundary condition zone*/
 /* Begin loop to determine the lowest x coordinate of the boundary condition zone*/
            begin_c_loop(c,t)
              {
               C_CENTROID(x,c,t);
               if ((x[0] <= xdist))
                {
                xdist = x[0]; /* get x coordinate */
                }
              }
            end_c_loop(c,t)

 /* Begin loop to determine the lowest z coordinate of the boundary condition zone*/
            begin_c_loop(c,t)
            {
              C_CENTROID(x,c,t);
              if ((x[2] <= zdist))
               {
                 zdist = x[2]; /* get z coordinate */
               }
              }
            end_c_loop(c,t)

/* Calculate y-velocity profile for boundary condition */
begin_c_loop(c,t)
 {
  C_CENTROID(x,c,t);
  C_PROFILE(c,t,position)=0.0001*(eps1*exp(-0.5*(pow(((10*(x[0]-xdist-0.3)-
eps2)/eps3),2)+pow((((10*(x[2]-zdist-0.35-0.1475))-eps4/eps5)),2))));
 }
end_c_loop(c,t)
}
```

ANNEX IV: St. Anna – building constructions

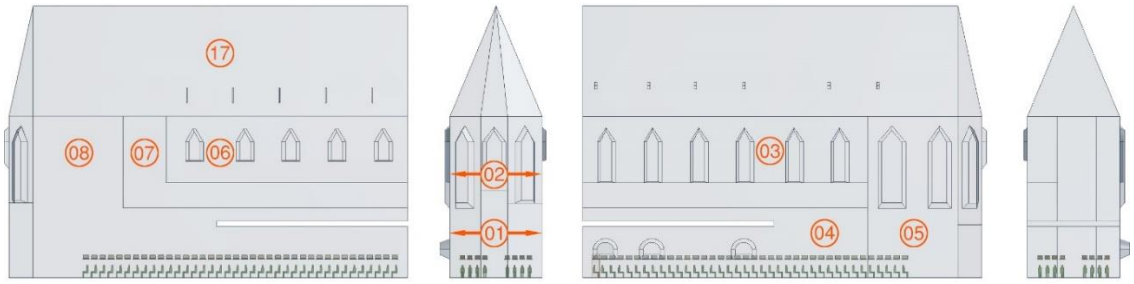

No.	Construction	*D* [m]	ρ [kg/m^3]	λ [W/m·K]	*c* [J/kg·K]
01	Wall apse A	1.2	2400	1.4	920
02	Wall apse B	1.4	2400	1.4	920
03	Wall south A	1.0	2400	1.4	920
04	Wall south B	1.4	2400	1.4	920
05	Wall south C	1.4	2400	1.4	920
06	Wall north A	1.0	2400	1.4	920
07	Wall north B	1.4	2400	1.4	920
08	Wall north C	1.4	2400	1.4	920
09	Wall west A	1.4	2400	1.4	920
10	Wall west B	0.8	2400	1.4	920
11	Wall west – to the tower A	1.4	2400	1.4	920
12	Wall west – to the tower B	0.8	2400	1.4	920
13	Niches apse	1.4	2400	1.4	920
14	Niches south wall	1.4	2400	1.4	920
15	Niches north wall	1.4	2400	1.4	920
16	Glass	0.01	2710	0.76	837
17	Roof – multilayer construction (layer order from inside to outside)				
	01 - Wooden cover	0.025	600	0.22	2510
	02 - Insulation layer	0.04	30	0.035	2000
	03 - Air gap	0.04	1.225	0.2	1010
	04 - Slate roofing tiles	0.005	2800	1.7	920
18	Floor – multilayer construction (layer order from inside to outside)				
	01 - Tiles	0.05	2000	0.96	840
	02 - Concrete	0.4	1700	0.57	850

ANNEX V: Compact disc